Scalable Vertiport Allocation Plan in Conjunction with Heterogeneous Fleet Sizing

MSc Thesis

S. F. Veldhuizen

TU Delft

MSc Thesis Report

2024/2025

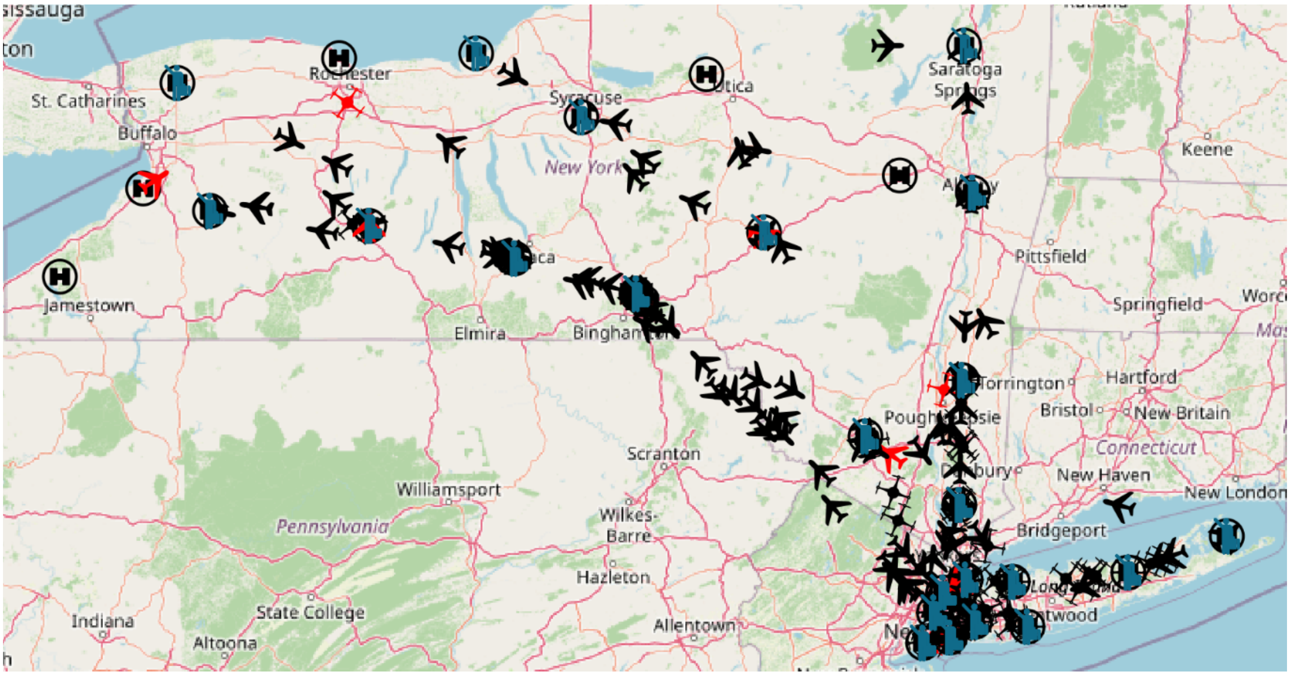

Unified Framework for a Scalable Vertiport Allocation Plan with System-performance-based Heterogeneous Fleet Sizing

Author:

Veldhuizen, Simone F.	4534441

Assessment committee:

Dr. Lima Pereira, Lourenco T.	Supervisor
Dr. Ribeiro, Marta J.	Supervisor
Dr. Oliviero, Fabrizio	Chair
Dr. Merino Martinez, Roberto	Examiner
Shiva Prakasha, Prajwal	Industry - DLR

Cover image: AI generated

TU Delft | Aerospace Engineering

Acknowledgements

I would like to thank my thesis supervisors, , for their support, feedback, discussions, patience and laughs throughout the entire project period. Marta, you were able to guide me through the complexities on the operational side of the AAM transportation system. Your overall perspective and knowledge helped me to formulate the appropriate level of detail for the research conducted. Discussions we have had pushed me to think critically as well as constrain the research where necessary. Tercio, your knowledge on aircraft performance and your eye for detail aided me in ultimately produce the quality of the results presented. Your positivity and enthusiasm constantly motivated me throughout the thesis to perform, while your critical thinking slowed me down and re-adjust where necessary. Ultimately, both of you played crucial roles in the formulation and the execution of the research, which I will forever be thankful for!

A big thank you to the COLOSSUS SoSID toolkit development team; for their support in the employment of the agent-based simulation tool, in particular, Timo Stienstra for your immaculately fast bug fixes and overall support; you aided me tremendously in conducting the research presented here.

I would like to thank my friends for their support, motivation and understanding throughout this period, walo lobi <3. A special thanks to Rax, Sol and Felix for the conversations, pointers, and time and energy put into proof-reading.

Finally, I would like to thank my family, in particular, my parents for raising me the way you have, and providing me with the opportunities to develop myself academically and as an individual. Your support and (at times, tough) love have motivated me to achieve what I have up until this point, realizing that it is a handful, while being humbled by the fact that this is just the start. Both of you, in your own ways, inspire me to do and be better, career-wise, as an individual and as a family member.

Simone F. Veldhuizen
Delft, February 2025

Contents

List of Figures

List of Tables

Introduction

The Master's thesis presented in this report was conducted at TU Delft in cooperation with the German Aerospace Center (DLR), within the context of the European project COLOSSUS, Collaborative System of Systems Exploration of Aviation Products, Services & Business Models.

The deployment of an advanced air mobility (AAM) transportation system requires a substantial amount of planning and analysis to function appropriately. On the operations side, it starts with the allocation of vertiports such that the system may respond to its demand. The established vertiport network and demand are then to be served by electric vertical take-off and landing (eVTOL) aircraft, which are to be sized such that they may transport passengers as effectively as possible between vertiports. However, the electric nature of eVTOL aircraft and current-day battery technology introduce drastic limitations on the missions they may serve. Consequently, a general distinction can be made between the types of trips within the AAM system between urban air mobility (UAM, ≤50 [km]) and regional air mobility (RAM, 50-200 [km]). This distinction in combination with the availability of distributed propulsion technology has enabled the establishment of a number of different eVTOL configuration architectures. The architectures may be split up into two main groups, where one is based on a rotary-wing cruise segment and the other on a fixed-wing cruise segment.

Generally, the rotary-wing types are better at performing shorter range trips due to its relatively efficient hover segment and inefficient cruise segment. On the other hand, the fixed-wing types have a less efficient hover segment, but more efficient cruise segment, making it better at performing longer range trips. As a result, given the potential presence of UAM and RAM trips within an AAM transportation system, it could be optimal to operate a heterogeneous fleet consisting of both types of aircraft. Furthermore, seeing as the development of the AAM network will take a considerable amount of time, the assessment of how it may evolve (progressive preliminary allocation of vertiports) and as a result, how its demand and distances of the routes will evolve, will allow for the study of the network-coupled optimal fleet and infrastructure.

As a result, this thesis aims to formulate a unified framework for the development of a scalable vertiport allocation plan in conjunction with heterogeneous fleet sizing. This is accomplished through the development of a synthetic demand generator which models semantic travel patterns based on county to county flows. Furthermore, a vertiport allocator is developed, which establishes the final network by employing a distance-based agglomerative clustering algorithm, followed by the progressive commute-distance-based vertiport elimination procedure, which includes redistribution of the demand among the available vertiports at each iteration. Vehicles are sized using an externally developed eVTOL vehicle sizing tool, and a parameter sweep is carried out across the size and composition of the fleet. All combinations of vertiport networks and fleet are implemented in an (externally developed) on-demand agent-based simulation, which determines the performance of the AAM transportation system. The optimal fleet per vertiport network size under investigation is then determined based on the total system performance metrics.

This report is structured as follows: Chapter 1 contains the scientific paper and Chapter 2 contains the literature review conducted in preparation of the development of the framework.

1

Scientific paper

Unified Framework for a Scalable Vertiport Allocation Plan with System-performance-based Heterogeneous Fleet Sizing

Simone F. Veldhuizen

Delft University of Technology, Faculty of Aerospace Engineering, Kluyverweg 1, 2629 HS Delft, Netherlands

The deployment and subsequent development of an Advanced Air Mobility (AAM) transportation system is expected to take an incredible amount of resources in terms of planning, time and capital. Due to the system not yet being operational anywhere, and consequently, the lack of clear operational boundaries set, researchers and developers are left with an enormous design space. Currently, parallel independent developments are taking place in all aspects of the system, and different perspectives have enabled a wide range of concepts to be formulated in each. Whereas independent assessments provide crucial insights into the individual components of the system themselves, they fail to capture the inherent interdependencies. They also do not capture the growth of the aircraft fleet in correlation with the growth of the vertiport network. This gives rise to the need for a framework which is capable of establishing a preliminary vertiport network to allow for the study of the aircraft, fleet and total system performance in a coherent manner, and the scalable correlated evolution thereof. Consequently, this study aims to develop a unified framework for the formation of a scalable vertiport allocation plan in conjunction with system-performance-based heterogeneous fleet sizing. The scalable vertiport allocator employs a distance-based agglomerative clustering algorithm to determine the clusters in the ultimate vertiport network and the k-means clustering algorithm to determine the preliminary location of the vertiport per cluster. This is followed by a commute-distance based vertiport elimination procedure to establish each vertiport network to be assessed. The optimal fleet at each stage of network growth is established through a parameter sweep conducted across the fleet size and composition. The system-based performance metrics of the combinations of vertiport network and fleet are then assessed using an on-demand agent-based simulation. The framework is applied to New York (NY) state and models of existing multi-rotor (MR) and tilt-rotor (TR) aircraft are utilized as test case. The test case results show the applicability of the framework in the establishment of a scalable preliminary vertiport allocation plan to maximize system commute distance, and the correlated growth of the optimal fleet based on the maximum system performance.

1. Introduction

Advancements in electric motors, distributed propulsion, artificial intelligence, etc. have allowed the emergence of a new segment within the aviation market, namely Advanced Air Mobility (AAM) or Innovative Air Mobility (IAM). Generally, aircraft within this new segment are capable of vertical take-off and landing operations, and are based on a fully electric powertrain (electric vertical take-off and landing, eVTOL, aircraft). Distributed propulsion and electric motors give way to a whole new and bigger design space for the aircraft. Consequently, a number of vehicle architectures have been established up to this point, where the two main branches are based on a fixed-wing cruise or a rotary-wing cruise [4] [5]. As a result, this new segment includes a wide range of operations e.g. last mile package delivery, emergency response services, passenger air taxi transportation system [2, 8, 9].

On the passenger transportation side, the AAM market segment can be split into Urban Air Mobility (UAM) and Regional Air Mobility (RAM), where the main difference lies in the latter covering longer range trips and the former shorter ranges. These passenger carrying flights are to be served through vertiports, which in terms of serving demand, should generally be placed in high traffic flow areas. Numerous studies on the allocation of vertiports have been performed and can be categorized into 4 main categories based on their approach, namely, location requirements and limitations approach [3, 10–13], geographic data comparison approach (GIS) [14–16], clustering approach [17–20] and objective-based approach [21–24]. Whereas these studies provide various state-of-the-art vertiport allocation methodologies, the majority provides a single set of vertiport locations. However, the need for a sequential allocation plan becomes evident when confronted with the planning efforts and infrastructure costs associated with the development of a single vertiport. This is emphasized by the very limited space available to place vertiports as a result of the already dense infrastructure found in the majority of global urban hubs.

On the vehicle sizing and performance side, aircraft concepts based on numerous architectures have been developed. The previously introduced rotary-wing cruise branch can further be split up into multi-rotor (MR, multiple smaller rotors and distributed propulsion) and the electric-helicopter (e-heli, single large rotor and conventional helicopter flight dynamics) types. On the other hand, the fixed-wing cruise types can be segmented into the tilt-rotor (TR), tilt-duct(TD) and lift+cruise types. All fixed-wing cruise types use the concept of distributed propulsion while in hover state, and transition to conventional aircraft dynamics in their cruise segments. To this extent, a number of studies on the architectural assessment of aircraft have been performed [7, 25]. Compared to conventional aviation, the limitations imposed on the aircraft range by current-day battery technology increase the complexity of the transportation system as a whole substantially, and emphasise the interdependencies between the various components of the system (e.g. aircraft sizing and performance, traffic management, vertiport allocation and operations).

Daskilewicz et al. [22] show progressive vertiport placement in three steps (small, medium and large vertiport network), by 'solving an integer program that maximizes the population-cumulative potential time savings compared to driving'. Whereas the authors do assess the effect of network growth on the mean distance in the network and correlate it to aircraft range requirements, the limitations imposed by the aircraft performance and its range are not incorporated. On the other hand, Prakasha et al. [1, 5] developed a system of systems (SOS) framework for the assessment of the transportation system as a whole along with the systems it contains (aircraft sizing, homogeneous fleet sizing, vertiport network). Ratei et al. [26] utilized this framework to assess the impact of homogeneous fleet operations on the top-level aircraft requirements of a multi-rotor and tilt-rotor eVTOL aircraft. Whereas these studies provide crucial insights into scalable vertiport allocation or homogeneous fleet sizing, they do not capture the sequential and correlated evolution of the vertport network and heterogeneous fleet (i.e. size and composition). Consequently, this study aims to **formulate a unified framework for the development of a scalable vertiport allocation plan in conjunction with heterogeneous fleet sizing**.

In order to establish the stepwise vertiport allocation plan, the framework starts with the development of a synthetic demand generator, which models semantic travel patterns based on county to county (C2C) flows. The synthetic demand generator produces a dataset containing origin-destination (OD) pairs along with accompanying departure times. The methodology applied to arrive at this synthetic demand dataset is provided in subsection 2.1. To determine the optimal sequential allocation of vertiports, a scalable vertiport allocator is developed. It starts by establishing the final network by using a distance-based agglomerative clustering algorithm to determine the clusters in the network, and the k-means clustering algorithm to determine the optimal preliminary location of the vertiport per cluster. This is followed by the progressive commute-distance-based vertiport elimination procedure, which includes redistribution of the demand among the available vertiports at each iteration using the K-Dimensional tree algorithm. The vertiport allocator is presented in subsection 2.2. The framework continues with the sizing and performance analyses of the aircraft included in this study through the use of an externally developed eVTOL aircraft sizing tool. The vertiport network, aircraft sizing and performance results, and fleet size and composition are combined and fed to an externally developed on-demand agent-based simulation tool, which conducts a full day of operations and gathers the data thereof. These tools are introduced in subsection 2.3. The data accumulated by the agent-based simulation tool are fed to the post-processor (subsection 2.4), which assesses a set of performance measures through value functions (VFs). The VFs are then combined along with their respective weights in the measure of effectiveness (MoE), which ultimately represents how well the system as a whole performs.

The framework is applied to a case study (Section 3) to assess its applicability and validity. The resulting total demand is presented and validated in subsection 4.1. The vertiport network results are provided in subsection 4.2, followed by the sizing and performance results of the aircraft in subsection 4.3. subsection 4.4 contains the system performance results, after which the fleet sizing results are detailed in subsection 4.5.

The overall results are discussed in subsection 4.6. The study concludes by summarizing the results and presenting potential future work in Section 5.

2. Methodology

The System of Systems (SoS) approach as established by Prakasha et al. [5] is adopted and expanded to arrive at the workflow presented in Figure 1.1. The workflow starts with a synthetic demand generator (module 1, subsection 2.1) which produces an origin-destination (OD) commute dataset based on semantic travel patterns. This allows for a more precise assessment of the demand which may be served by the AAM transportation system, seeing as realistically, only a portion of commutes experience time savings when comparing the AAM trip to a car-based trip. This in turn results in a more realistic top-level AAM performance assessment.

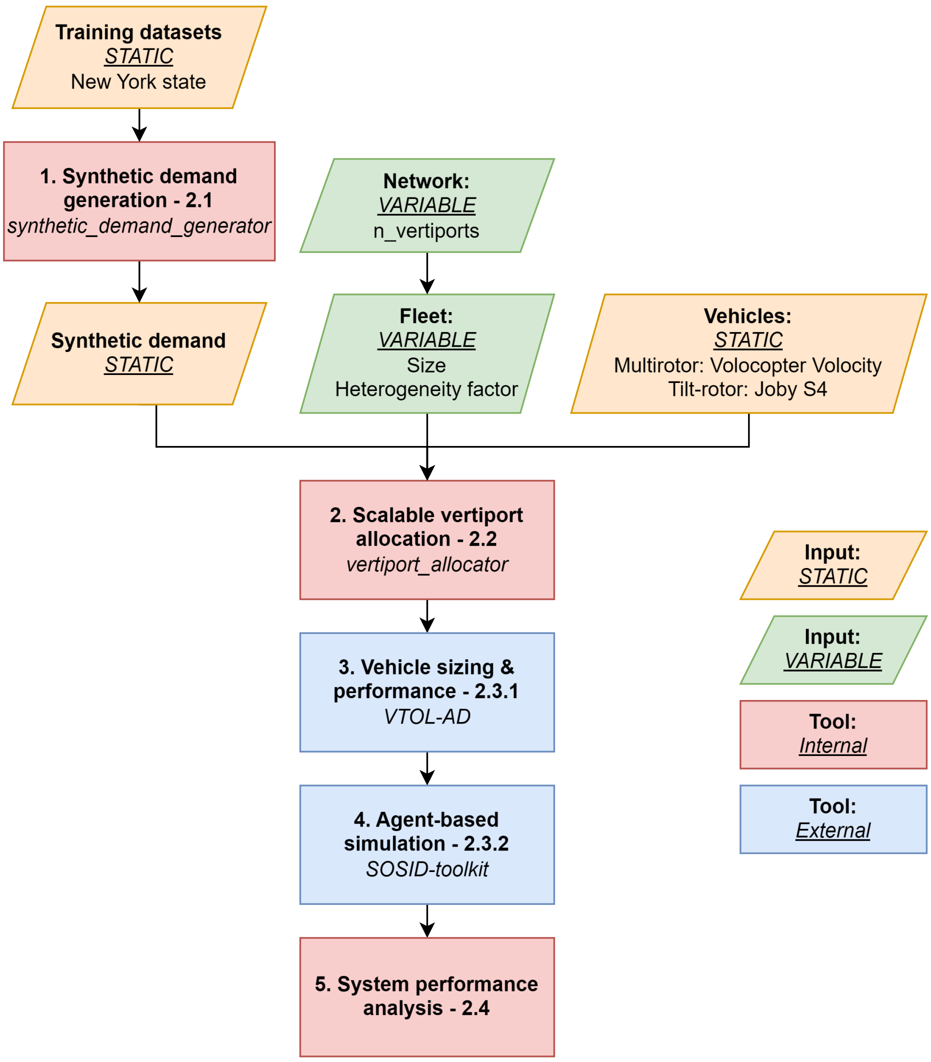

Figure 1.1: Scalable vertiport allocation and heterogeneous fleet assessment workflow

The synthetic demand dataset is fed to the scalable vertiport allocator (module 2, subsection 2.2), which starts by establishing the 'final' vertiport network through a distance-based agglomerative clustering algorithm. A distance-based clustering algorithm is opted for such that a vertiport network based on a minimum distance between vertiports is established. In this way, the optimal number of vertiports is determined by the clustering algorithm rather than having to provide it as input, which is the case for the widely adopted k-means clustering algorithm [17–20, 27]. The scalable aspect is then accounted for by adopting an iterative commute-distance based vertiport scoring system and demand redistribution (among the available vertiports using a KD-tree algorithm), and eliminating the bottom vertiport until the intended number of vertiports in the network is achieved. The vertiport allocator is further elaborated upon in subsection 2.2.

For the vehicle sizing and performance aspect (module 3, subsubsection 2.3.1) of the workflow, the vehicle sizing tool VTOL-AD developed by Ratei [4] is used. The vertiport-based (filtered) demand, vertiport network, vehicles, and fleet are combined and fed to the agent-based simulation tool developed by Prakasha et al. [5]. The agent-based simulator (module 4, subsubsection 2.3.2) performs operations that span the operating hours of the system in a day and collects the data. Based on the data, a top-level system performance assessment is performed in the post-processing step (module 5, subsection 2.4). A parameter sweep is conducted across the number of vertiports (scalable network size), fleet size and heterogeneity factor (ratio of multi-rotor vehicles over total number of vehicles) such that a correlated assessment between growth of the network and the fleet can be made.

2.1. Synthetic demand generation

The vertiport allocator requires a commute dataset containing longitudes and latitudes of OD pairs as well as accompanying departure times. Seeing as such data is not readily available to the public due to privacy reasons, the synthetic demand generator (module 1 in Figure 1.1) is developed. The workflow implemented in this generator is provided in Figure 1.2.

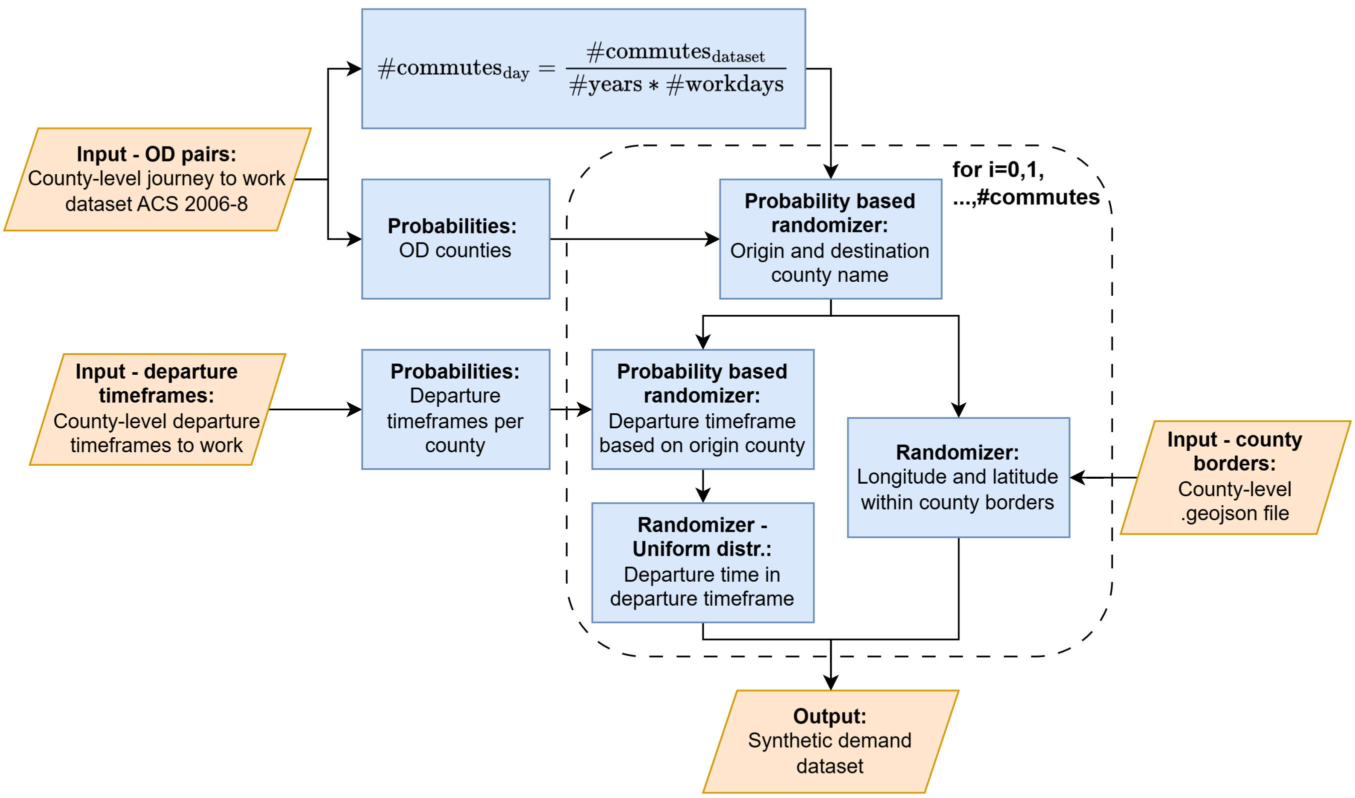

Figure 1.2: Workflow - Module 1 - Synthetic demand generator

To establish the origin and destination locations, the generator starts with a county-level journey to work (C2C) dataset [28], which contains the number of commutes between counties over a three year period. Based on this dataset, the number of commutes within a day is determined by normalizing the number of commutes in the C2C dataset by 3 years, containing 260 workdays each. The C2C dataset is also used to determine the probabilities of commutes between each combination of counties within the dataset (OD probabilities). This is done as a means to model semantic travel patterns i.e. restricted to commutes to work within the context of the research presented here. In order to determine the departure time, a county-level dataset containing the number of commutes within given departure timeframes is adopted [29]. Based on this dataset, the probabilities of commutes within the timeframes is established per county (timeframe probabilities). The longitudes and latitudes of the OD pairs are determined using the final input dataset, which contains the coordinates of the borders (excluding water) per county [30].

The datasets used to train the synthetic demand generator are all based on New York state. However, the generated synthetic demand dataset may be created for any location assuming the availability of data on the population count and borders per county, and the number of target counties do not exceed the number of training counties. New York state has been chosen seeing as it contains a high population count and a high traffic flow. It also contains a variation in commute distances, indicating the potential for UAM as well as RAM trips. Finally, the datasets required for the demand generator are available to the public for New York state.

For the number of commutes in a day, the origin and destination county names are determined per commute using a randomizer based on the OD probabilities. This is followed by the longitudes and latitudes being determined by the location randomizer using the county borders. On the other hand, the departure timeframe is determined based on the origin county name and the respective departure timeframe probabilities. Finally, a randomizer based on a uniform distribution is used to determine the exact departure time within the selected timeframe.

2.2. Scalable vertiport allocator

The previously established synthetic demand dataset is used as input for the scalable vertiport allocator (module 2 in Figure 1.1). This vertiport allocator contains 2 iterative loops; the first establishes the 'final' vertiport network, and the second establishes a vertiport network based on the intended number of vertiports. The 'final' vertiport network in this case represents the potential final number of vertiports based on a minimum distance between vertiports. The workflow implemented in the vertiport allocator is provided in Figure 1.3.

Before the vertiports are placed, the synthetic commute dataset established by the synthetic demand generator is filtered such that only trips which have a straight-line distance larger than 5 [km] (filter 1) are considered in the allocation process. The clusters are then established using a distance-based agglomerative clustering algorithm. This is done in the first iterative process, where the distance threshold is varied until a minimum distance between vertiports between 10 to 12 [km] is attained. This minimum distance has been assumed at this stage to account for the limited airspace capacity, especially in the vicinity of vertiports. Based on the established clusters, the preliminary vertiport location per cluster is then determined by employing the k-means clustering algorithm. The vertiport locations established in this study are limited to preliminary locations since the methodology does not account for the infrastructure density and accordingly, the possibility to place the vertiports at the locations determined by the k-means algorithm. Seeing as the development of the network will take a considerable amount of time in reality, a scalable allocation procedure based on an iterative vertiport elimination process is included. For the scalable part to start, the vertiports are scored based on the total incoming and outgoing kilometres directly travelled (i.e. direct flights between vertiports) to and from the vertiports.

Accordingly, the second iterative process starts by eliminating the vertiport with the worst score (least km travelled). This is followed by redistribution of the synthetic commutes to their nearest vertiports using the K-dimensional (KD) tree algorithm. The redistributed commutes are then filtered based on the pre- and post-flight commute distance (filter 2), AAM commute compared to commute by car (filter 3) and AAM operating hours (filter 4). The last filter ensures that commutes which have the same origin and destination vertiports are not considered (filter 5). As can be seen below, filter 3 determines the (AAM) validity of the commute based on the added benefit as opposed to an equivalent car-based trip. To determine the car-equivalent trip details, a re-routing factor of 1.68 is used to estimate the actual distance travelled based on the straight-line distance [31]. Furthermore, depending on the distance travelled, a different average velocity is used to account for the difference between trips confined to a city centre compared to those including a freeway. The final step of the second iterative process pertains re-scoring of the remaining vertiports. This iterative process takes place until the desired number of vertiports is attained.

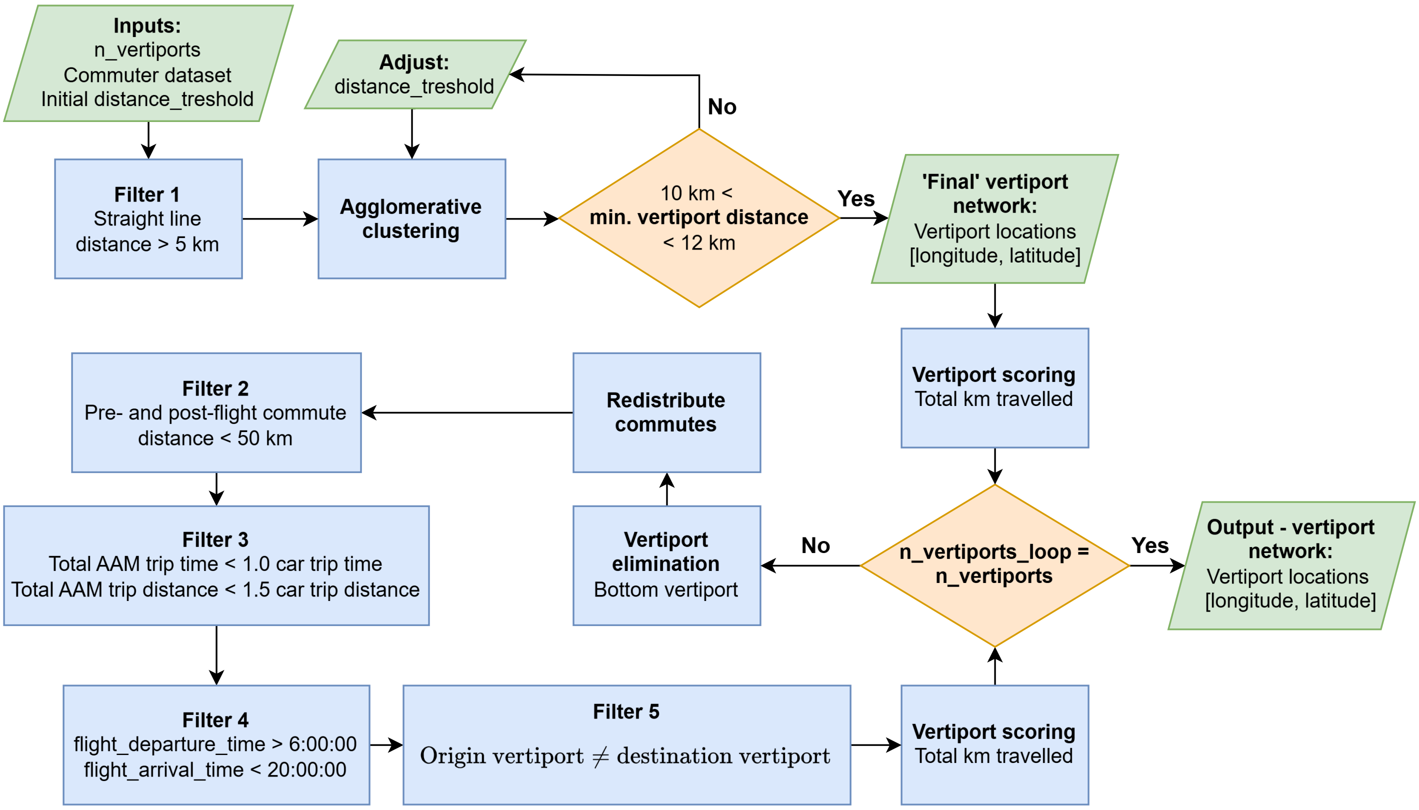

Figure 1.3: Workflow - Module 2 - Scalable vertiport allocator

Demand filters:

1. Straight-line distance > 5 [km]
2. Pre- and post-flight commute distance < 50 [km]
3. AAM vs. Car:
   - Total AAM distance < 1.5 Car distance
   - Total AAM travel time < 1.0 Car travel time
   - Car-equivalent trip constants:
     - Re-route factor = 1.68
     - Car-based distance < 5 [km]: Average velocity = 30 [km/h]
     - Car-based distance > 5 [km]: Average velocity = 70 [km/hr]
4. Operating hours:
   - $t_{dep_{AAM}} > 6{:}00{:}00$
   - $t_{arr_{AAM}} < 20{:}00{:}00$
5. Origin vertiport ≠ destination vertiport

Once the commutes have been filtered out and assigned to their vertiports, the number of incoming and outgoing commutes per hour are established for each vertiport. A Gaussian distribution is then applied to the hourly data to formulate the demand distributions for the agent-based simulation (SOSID toolkit [5]) introduced in subsubsection 2.3.2.

2.3. Tools

The results of the synthetic demand generator (module 1) and the scalable vertiport allocator (module 2) form the basis for the operations side of the AAM transportation system. The next step regards the vehicles which are to serve the system. As such, information on their size and performance is required. Apart from the top-level aircraft requirements (TLARs, i.e. range, passenger capacity, cruise speed) and maximum take-off mass (MTOM), information on existing eVTOL aircraft is generally not published by the manufacturers.

2.3.1. Vehicle sizing and performance - VTOL-AD

Seeing as the information generally is not available to the public, the vehicle sizing and performance assessment tool (VTOL-AD) developed by Ratei [4] is utilized and represents the third module as seen in Figure 1.1. With regards to the aircraft considered in this study, two different types of eVTOL aircraft are opted for. The first is based on a multi-rotor architecture and is chosen since overall, this type performs best in serving short-range trips (UAM demand) compared to the other vehicle architectures [32, 33]. The second is a tilt-rotor aircraft, and is chosen to serve the longer-range trips (RAM) based on their overall best performance compared to its counterparts [7, 33]. Even though it is expected that the vehicles will perform various missions as a result of the inherent differences in architectures and even more so, limitations imposed by air traffic management, it is assumed at this stage that all aircraft operating within the system will perform the same mission profile. Accordingly, they are sized based on the same segment altitudes. On the other hand, the differences in the top level aircraft requirements (TLARs) between the two aircraft types are accounted for. Furthermore, battery swapping is disabled for both aircraft seeing as it would induce an increase in empty weight to account for the required structure to house the battery safely.

2.3.2. Agent-based simulation - SOSID toolkit

Once the operations side and the vehicles which are to serve the system have been established, an assessment of their combined performance is to be made. In order to assess the system performance, the on-demand agent-based simulation tool (SOSID toolkit) developed by Prakasha et al. [5] is adopted (module 4 in Figure 1.1).

The agent-based simulation requires the number of vehicles per vehicle type at each vertiport at the start of the simulation (initial vehicle distributions). Rather than choosing a uniform initial distribution, the assumption is made that the AAM system will operate using data gathered through operations, and consequently, will be able to make predictions such that vehicles may be (re-)distributed accordingly. Accordingly, the filtered demand is split up into UAM and RAM trips, where the distinction is made based on the range of the multi-rotor vehicle. For both, the hourly demand per vertiport is established. This is followed by identifying the hours and magnitudes of the peaks per vertiport. Finally, the initial vehicle distribution for the multi-rotor (UAM) and tilt-rotor (RAM) configurations are determined using Equation 1.1 and Equation 1.2, respectively. The heterogeneity factor (Equation 1.3) represents the ratio of multi-rotor aircraft over the total fleet size. A potential correction is applied in case the distributed number of vehicles does not match the intended number of vehicles.

$$\#\text{vehicles}_{\text{UAM}_i} = \frac{\text{magnitude}_{\text{UAM}_i}}{\sum_{i=1..n} \text{magnitude}_{\text{UAM}_i}} * \#\text{vehicles}_{\text{total}} * \text{heterogeneity factor} \tag{1.1}$$

$$\#\text{vehicles}_{\text{RAM}_i} = \frac{\text{magnitude}_{\text{RAM}_i}}{\sum_{i=1..n} \text{magnitude}_{\text{RAM}_i}} * \#\text{vehicles}_{\text{total}} * (1 - \text{heterogeneity factor}) \tag{1.2}$$

$$\text{heterogeneity factor} = \frac{\#\text{multi-rotor aircraft}}{\text{fleet size}} \tag{1.3}$$

In this agent-based simulation, it is assumed that deadhead flights are performed autonomously, whereas all passenger-carrying flights are piloted. Furthermore, the agent-based simulation tool accounts for the range limitations of the aircraft by allowing for multi-legged trips where necessary. Charging of the vehicles occurs the moment the vehicle enters idle mode, and the vehicles are simulated to charge with a c-rate equal to 2.0C. The simulator conducts a full day of operations and gathers the results thereof. These results are fed to the post-processor, namely, the system performance analysis. The definition of the performance measures used in this study are provided in subsection 2.4.

2.4. System performance analysis

The final step of the workflow pertains the assessment of the total system performance as a result of the combination of vertiport network, fleet size and composition, and the vehicles in the fleet. The concept of measure of effectiveness (MoE) as defined by Ratei et al. [26] is adopted to assess the system performance. The normalization method applied to the value functions is adapted as opposed to that defined by Ratei et al. and follows the normalization of multi-objective optimization methods defined by Arora [34]. Furthermore, the average time saved is also incorporated in the MoE to account for the potential cruise velocity superiority of one aircraft type over the other. Ultimately, the MoE used in this study is provided in Equation 1.4.

The first performance measure (VF_I, Equation 1.5) in the MoE pertains the share of AAM trips over the total number of trips under consideration or rather, the ratio of served demand over filtered demand. The served demand is the number of trips served by the AAM transportation system within a day of operations and depends on the filtered demand provided to the agent-based simulation. The agent-based simulation converts trip requests to AAM trips based on the potential time savings compared to a car-based trip i.e. if the AAM trip is slower than the car-based trip, the passenger chooses to travel by car. Based on this definition, it is clear that the filtered and, accordingly, served demand vary as the number of vertiports in the network is adapted (Equation 1.5). Ultimately, VF_I provides information on how well the fleet can respond to demand within the formulated network and, as originally defined, aims to maximize the revenue generated by the AAM transportation system.

$$\mathrm{MoE} = w_I VF_I + w_{II} VF_{II} + w_{III} VF_{III} + w_{IV} VF_{IV} \tag{1.4}$$

In which: $w_I = 0.4$ $w_{II} = 0.3$ $w_{III} = 0.1$ $w_{IV} = 0.2$

$$VF_I = \frac{\text{converted requests}_i(\text{fleet size, heterogeneity factor}) - \text{converted requests}_{i_{min}}}{\text{converted requests}_{i_{max}} - \text{converted requests}_{i_{min}}} \tag{1.5}$$

$$VF_{II} = 1 - \frac{\text{fleet energy}_i(\text{fleet size, heterogeneity factor}) - \text{fleet energy}_{i_{min}}}{\text{fleet energy}_{i_{max}} - \text{fleet energy}_{i_{min}}} \tag{1.6}$$

$$VF_{III} = \frac{\text{average load factor}_i(\text{fleet size, heterogeneity factor}) - \text{average load factor}_{i_{min}}}{\text{average laod factor}_{i_{max}} - \text{average load factor}_{i_{min}}} \tag{1.7}$$

$$VF_{IV} = \frac{\text{average time saved}_i(\text{fleet size, heterogeneity factor}) - \text{average time saved}_{i_{min}}}{\text{average time saved}_{i_{max}} - \text{average time saved}_{i_{min}}} \tag{1.8}$$

The second performance measure (VF_{II}, Equation 1.6) aims to minimize the total fleet energy and as presented by Ratei et al. [26] serves to minimize the operational costs of the transportation system. This has effect on the size of the fleet, seeing as more vehicles require more energy to operate. Apart from the fleet size, this also affects the optimal heterogeneity factor (fleet composition) due to the varying power output profiles, and flight envelopes of the multi-rotor and tilt-rotor aircraft. This is further elaborated upon in Section 3.

The third performance measure (VF_{III}, Equation 1.7) aims to maximize the average load factor of the fleet as a way to maximize its utilization. The average load factor is determined through Equation 1.11, where the average capacity of the entire fleet and the average operational capacity (i.e. averaged over all performed missions, including autonomous deadhead flights) are determined using Equation 1.9 and Equation 1.10, respectively. These are all affected by the number of vertiports in the network, the fleet size and the heterogeneity factor. Furthermore, the definition of the average load factor indirectly implies a minimization of the number of deadhead flights.

$$\text{fleet average capacity} = \frac{\#\text{vehicles}_{\text{MR}}\ \text{capacity}_{\text{MR}} + \#\text{vehicles}_{\text{TR}}\ \text{capacity}_{\text{TR}}}{\text{fleet size}} \tag{1.9}$$

$$\text{fleet average operating capacity} = \frac{\#\text{revenue flights} * \text{average revenue capacity}}{\#\text{revenue flights} + \#\text{deadhead flights}} \tag{1.10}$$

$$\text{average load factor} = \frac{\text{fleet average operating capacity}}{\text{fleet average capacity}} \tag{1.11}$$

The fourth performance measure (VF_{IV}, Equation 1.8) is incorporated to maximize the time saved opposed to an equivalent car-based trip. This relates back to the users' willingness to pay [35] [36]. With regards to fleet sizing, a bigger fleet results in the higher probability of a vehicle being present when a trip is requested. On the other hand, the multi-rotor and tilt-rotor have different cruise velocities based on their type of cruise segment i.e. rotary-wing, low-speed vs fixed-wing, medium- to high-speed cruise, respectively.

Finally, these performance measures are combined in Equation 1.4, in which weights are also applied to each. The weights represent a trade-off between the importance of AAM share (w_I), fleet energy (w_{II}), load factor (w_{III}) and time saved (w_{IV}). As can be seen in Equation 1.4, the ability of the fleet to respond to demand and, consequently, generate revenue is given the highest priority (VF_I, w_I). This is followed by the fleet energy (VF_{II}, w_{II}) to account for operating costs of the system. The average time saved (VF_{IV}, w_{IV}) and the load factor (VF_{III}, w_{III}) are given the lowest weights such that the efficiency of operations is considered in a limited manner since it is mainly driven by the filtered demand and the scheduler implemented in the agent-based simulation tool. As is evident based on the definition of the parameters detailed in this section, they vary according to the number of vertiports (subscript i in Equation 1.5-1.8) in the network, and fleet size and composition.

3. Case study

3.1. Location

The synthetic demand generator presented in subsection 2.1 generates a single (three-year-averaged) commuter dataset spanning over a day for New York state. This has been chosen since the semantic travel patterns modelled in the synthetic demand generator represent that of New York state, and accordingly, are most representative of reality compared to inducing a re-location. The generated synthetic demand dataset then represents the total demand in the system in a day. Whereas optimally, one would account for a variable demand based on population growth and redistribution over time (i.e. as vertiports are added to the network), for the purpose of providing the first insights into the correlated growth of the AAM network and the heterogeneous fleet which serves it, the total demand is kept static throughout the analyses presented in this study.

3.2. Aircraft

Models of existing aircraft are used in this study rather than new aircraft concepts, namely following the concepts of the multi-rotor Volocopter Volocity (Figure 1.4 [1]) and the tilt-rotor Joby S4 (Figure 2.11 [2]). These concepts have been chosen due to their advanced stage of development in comparison to their competitors. Furthermore, models of existing aircraft have been chosen such that the results will provide insights as to how a fleet containing those will evolve with growth in the AAM network.

[1] Volocopter Volocity: `https://evtol.news/volocopter-volocity/` [accessed 02.02.24]
[2] Joby S4: `https://www.jobyaviation.com/` [accessed 25.06.24]

Figure 1.4: UAM - Multi-rotor aircraft: Volocopter Volocity

Figure 1.5: RAM - Tilt-rotor aircraft: Joby S4

The maximum disk loading, details on the powertrain and the mission used to size both aircraft are provided in Table 1.1. Furthermore, the top-level aircraft requirements (TLARs) of both aircraft are provided in Table 1.2 for each type. As evident based on the table, it is assumed that the vertiports are located at sea-level altitude, and both aircraft perform the same mission profile (i.e. altitudes). In reality, this will vary across the vehicles and trips, and overall, will be highly dependent on the manner in which Air Traffic Management (ATM) is integrated (e.g. flight corridors, flight levels, fully autonomous) in the location in question. Accordingly, this is not accounted for within the context of this study.

Table 1.1: Vehicle constants and mission profile: multi-rotor (Volocopter Volocity model) and tilt-rotor (Joby S4 model)

Variable	**Value**	**Unit**
Maximum disk loading	750.0	[N/m^2]
Powertrain efficiency	0.912375	[-]
Propeller efficiency	0.8	[-]
Battery specific energy	235.0	[Wh/kg]
Battery specific power	2.0	[kW/kg]
Altitude - Vertiport	0.0	[m]
Altitude - Vertical climb	15.24	[m]
Altitude - Cruise	457.2	[m]
Taxi time	120	[s]
Transition time MR	35.69	[s]
Transition time TR	71.38	[s]
Vertical climb and descent rate	0.508	[m/s]
Cruise climb and descent rate	3.556	[m/s]
Passenger carrying flight	Piloted	[-]
Deadhead flight	Autonomous	[-]
Battery swap enabled	False	[-]
Charge rate	2C	[-]

Table 1.2: Top level aircraft requirements (TLARs) used for the multi-rotor (Volocopter Volocity model) and tilt-rotor (Joby S4 model) aircraft.

Variable	**Multi-rotor**	**Tilt-rotor**	**Unit**
Persons on board (incl. pilot)	2	5	[pax]
Payload mass	180.0	450.0	[kg]
Cruise speed	35.0	70.0	[m/s]
Range	30.0	150.0	[km]

3.3. Parameter sweep - Independent variables

Finally, the variable inputs as seen in Figure 1.1 represent the parameter sweep conducted in this research. The first pertains the number of vertiports in the network. This is varied to assess the progressive growth of the network. The first and smallest network analysed in this study contains 5 vertiports. This is followed by the addition of 5 vertiports to the network at every next analysis point. Furthermore, the optimal fleet to serve the AAM network at each analysis step is determined by varying the fleet size from 20 to 500 in steps of 20 [vehicles]. The composition of the fleet is represented by the heterogeneity factor, where the heterogeneity factor represents the ratio of multi-rotor vehicles over total number of vehicles in the fleet (fleet size), see Equation 1.3. Naturally, (1-heterogeneity factor) represents the ratio of tilt-rotor vehicles over fleet size. The heterogeneity factor is varied from 0 to 1 with steps of 0.05 [-]. The complete parameter sweep performed in this research is provided in Table 1.3.

Table 1.3: Parameter sweep variables

Variable	**Value**
Number of vertiports	5, 10, 15,..., 40, 45, 50
Fleet size	20, 40, 60,..., 480, 500
Heterogeneity factor	0.00, 0.05, 0.10,..., 0.95, 1.00

4. Results and discussion

The framework established in Section 2 is applied to the case study outlined in Section 3. Accordingly, the synthetic demand generated for NY state is provided in subsection 4.1. The results of the scalable vertiport allocator and subsequent filtered demand are presented in subsubsection 4.2.1. The resulting progression of the network distances (i.e. between vertiports) as a result of the number of vertiports in the network is provided in subsubsection 4.2.2. subsection 4.3 contains the aircraft sizing and performance results of the MR and TR aircraft. This section continues by displaying the system-based performance results in subsection 4.4. The results of the subsequent optimal fleet sizing analysis are presented in subsection 4.5. Finally, the overall results are discussed in subsection 4.6.

4.1. Total demand

The synthetic commute dataset generated for NY state (output of module 1 in Figure 1.1, subsection 2.1) is visualized in Figure 1.6. The red and blue dots represent the origin and destination locations of the commutes, respectively. The origin and destination locations are connected by the grey lines. Figure 1.6 shows the highest concentration of commutes to be located in the NY counties in NY metropolitan area. Furthermore, clusters can be observed in Buffalo, Rochester, Syracuse and Albany. One can see the presence of UAM and RAM trips, as well as a number of long-distance commutes (>400 [km]), which exceed the attainable range of the eVTOL aircraft modelled in this study (Table 1.2). As a result, these trips will need to be performed through multiple legs, which is enabled in the agent-based simulation tool.

The synthetic demand dataset has been compared to the county-to-county commutes training dataset for validation purposes. The correlation between the two was determined to be 0.9985, which indicates that the synthetic demand dataset closely follows the distribution of commutes as found in the training dataset. Furthermore, the KL divergence was found to be equal to 0.0167, which indicates that the probabilities of commutes between counties of the generated and training dataset resemble one another closely. Finally, these validation results can be seen in Figure 1.7, where the red dashed line represents a perfect match between the training and synthetic datasets. The blue dots represent the number of commutes of each OD-county-pair in the training and synthetic datasets.

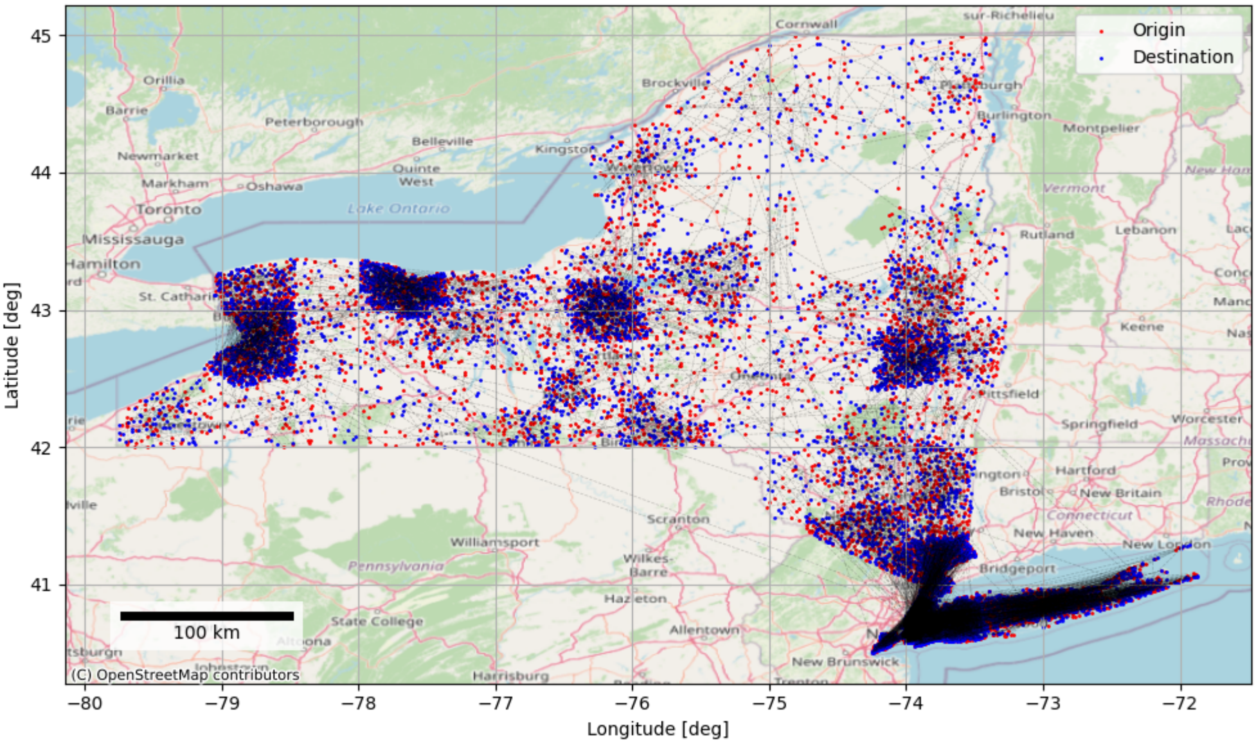

Figure 1.6: Result of the synthetic demand generator; total demand of the system and kept static throughout the parameter sweep.

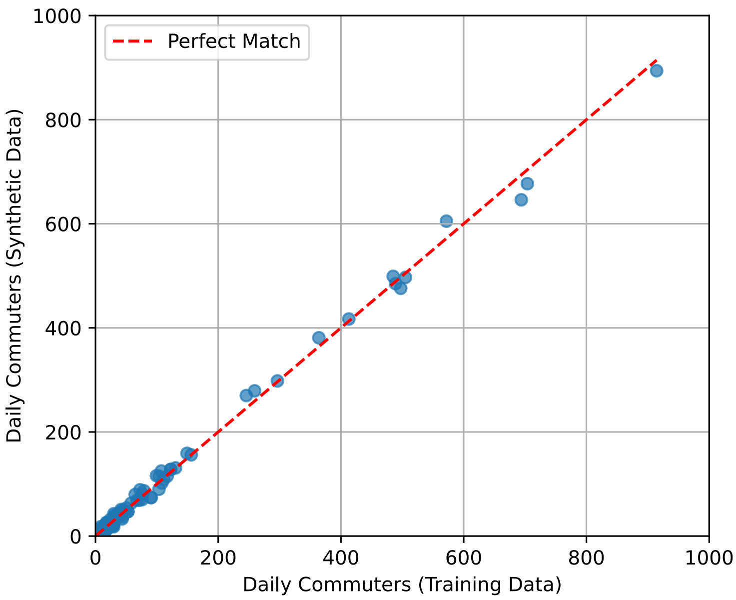

Figure 1.7: Comparison in counts of origin and destination county pairs between training (county-to-county) and the generated (synthetic) demand dataset.

4.2. Scalable AAM network

4.2.1. Vertiport locations and filtered demand

The sequential allocation of vertiports (in steps of 5 vertiports) can be seen in Figure 1.8. Figure 1.8a illustrates that the optimal placement of the first five vertiports (the deployment of the AAM transportation system in NY State) is constrained to the NY counties within the NY metropolitan area. This is in line with the highest concentration of commutes as seen in the visualization of the total demand (Figure 1.6). Figure 1.8b shows a further expansion of the network within the NY metropolitan area. Figure 1.8c shows that as vertiports are added, there is more benefit in the formulation of a separate network in and near Buffalo, rather than only further expansion in the NY metropolitan area. This is followed by growth of both networks separately as the number of vertiports in the total NY state network increases (see Figure 1.8d) until they are connected through Syracuse once the network reaches a size of 30 vertiports as seen in Figure 1.8e.

The available routes in the network along with the ranges of both aircraft show that the connection between the previously separate networks can only be served by the TR aircraft. Furthermore, the inability of the MR aircraft to respond to the filtered demand is evident based on its range and the network routes. Ultimately, the state-wide AAM network grows as the number of vertiports is increased beyond 30 as can be seen in Figure 1.8e-1.8f. This scalable vertiport allocation plan is based on the demand in NY state and accordingly, will differ as the semantic travel patterns of commuters in other locations vary from those in New York state. As a result, the vertiport allocation strategy is expected to differ to that of NY state, depending on the location under consideration. Figure 1.8 details the vertiport networks that produce the most significant differences in results; for a complete overview of all produced networks, and the longitudes and latitudes of the fifty vertiport locations, the reader is referred to Appendix A.

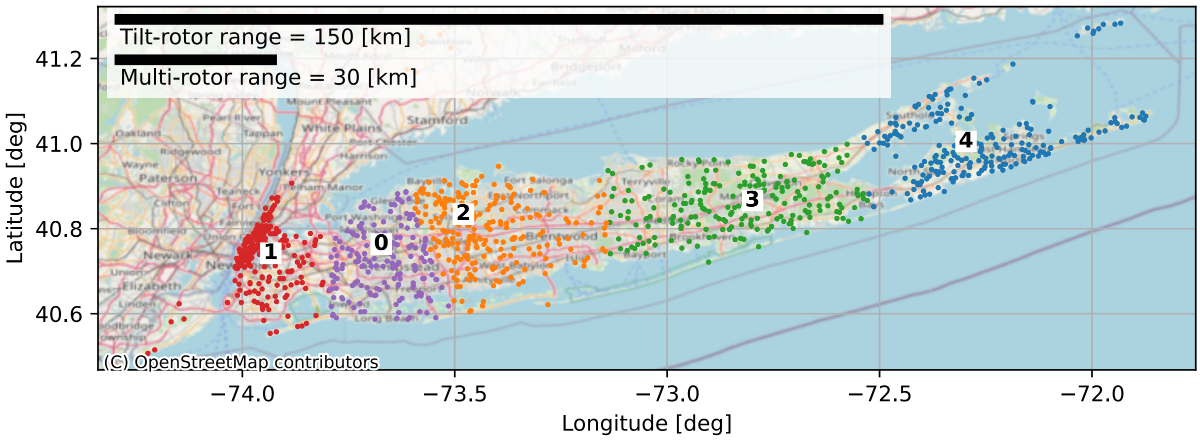

(a) 5 Vertiport network

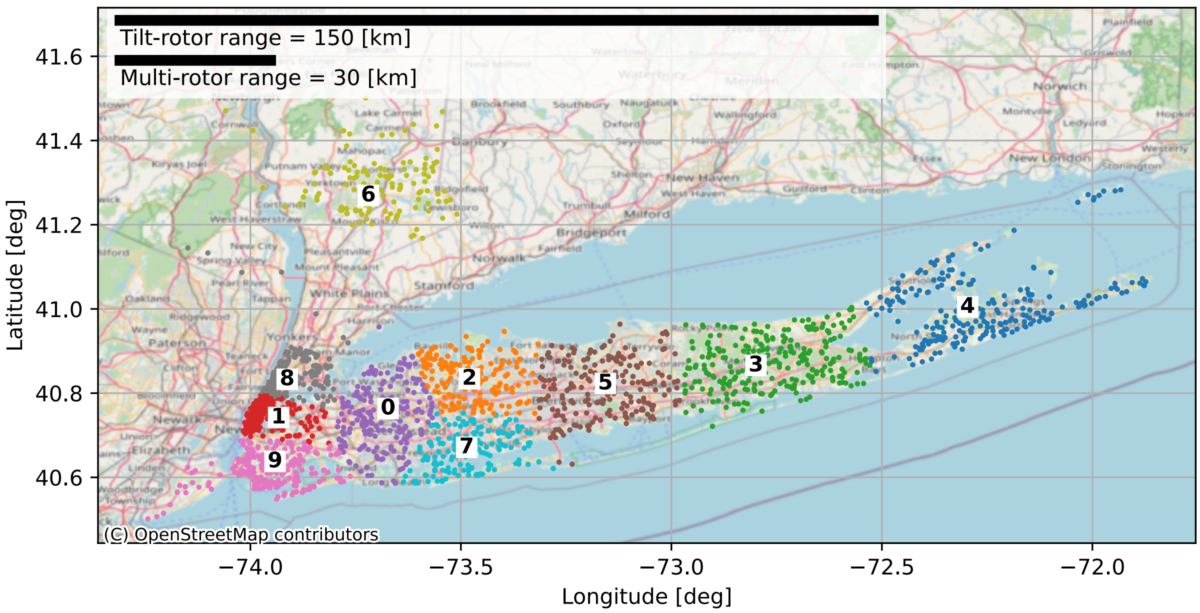

(b) 10 Vertiport network

Figure 1.8: Vertiport locations and filtered demand as a result of varying number of vertiports. The bars show the range of the multi-rotor (MR) and tilt-rotor (TR) aircraft.

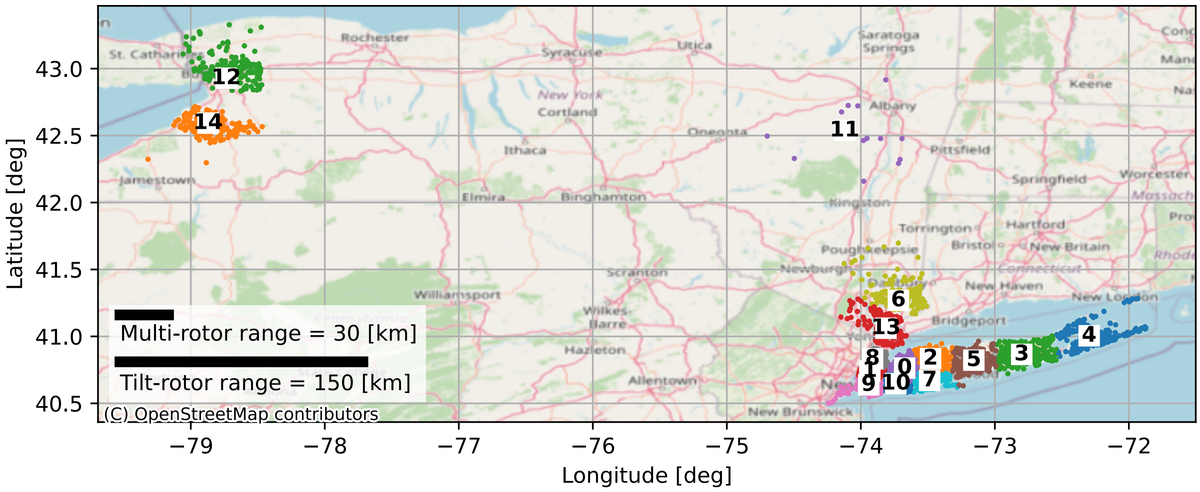

(c) 15 Vertiport network

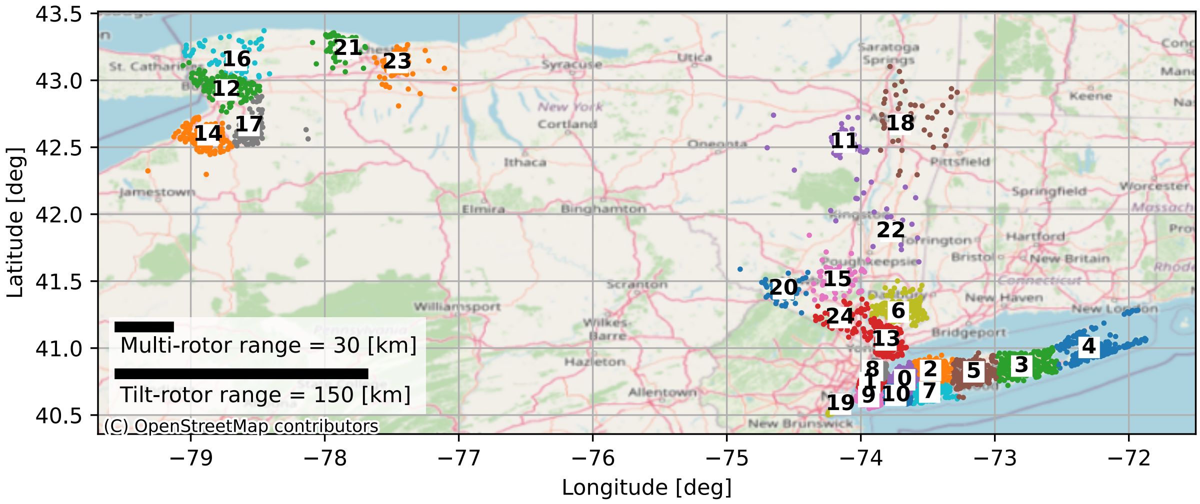

(d) 25 Vertiport network

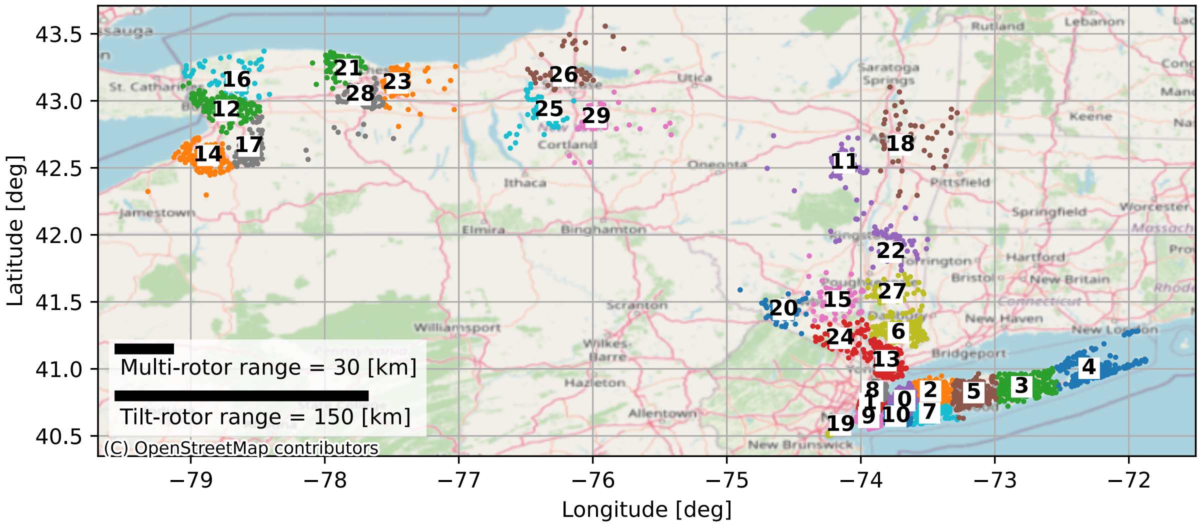

(e) 30 Vertiport network

Figure 1.8: Vertiport locations and filtered demand as a result of the number of vertiports in the AAM network. The bars show the range of the multi-rotor (MR) and tilt-rotor (TR) aircraft.

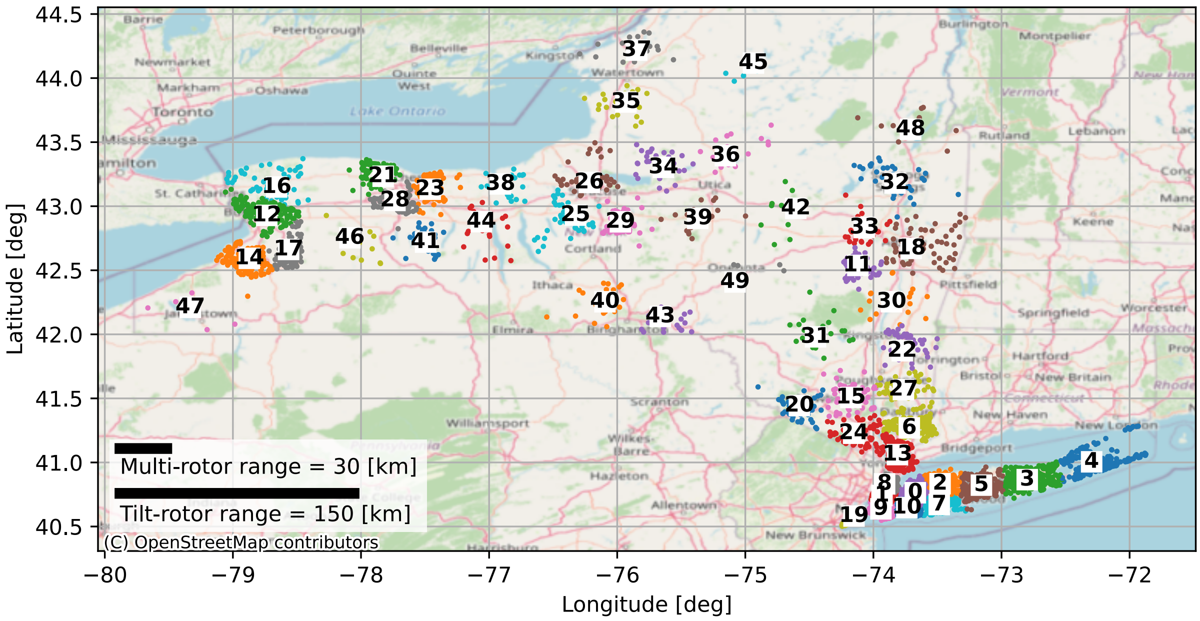

(f) 50 Vertiport network

Figure 1.8: Vertiport locations and filtered demand as a result of the number of vertiports in the AAM network. The bars show the range of the multi-rotor (MR) and tilt-rotor (TR) aircraft.

Apart from the vertiport locations, Figure 1.8 shows the progression of filtered demand as the vertiport network grows. The addition of vertiports also shows the redistribution of filtered demand to a vertiport closer by, based on its availability. One can observe this most effectively when comparing the clusters in the network containing 5 vertiports (Figure 1.8a) to the clusters in the network containing 10 vertiports (Figure 1.8b) e.g. red to grey and pink dots, orange to light blue and brown dots. Accordingly, the demand and resulting throughput per vertiport is affected by this redistribution. Overall, an increase in the filtered demand in the system can be observed as the number of vertiports in the network increases. However, comparing the filtered demand in the largest network (Figure 1.8f) to the total demand (Figure 1.6), one can see a significant difference in number of commutes. This is the result of the range of filters applied to the demand in the vertiport allocator (subsection 2.2) and reflects the fraction of trips that experience time savings compared to a car-based trip.

4.2.2. Network distances

The minimum (R_min), mean (R_mean) and commute-averaged mean (R_net_mean) distances between vertiports as the network grows are provided in Figure 1.9. The figure also contains the range of both aircraft, and accordingly shows the range deficit of both aircraft in terms of being able to serve the available routes in the network once it grows from 10 to 15 vertiports. On the other hand, the commute-averaged range shows that the tilt-rotor (TR) aircraft can serve the majority of (if not all) travelled routes, whereas the multi-rotor (MR) aircraft may not.

The range deficit can further be observed in the distances between vertiports and the ranges of the aircraft in Figure 1.8. Figure 1.8a shows that the MR aircraft may only serve 2 out of 10 available routes. Once the network grows to 10 vertiports, the MR aircraft is able to respond to 12 out of 45 routes. Contrary to the MR aircraft, the TR aircraft is able to serve all available routes in case of the 5 as well as 10 vertiport networks. Once the network grows beyond 10 vertiports, the TR aircraft becomes unable to serve all available routes, causing the separate network in the north-west corner of NY state to be formed as can be seen in Figure 1.8c). This causes the jump in R_mean as observed in Figure 1.9.

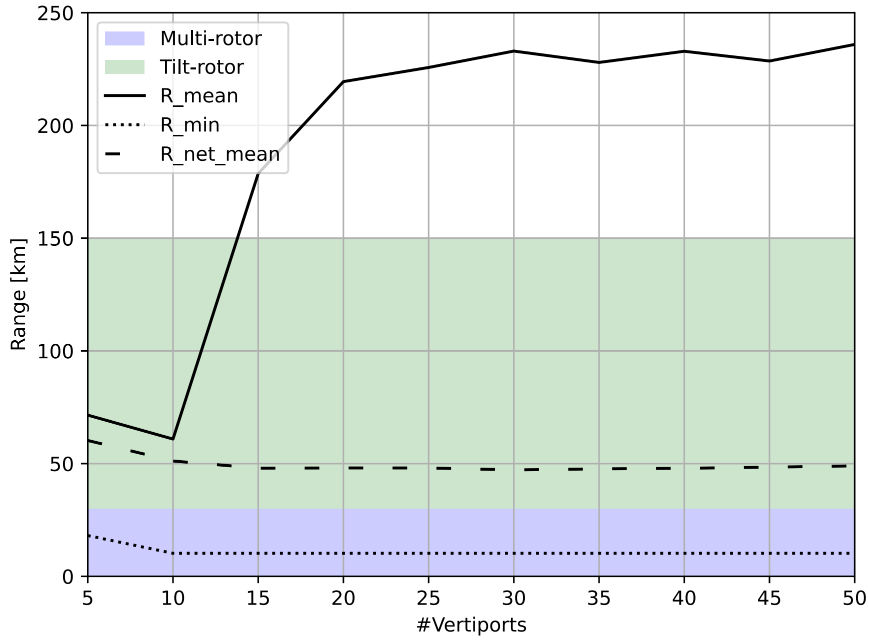

Figure 1.9: Progression of the distance between vertiports as the number of vertiports in the network is increased. The blue and green areas represent the range attainable by the modelled multi-rotor and tilt-rotor aircraft, respectively.

4.3. Aircraft sizing and performance

The sizing and performance results of both aircraft are provided in Table 1.4 and 1.5. The resulting masses of both aircraft are compared to the respective results established by Shim et al. [6] for validation purposes. Whereas the maximum take-off mass (MTOM) of the Joby S4 model determined using VTOL-AD resembles the reference results, a 20% difference can be seen for the Volocopter Volocity model. Furthermore, other discrepancies may be observed in the various component masses. These discrepancies may be attributed to the differences in missions for which they were sized (e.g. modelled flight segments, altitudes, times).

Table 1.4: VTOL-AD sizing results of the multi-rotor (Volocopter Volocity model) and tilt-rotor (Joby S4 model) aircraft.

Variable	**Multi-rotor**	**Tilt-rotor**	**Unit**
Disk loading	141.1761	150.0	[N/m^2]
Best endurance speed	20.836	46.314	[m/s]
Best range speed	27.422	60.953	[m/s]

Table 1.5: VTOL-AD mass sizing results of the multi-rotor (Volocopter Volocity model) and tilt-rotor (Joby S4 model) aircraft compared to reference sizing results [6].

	Multi-rotor			**Tilt-rotor**		
	VTOL-AD [kg]	Reference [6] [kg]	Difference [%]	VTOL-AD [kg]	Reference [6] [kg]	Difference [%]
MTOM	1076.6	900.0	19.62	2236.5	2177.0	2.73
Payload mass	180.0	200.0	-10.00	450.0	453.6	-0.79
Empty mass	554.9	504.2	10.05	1056.8	898.6	17.60
Battery mass	341.7	195.8	74.55	729.7	824.8	-11.53

The resulting power requirements per flight segment for both aircraft can be seen in Figure 1.10. One can observe 3 different power requirement trends for the multi-rotor aircraft, which are based on the different loading scenarios i.e. number of people on board. The loading scenario which contains zero passengers represents an autonomous flight, which is applicable for all deadhead flights in the agent-based simulations. On the other hand, all passenger-carrying flights are piloted. The same variation in loading profiles can be observed for the tilt-rotor aircraft.

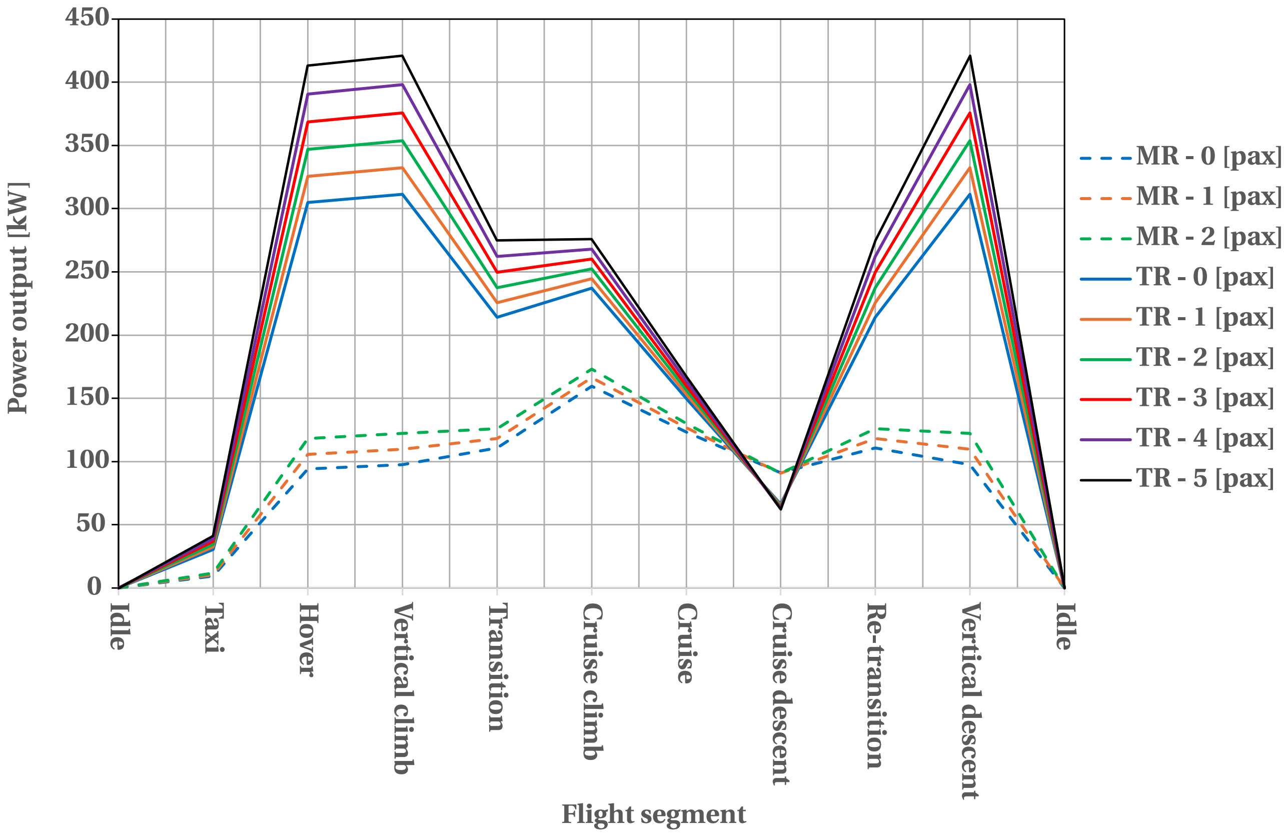

Figure 1.10: Power requirements per flight segment - Muti-rotor (MR, Volocopter Volocity model) and tilt-rotor (TR, Joby S4 model).

4.4. System performance

Before diving into the system performance measures, the demand and fleet energy are assessed in order to validate the workings of the scalable vertiport allocator and agent-based simulation (subsubsection 4.4.1). This is followed by the resulting value functions ($VF_{I\text{-}IV}$) and the assessment thereof. Finally, the ultimate system performance (MoE) analysis results are presented and discussed in subsubsection 4.4.3.

4.4.1. Validation

Figure 1.11a shows the filtered demand as the vertiport network increases in size, as well as the served demand when operating homogeneous (MR and TR) fleets consisting of 500 aircraft each (maximum fleet size). Overall, the filtered demand can be seen to increase and plateau as the networks size increases. This validates the workings of the scalable vertiport allocator, which scores vertiports based on the total commute distance travelled to and from that vertiport in a single-legged trip.

Observing the progression of served demand (Figure 1.11a) as the network grows, when operating homogeneous fleets, one can observe major differences between the two. The trend for the TR fleet follows that of the filtered demand very closely until a network size of 10 vertiports is reached. As the network grows from 10 to 15 vertiports, the separate vertiport network (connecting suburban counties) is formed. Looking at the jump in R_mean (Figure 1.9), the vertiport networks (Figure 1.8b and Figure 1.8c), and the difference in filtered and served demand Figure 1.11a when expanding the network from 10 to 15 vertiports, one can conclude that trips are requested from one part of the network to the other, which both aircraft are unable to serve based on the ranges for which they have been sized.

The expansion of both individual parts of the network (15 to 25 vertiports) can be seen in the slight increase in served demand. Once the network is expanded from 25 to 30 vertiports, the state-wide connection is formed. This allows for the previously not serviceable demand to be completed through multi-legged trips and causes the jump in served demand (Figure 1.11a). The discrepancy between the filtered demand and the demand served by the TR fleet once the network reaches 30 vertiports can be attributed to a combination of limited maximum fleet size assessed and potential planning inefficiencies of the scheduler implemented in the agent-based simulation tool. This will be discussed from a system-performance fleet sizing perspective in detail in subsection 4.5.

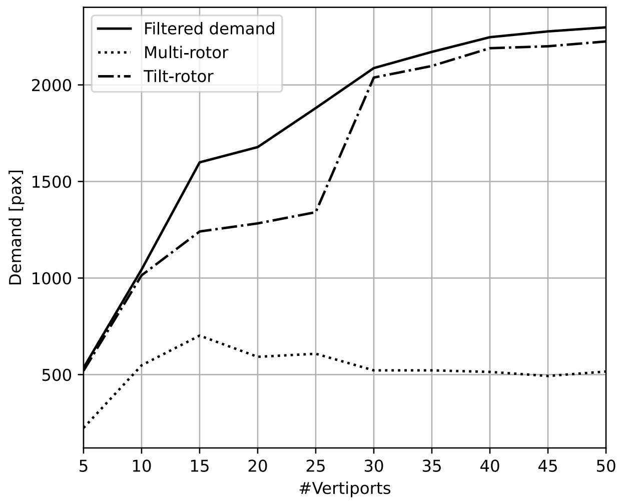

(a) Demand vs #Vertiports - Homogeneous fleet - Fleet size = 500 aircraft.

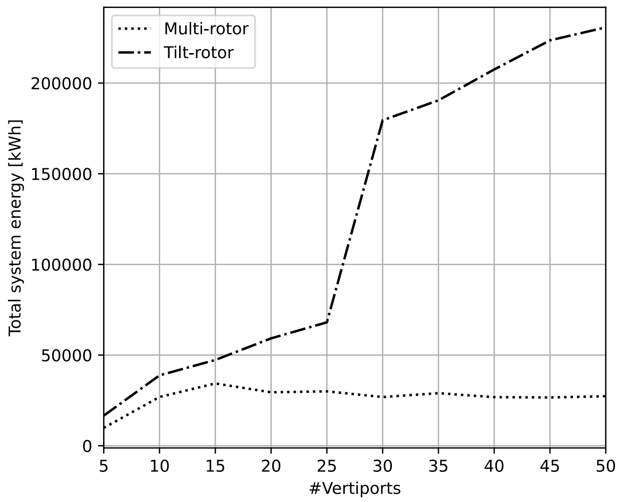

(b) Fleet energy vs #Vertiports - Homogeneous fleet - Fleet size = 500 aircraft.

A difference between MR served demand, and filtered and TR served demand can be observed at 5 vertiports (Figure 1.11a). This is in line with the inability of the MR aircraft to serve the majority of requested trips. Some trips could be conducted through multi-legged trips. However, when considering the relatively low cruise velocity of the MR aircraft in combination with the wait time (on-demand system) and time lost as a result of the multi-legged nature of the trip, the probability of potential time savings becomes very small. Consequently, it is more advantageous for the commuter to employ a car-based trip rather than make use of the AAM transportation system (logic implemented in agent-based simulation scheduler). Furthermore, the MR served demand can be seen to increase as the network expands from 5 to 15 vertiports. This is in line with the predominant increase in vertiport density in the network (Figure 1.8a-1.8c), and consequently, the decrease in commute-averaged trip distance (R_net_mean) as seen in Figure 1.9. As the network grows beyond 15 vertiports, the minor variations in R_net_mean along with the increase in R_mean (subsubsection 4.2.2) emphasize the MR range limitation and cause the initial decrease, and ultimately, relatively constant MR served demand.

These characteristics can further be observed in the fleet energy as a result of the network size (Figure 1.11b) when operating homogeneous (MR and TR) fleets consisting of 500 aircraft each. The initial discrepancy between MR and TR served demand naturally causes the difference in fleet energy observed in Figure 1.11b. The further similarities between the MR served demand and MR fleet energy trends show the lack of unnecessary deadhead flights and consequently, the validity of the scheduler implemented in the on-demand agent-based simulator. The same can be concluded for the TR fleet, where similarities between the TR served demand Figure 1.11a and TR fleet energy trends (Figure 1.11b) can be observed as well. The jump in fleet energy as a result of the expansion from 25 to 30 vertiports is emphasized compared to the jump in served demand due to the combination of increase in served demand and increase in served trip distance. This is discussed in detail in subsection 4.6.

4.4.2. Value Functions

Following the validity of the agent-based simulator, the system performance measures (subsection 2.4) based on the parameter sweep (Table 1.3) are processed and assessed. Figure 1.12 shows the AAM served demand w.r.t. filtered demand (VF_I) as a result of the number of vertiports in the network, fleet size and fleet composition. In order to serve the highest number of requested trips in a vertiport network consisting of the first five vertiports, a fleet consisting of 240 vehicles and a heterogeneity factor of around 0.7 can be observed. As the network grows, the yellow region can be seen to become smaller and shift to the bottom right, indicating a growing fleet size and decreasing heterogeneity factor. Furthermore, the yellow area around a heterogeneity factor equal to zero for a vertiport network consisting of more than five vertiports, shows that the optimal fleet based on VF_I consists only of tilt-rotor vehicles. This can be attributed to the superior cruise speed, range and passenger capacity of the TR aircraft compared to the MR aircraft.

On the other hand, observing the progression of the blue region, one can see that it remains in the upper left corner, but grows as the vertiport network grows. This is a result of the increasing inability of the multi-rotor aircraft to respond to an increasing number of requested trips due to its limited range of 30 [km]. Figure 1.12 shows the outcomes for the vertiport networks that yield the most significant shifts in the contour plots; readers should consult Appendix B for the outcomes of all assessed vertiport networks.

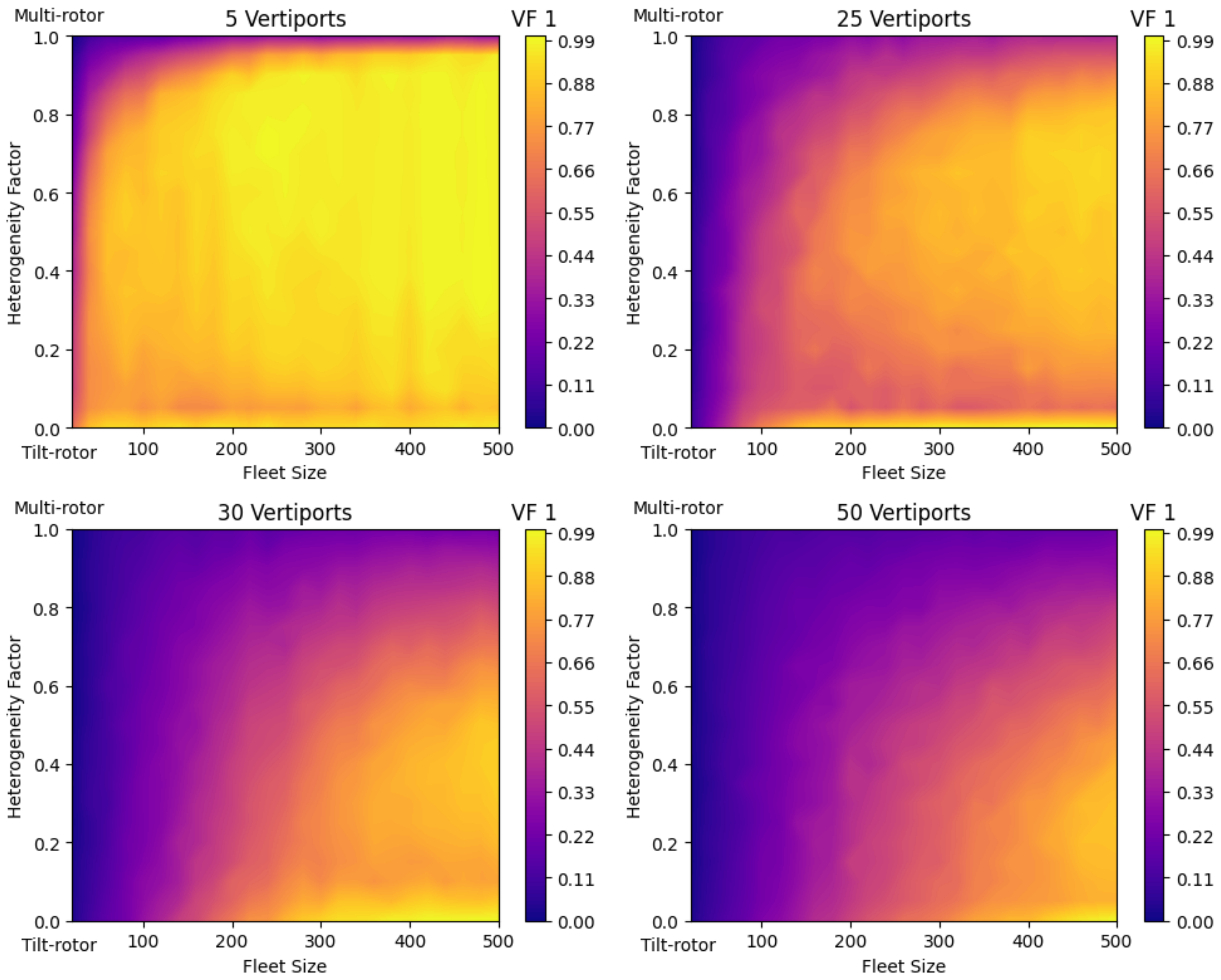

Figure 1.12: VF_I - Ability of the fleet to respond to the filtered demand as a result of the number of vertiports, fleet size and fleet composition

Figure 1.13 shows the inverse of fleet energy (VF_{II}) as a result of the network size and fleet. The yellow regions can be observed at lower fleet sizes and generally, higher heterogeneity factors. This is in line with the fact that a smaller fleet will use a lower total amount of energy. Furthermore, the higher heterogeneity factor represents a fleet consisting of more MR aircraft compared to TR aircraft, which follows the lower overall segment power requirements of the MR aircraft (Figure 1.10) in combination with its inherent inability to serve all requested trips while enabling a shorter trip time (as elaborated upon in subsubsection 4.4.1).

Furthermore, as the network size increases, the yellow region remains at its initially described location, but can be seen to grow in size. This can be attributed to the inability of the MR aircraft to serve increasing number of requested trips, resulting in a decreased number of trips served and consequently, a lower amount of energy used. Ultimately, Figure 1.13 shows that with regards to energy consumption, a smaller fleet consisting of as much MR aircraft is preferred. However, this entails the increasing inability of the transportation system to respond to the requested trips. Figure 1.13 displays the outcomes of the vertiport networks that produce the most notable shifts; readers are encouraged to refer to Appendix B for a complete overview of the results from all evaluated networks.

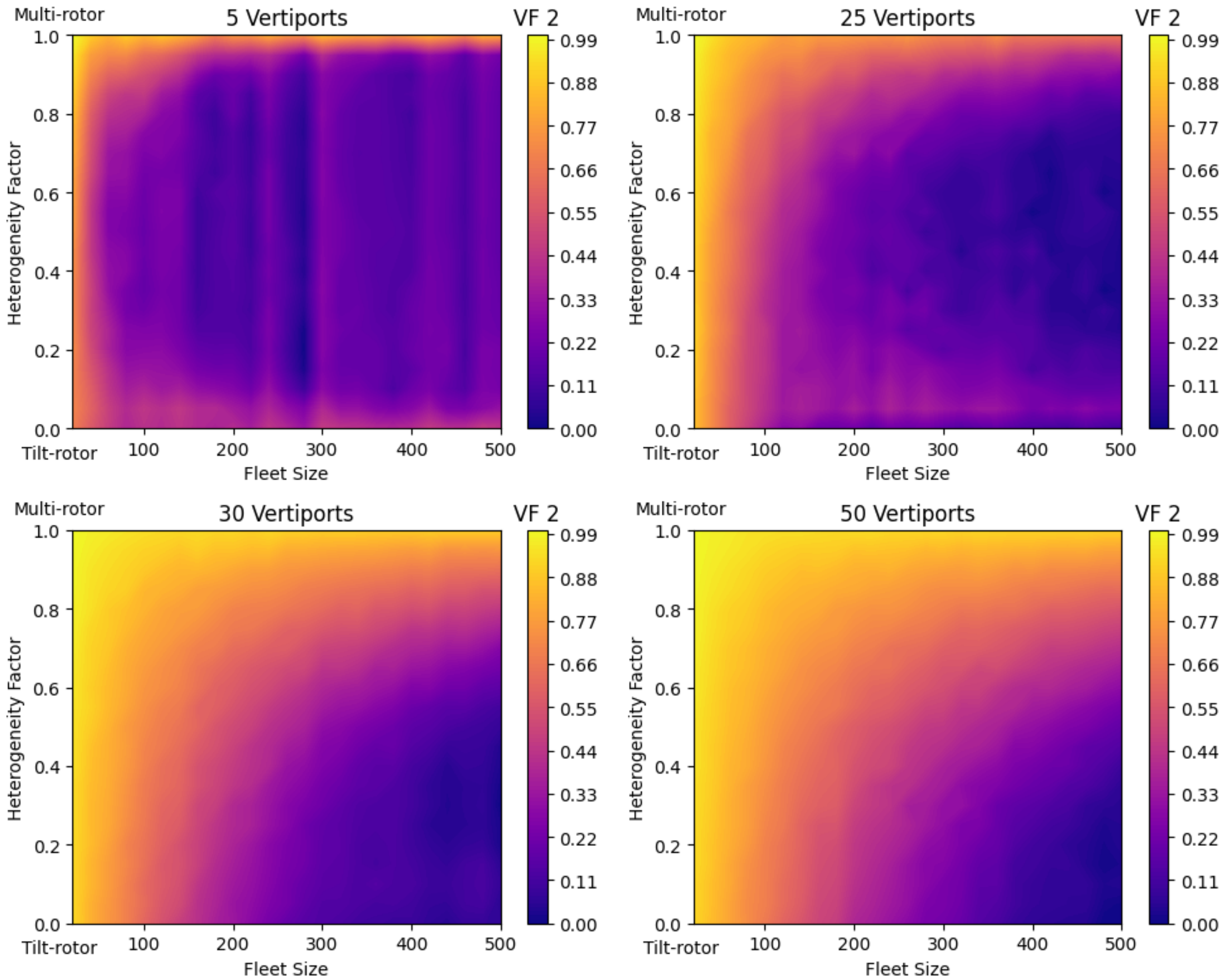

Figure 1.13: VF_{II} - Fleet energy as a result of the number of vertiports, fleet size and fleet composition

The average fleet load factor (VF_{III}) as a result of the vertiport network size and fleet can be observed in Figure 1.14. The optimal fleet (yellow region in contour plot) for the best average load factor can be observed to be composed of mainly multi-rotor (MR, heterogeneity factor around 1.0) aircraft, irrespective of the network size under consideration. This can be attributed to the fact that the passenger capacity of the MR aircraft is limited to one passenger (excl. pilot), resulting in either a load factor of zero (deadhead flight) or one (passenger-carrying flight). Furthermore, multiple yellow regions may be observed and vary depending on the network size under investigation. This translates into multiple local optimum fleet sizes and heterogeneity factors.

On the other hand, the dark blue region indicates the fleet corresponding to the lowest load factor, which is located in the bottom right corner of the graph. This translates into larger fleet sizes and more TR aircraft compared to MR aircraft. As the network expands, the blue region can be seen to dissipate, indicating increasing efficiency and effectiveness. This can be attributed to the filtered demand and average served distance increasing as the network expands. The biggest shift can be observed when expanding the network from 25 to 30 vertiports. This aligns with the connection between the initially separate parts of the network being made (Figure 1.8d and Figure 1.8e), and the jumps in served demand Figure 1.11a and fleet energy (Figure 1.11b).

Overall, the average load factor gives preference to a fleet consisting of a medium to low number of aircraft and a high heterogeneity factor. Figure 1.14 presents the results of the vertiport networks which cause the biggest changes in results; the attention of the reader is directed to Appendix B for the full range of results of the vertiport networks assessed in this study.

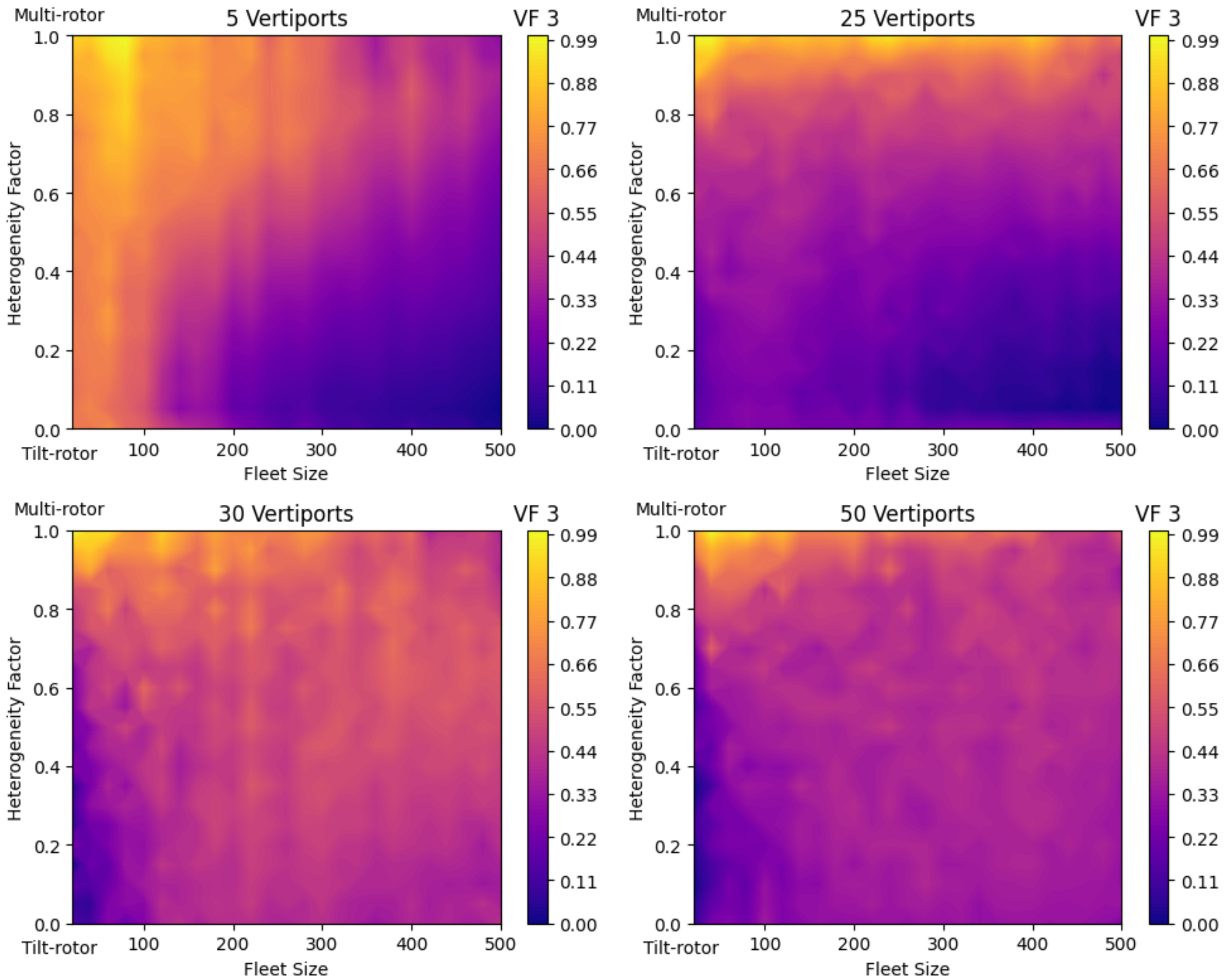

Figure 1.14: VF_{III} - Average fleet load factor as a result of the number of vertiports, fleet size and fleet composition

The last value function pertains the average time saved of trips served (VF_{IV}, Figure 1.15) as a result of the network size, and fleet size and composition. Multiple yellow regions may be observed for networks consisting of 5 to 25 vertiports, indicating the presence of multiple local optimum fleet sizes; the heterogeneity factor for all can be seen to be equal to around 0.05. Once the network reaches a size of 30 vertiports, they seem to dissipate. This may be a result of the 2 separate vertiports networks being connected at this stage and the maximum fleet size assessed in the parameter study being to low to be able to observe the local optima clearly.

Overall, the optimal fleet size can be observed to increase as the network expands. The optimal heterogeneity factor can be seen to be relatively constant around 0.05 for all vertiport networks. Accordingly, the average time saved shows the benefit of a heterogeneous fleet in the case of the NY state vertiport network. However, the superior cruise speed and range of the TR aircraft is reflected in very low heterogeneity factor. Figure 1.15 illustrates the findings for the vertiport networks that exhibit the most pronounced impact on the outcomes; please refer to Appendix B for the complete set of results from all networks evaluated in this study.

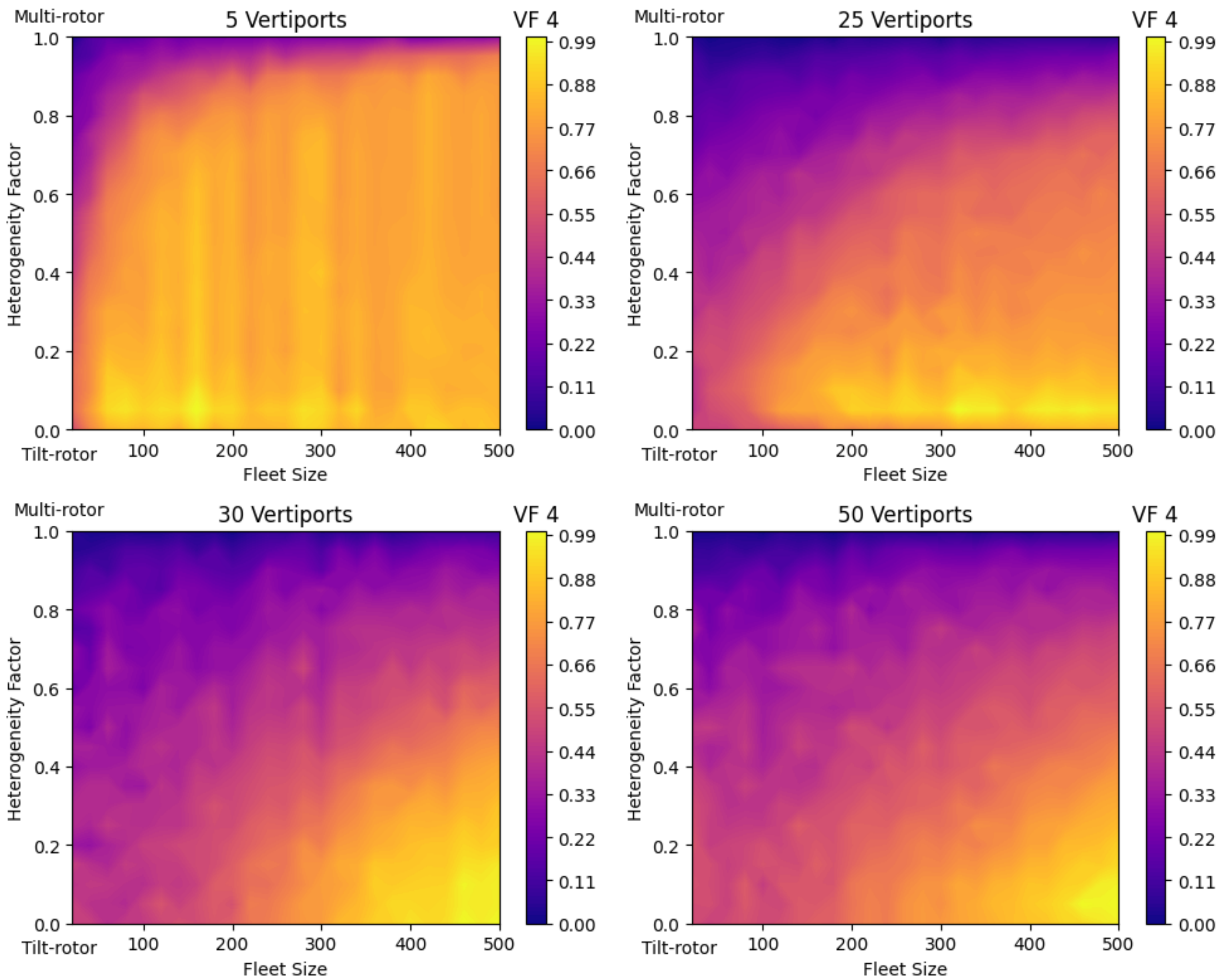

Figure 1.15: VF_{IV} - Average time saved as a result of the number of vertiports, fleet size and fleet composition

4.4.3. Measure of Effectiveness

The value functions presented and discussed in subsubsection 4.4.2 are combined along with their assigned weights (Equation 1.4) to arrive at the Measure of Effectiveness (MoE, Figure 1.16) as a result of the number of vertiports, and fleet size and composition. Overall, the optimal fleet size can be seen to increase as the network expands, whereas the optimal heterogeneity factor is equal to zero, irrespective of the network size under investigation.

The maximum magnitude of the MoE can be seen to decrease as the network grows from 5 to 25 vertiports, indicating a decrease in system performance. This could be a result of the changes in the network and consequently, network distances while not allowing for variations in top level aircraft requirements (TLARs). Further expansion of the network to 30 vertiports causes an increase in maximum MoE and is the point at which the connection between the two separate parts of the network is made (Figure 1.8d to Figure 1.8e). This is followed by further decrease in system performance until the maximum network size assessed in this study. This may be attributed to the limited maximum fleet size (500 aircraft) simulated in this study to serve the AAM transportation system. This is further discussed from a fleet sizing perspective in subsection 4.5. Figure 1.16 presents the outcomes for the vertiport networks that generate the most substantial differences in results; for a comprehensive overview of all evaluated networks, please see Appendix C.

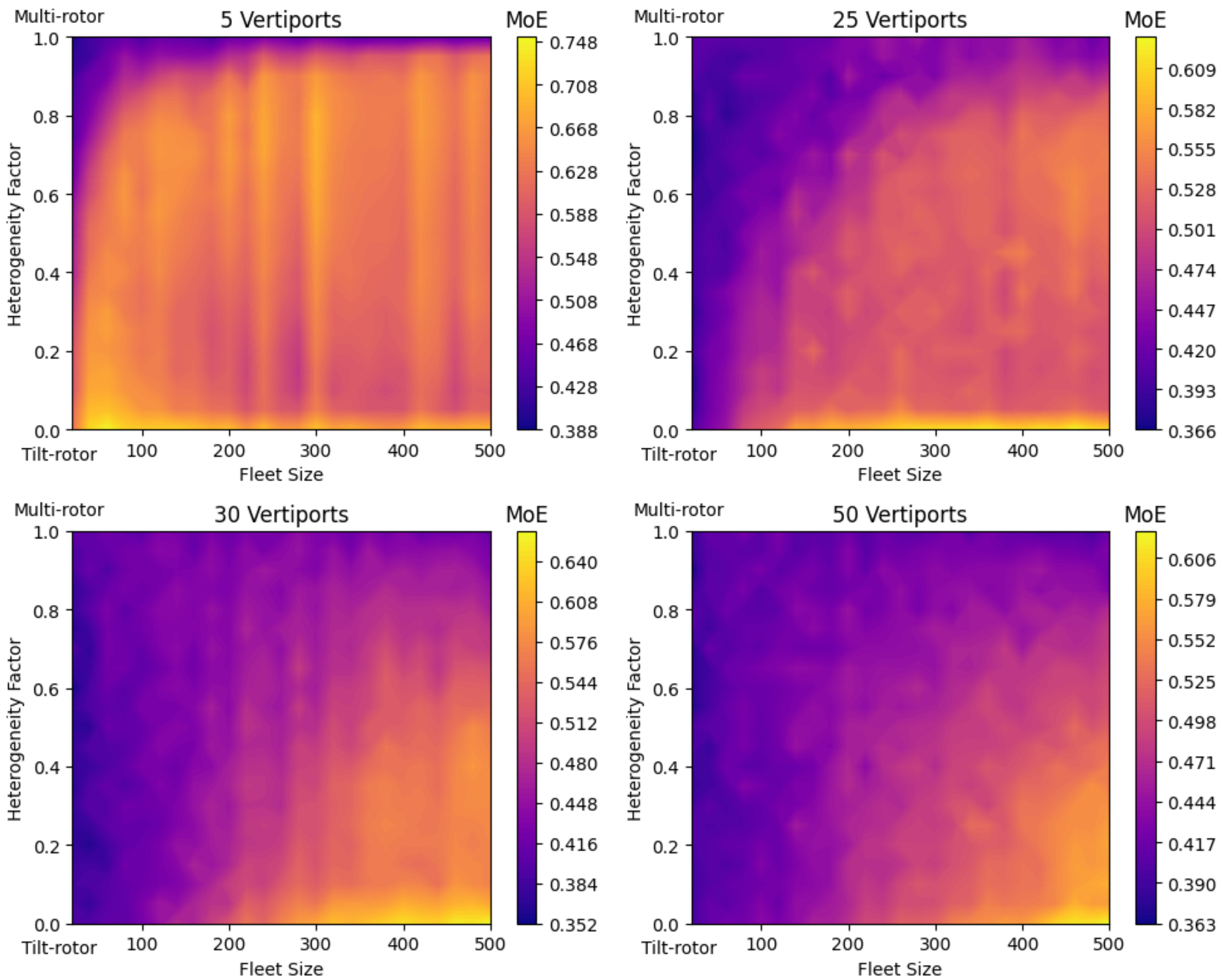

Figure 1.16: Measure of effectiveness (MoE) based on the network size, fleet size and fleet composition.

4.5. Fleet sizing

4.5.1. Optimal fleet

The progressions of optimal fleet size and composition based on each of the value functions (subsection 2.4) as a result of the network size are provided in Figure 1.17a. Looking at the fleet size, one can observe how it behaves rather erratically in the case of VF_{I}, VF_{III} and VF_{IV}. However, the fleet sizes according to VF_{I} and VF_{IV} can be seen to increase overall as the network expands, whereas in case of VF_{III}, the fleet size decreases. VF_{II} causes a constant fleet size of 20 aircraft, irrespective of network size. With regards to the fleet composition, VF_{I} and VF_{IV} give preference to the TR aircraft, and the opposite holds for the optimal heterogeneity factor based on VF_{II} and VF_{III}. In all cases, the heterogeneity factor can be seen to remain relatively constant throughout the vertiport network evolution. The initial heterogeneity factor of 0.7 as a result of VF_{I} (served/filtered demand) shows the benefit of a heterogeneous fleet over a homogeneous fleet.

Based on the MoE as presented in Figure 1.16, the optimal fleet size is determined per vertiport network size and is provided in Figure 1.17b. The optimal fleet size can be observed to increase as the vertiport network grows. This occurs until a vertiport network consisting of 30 vertiports is reached at which point the optimal fleet size becomes equal to the maximum size (500 aircraft) assessed in this study and remains constant. This indicates the need for an expansion of fleet sizes assessed in the parameter sweep. However, the combination of the agent-based simulation runtime and the limited research time have prohibited the inclusion of a higher fleet size within the scope of the research presented here.

One can observe a constant optimal heterogeneity factor equal to zero, irrespective of the vertiport network size. This is in line with the overall findings of VF_I as seen in Figure 1.12, which predominantly drives the MoE given the weight assigned (Equation 1.4). However, even though the heterogeneity factor as a result of VF_I at 5 vertiports is equal to 0.7, the optimal heterogeneity factor is equal to zero. This is a result of the combination of value functions, which cause a superior MoE. As previously elaborated, this can mainly be attributed to the combination of vertiport networks established in NY state and the inability of the MR aircraft to serve the majority of available routes. Furthermore, as the trip distance increases, the higher cruise power requirement of the MR aircraft causes it to become less effective, while the opposite holds for the TR aircaft.

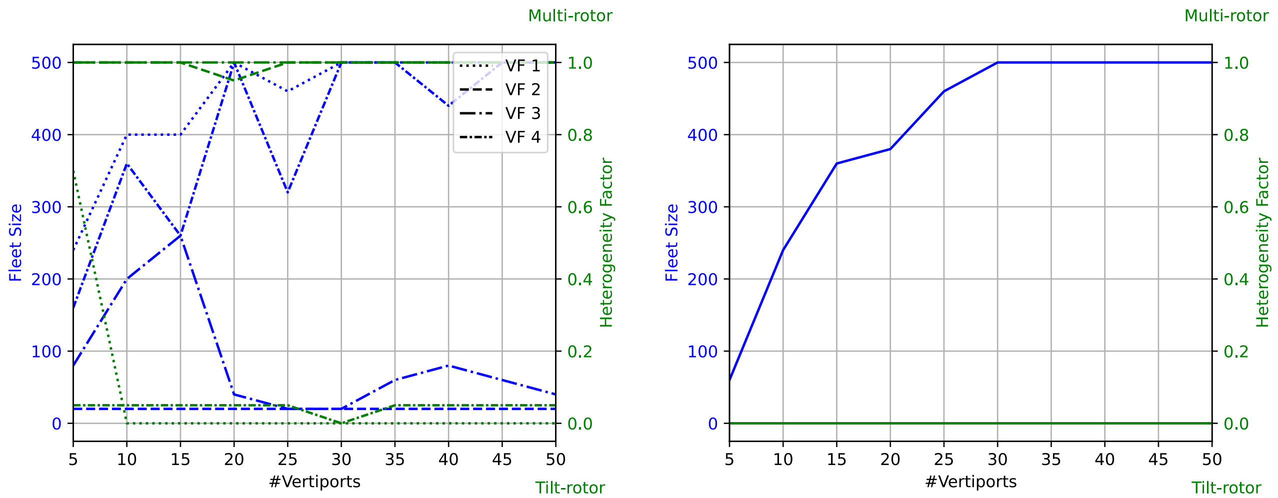

(a) Optimal fleet progression based on each value function (VF) for per network size assessed in this study.

(b) Optimal fleet progression as a result of the Measure of Effectiveness (MoE) for each network size.

4.5.2. Validation

In order to assess the validity of the optimal fleet based on the MoE, the number of revenue and deadhead flights conducted by the homogeneous fleets (500 aircraft each) as well as the optimal fleet are plotted against the AAM network size in Figure 1.18a. Seeing as the optimal fleet is homogeneous, consisting of only TR aircraft, it closely follows and in certain regions, overlaps the homogeneous TR fleet of 500 aircraft. At 5 vertiports, the homogeneous fleets and optimal fleet complete the same number of flights even though the optimal fleet size is significantly smaller than the homogeneous fleet size. Once the vertiport network reaches 10 vertiports, a discrepancy in the number of revenue flights conducted by the optimal fleet and homogeneous fleet can be seen. This is caused by the difference in fleet size between the two as seen in Figure 1.17b. Once the network size reaches 30 vertiports, the optimal and homogeneous TR fleets are the exact same, causing them to overlap.

The number of revenue and deadhead flights completed by the homogeneous MR and TR fleets can be seen to overlap in a network consisting of 5 to 15 vertiports. This is a result of an aircraft being available for the majority of requested flight. Once the network expands to 20 vertiports, major discrepancies can be observed between the number of flights conducted by the homogeneous MR and TR fleets. This is a result of the range limitations of the MR aircraft and can further be observed in the average deadhead and revenue distances of the flights in case of the homogeneous fleets as well as the optimal fleet (Figure 1.18b). The average revenue distance flown by the optimal and the homogeneous TR fleet can be seen to be higher than than that by the homogeneous MR fleet, irrespective of the network size. Furthermore, the average revenue distance in case of the homogeneous MR fleet remains relatively constant throughout the expansions in network size, showing again, the increasing inability of the MR aircraft to serve the demand due to its range limitation.

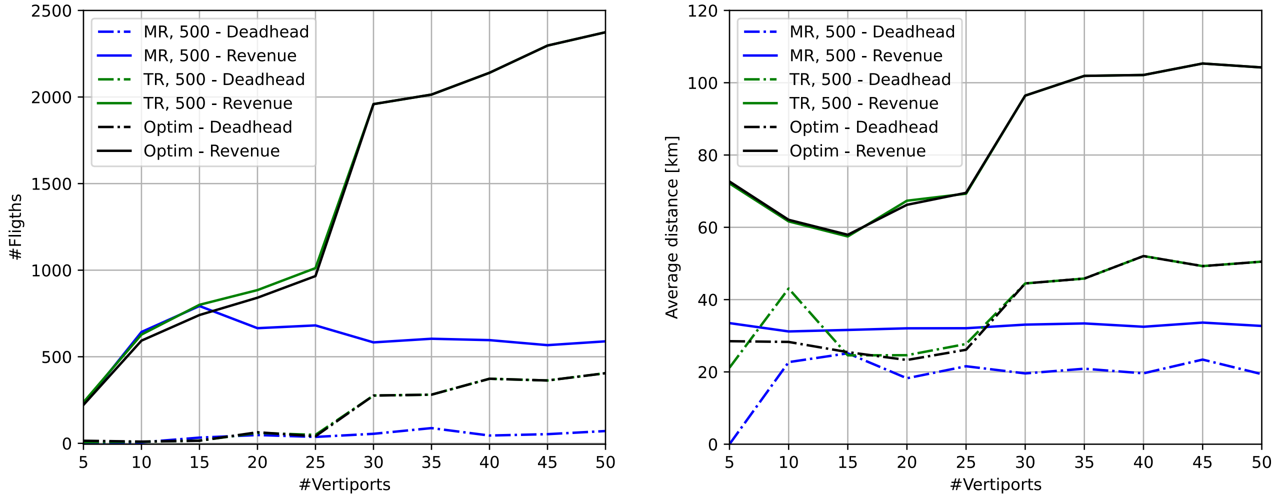

(a) Number of served and deadhead flights vs number of vertiports in the AAM network. Provided for homogeneous fleets consisting of 500 aircraft each as well as the optimal fleet based on maximum MoE.

(b) Average served and deadhead distance vs number of vertiports in the AAM network. Provided for homogeneous fleets consisting of 500 aircraft each as well as the optimal fleet based on maximum MoE.

On the other hand, the homogeneous TR fleet and optimal fleet (in Figure 1.18b) follow the same trends, which again, is a result of the identical heterogeneity factors of both. However, in case of the 5 vertiport network, the average deadhead distance flown by the optimal fleet is higher than that flown by the homogeneous TR fleet. This is a result of the optimal fleet consisting of less aircraft and consequently, the need to redistribute aircraft during operational hours. As the network grown, the average deadhead distance flown by the homogeneous TR fleet is higher or equal to that flown by the optimal fleet, while the average revenue distances are nearly identical. Considering the fact that the optimal fleet contains considerably less aircraft compared to the homogeneous (500 aircraft) TR fleet until the network size reaches 30 vertiports, it can be concluded that the optimal fleet is able to serve the demand in a more efficient manner in comparison.

4.6. Discussion

The framework has been applied to NY state as test case, where the demand has been generated solely based on commutes-to-work. Consequently, the results show that the optimal locations for the introduction of the AAM transportation system are constrained to the NY counties in the NY metropolitan area. This is followed by further expansion within the NY metropolitan area until a separate vertiport network, which connects suburban counties, is formed. As vertiports are added, both vertiport networks are expanded independently, until a state-wide vertiport network is established at 30 vertiports.

The system performance assessment (outlined in subsection 2.4) has shown that even though a heterogeneous fleet consisting of the modelled multi-rotor and tilt-rotor aircraft concepts is possible, a homogeneous fleet consisting of only tilt-rotor aircraft is able to serve the system best overall. This holds for all vertiport networks assessed, and shows a growing trend in fleet size as the vertiport network expands. This can be attributed to the superior range, cruise speed and passenger capacity of the modelled Joby S4 concept over that of the Volocopter Volocity concept.

The results presented in this study are solely based on New York state. Consequently, if one were to apply the framework to another location, inherently different results are expected. Furthermore, the vertiport network has been established based on a minimum distance between 10 and 12 [km]. Making changes to this constant is expected to affect the vertiport network results, and consequently, the system performance results. Decreasing the minimum distance will increase the applicability of the MR aircraft, seeing as its performance improves as the cruise range decreases.

5. Conclusion and future work

This study presented a scalable vertiport allocation plan in conjunction with system-performance-based heterogeneous fleet sizing. The primary interdependencies between operations and vehicle performance are captured through the adoption of a System of Systems (SoS) approach. The framework starts by establishing the ultimate vertiport network using a combination of distance-based agglomerative and k-means clustering algorithm based on a (3-year averaged) commute-to-work origin-destination pairs dataset spanning over a day. This is followed by the iterative commute-distance-based vertiport scoring and elimination procedure, which includes re-distribution of the demand among the available vertiports at every iteration using a K-dimensional tree algorithm. With regard to vehicles, this study modeled existing eVTOL aircraft for the purpose of sizing a heterogeneous fleet based on current-day technology. Finally, a parameter sweep is conducted across the fleet size and composition for each stage of vertiport network growth, and the combinations are inserted into an on-demand agent-based simulator, which models a full day of operations to determine the total system performance. The optimal fleet is then determined based on the overall system performance (measure of effectiveness, MoE) for every vertiport network size assessed in this study.

The NY state test case proved the applicability of the framework in terms of providing initial insights into the correlated growth of the AAM network and the (potentially) heterogeneous fleet to serve it. Overall, this framework serves to provide the applicable stakeholders with a scalable AAM transportation system plan in terms of vertiport allocation and subsequent fleet sizing. The application of this framework to a different location is expected to produce different results, based on inherent differences in demand. Consequently, it is advised to use commuter data which has been accumulated over an extended period and includes all commuter types (i.e. not only commutes to work) for that location. Furthermore, the vertiport locations determined by the vertiport allocator represent the optimal preliminary locations. This is due to the density of existing infrastructure in the majority of urban hubs in the world and the consequential limitations imposed on the precise allocation. Therefore, it is advised to determine suitable vertiport locations by employing a GIS-based approach followed by placement of the vertiports as close to the optimal locations as established by the scalable vertiport allocator.

Ultimately, the framework is capable of assessing the success of the AAM transportation system in any location, and provides a correlated scalable vertiport allocation and fleet sizing plan. Although the framework and test case presented in this study provide crucial insights into the growth of the AAM transportation system, it leaves room for improvements, namely:

1. **Demand:** The test case is based on a static synthetic commute-to-work demand dataset, spanning over a single day.
    - **Population growth:** Optimally, multiple demand datasets are used to account for population growth and relocation over time. This would allow for more precise modelling of growth of the AAM transportation network over time.
    - **Overall demand:** Use a demand dataset which considers various types of demand, not only based on commutes-to-work.
2. **Path planning:** Current version of the framework has included air traffic management and path planning in a very limited manner, namely by assuming a minimum distance between vertiports. Accordingly, there are a number of defining factors which need to be incorporated in order to ensure safe and orderly operation of the AAM transportation system.
    - **Airspace structure and air traffic management:** A number of airspace structure concepts have been developed (e.g. air corridors, flight levels) up to this point. This will greatly affect the way in which air traffic management is developed, and will also play a significant role in the maximum airspace capacity in order to ensure safe operation. As a result, this will not only affect the overall operations side, but more importantly, will play a key factor in each flight path.

- **Noise assessment:** The allowable noise level is expected to vary per location based primarily on legislation. Accordingly, the noise generated by the eVTOL aircraft, and a fleet thereof even more so, can have significant impact on the locations of the vertiports as well as the airspace in which the aircraft may operate (e.g. no-fly zones, low-noise residential areas). This will affect the flight path of each mission as well as the airspace density.
- **Vertiport capacity:** Currently, there are no limitations imposed on the vertiport capacity to park aircraft. Furthermore, a vertiport turnaround time of 15 seconds is assumed in the on-demand agent-based simulation tool. In reality, every vertiport will have a maximum parking capacity and the vertipad turnaround time is expected to vary per flight. This is expected to affect the overall AAM operations, but more importantly, each flight path.

3. **Scalable vertiport allocator:** include a routing step in the commute-distance-based vertiport elimination procedure, which accounts for the maximum range of the vehicles in the fleet for the establishment of multi-leg trips where necessary. In doing so, a more precise estimate of the total commute distance to and from each vertiport may be determined.
4. **Cost analysis:** Current optimal fleet is determined based on the overall system performance metrics, which have an impact on the overall economic aspect of the system, but do not represent the revenue and cost breakdown. Consequently, a system revenue/cost assessment could provide detrimental insights into the ultimate applicability of the AAM transportation system in a location.
5. **TLARs variations:** The optimal fleet is established based on models of existing aircraft concepts, of which the TLARs were kept constant. In order to provide insights into the optimal sizing of the aircraft, it would be beneficial to conduct a parameter sweep across the top-level aircraft requirements and determine the optimal set thereof accordingly per vehicle type and as the network expands.
6. **Multi-modal agent-based simulations:** The research presented here only accounts for car-based trips as alternative transportation method. Furthermore, it also only assesses the missions starting at the departure vertiports. Optimally, this is altered to include a multi-modal agent-based simulation which accounts for all available modes of transportation in the location under consideration. Furthermore, altering the agent-based simulation to simulate the mission from the moment the passenger leaves its origin location until it reaches its destination location, rather from origin vertiport to destination vertiport.

Bibliography

[1] Shiva Prakasha, P., Naeem, N., Ratei, P., and Nagel, B., "Aircraft architecture and fleet assessment framework for urban air mobility using a system of systems approach," Aerospace Science and Technology, Vol. 125, 2022.

[2] Asmer, L., Pak, H., Shivaprakasha, P., Schuchardt, B., Weiand, P., Meller, F., Torens, C., Becker, D., Zhu, C., Schweiger, K., Volkert, A., and Jaksche, R., "Urban Air Mobility Use Cases, Missions and Technology Scenarios for the HorizonUAM Project," 08 2021.

[3] EASA, Prototype technical specifications for the design of VFR vertiports for operation with manned VTOL-capable aircraft certified in the enhanced category, 2022.

[4] Ratei, P., Wagner, M., and Shiva Prakasha, P., Conceptual Aircraft Design and Comparison of different eVTOL Aircraft for Urban Air Mobility, Master's thesis, HAW Hamburg, 2021.

[5] Shiva Prakasha, P., Ratei, P., Naeem, N., Nagel, B., and Bertram, O., "System of Systems Simulation driven Urban Air Mobility Vehicle Design and Fleet Assessment," 08 2021.

[6] Shim, S., Ahn, C., Chang, Y., Cha, W., minho hwang, Park, S., and Shin, S. J., Weight Fraction Estimation for EVTOL Vehicle Sizing, 2023.

[7] Ugwueze, O., Statheros, T., Horri, N., Bromfield, M., and Simo, J., "An Efficient and Robust Sizing Method for eVTOL Aircraft Configurations in Conceptual Design," Aerospace, Vol. 10, 03 2023.

[8] Moradi, N., Wang, C., and Mafakheri, F., "Urban Air Mobility for Last-Mile Transportation: A Review," Vehicles, Vol. 6, No. 3, 2024.

[9] Goyal, R., Reiche, C., Fernando, C., and Cohen, A., "Advanced air mobility: Demand analysis and market potential of the airport shuttle and air taxi markets," Sustainability (Switzerland), Vol. 13, No. 13, 2021.

[10] Brunelli, M., Ditta, C. C., and Postorino, M. N., "New infrastructures for Urban Air Mobility systems: A systematic review on vertiport location and capacity," Journal of Air Transport Management, Vol. 112, 2023.

[11] Feldhoff, E. and Soares Roque, G., "Determining infrastructure requirements for an air taxi service at Cologne Bonn Airport," CEAS Aeronautical Journal, Vol. 12, No. 4, 2021, pp. 821 – 833.

[12] Antcliff, K. R., Moore, M. D., and Goodrich, K. H., "Silicon valley as an early adopter for on-demand civil VTOL operations," American Institute of Aeronautics and Astronautics Inc, AIAA, 2016.

[13] Otte, T., Metzner, N., Lipp, J., Schwienhorst, M. S., Solvay, A. F., and Meisen, T., "User-centered integration of automated air mobility into urban transportation networks," Vol. 2018-September, Institute of Electrical and Electronics Engineers Inc., 2018.

[14] Delgado González, C. J., Rooftop-place suitability analysis for urban air mobility Hubs: A GIS and neural network approach, Master's thesis, Universidade Nova de Lisboa, 2020.

[15] Fadhil, D. N., Rothfeld, R., and Moeckel, R., A GIS-based Analysis for Selecting Ground Infrastructure Locations for Urban Air Mobility, Master's thesis, Technical University of Munich, 2018.

[16] Kim, N. and Yoon, Y., "Regionalization for urban air mobility application with analyses of 3D urban space and geodemography in San Francisco and New York," Procedia Computer Science, Vol. 184, 2021, pp. 388–395.

[17] Lim, E. and Hwang, H., "The Selection of Vertiport Location for On-Demand Mobility and Its Application to Seoul Metro Area," International Journal of Aeronautical and Space Sciences, Vol. 20, No. 1, 2019, pp. 260 – 272.

[18] Jeong, J., So, M., and Hwang, H.-Y., "Selection of Vertiports Using K-Means Algorithm and Noise Analyses for Urban Air Mobility (UAM) in the Seoul Metropolitan Area," Applied Sciences, Vol. 11, No. 12, 2021.

[19] Rajendran, S. and Zack, J., "Insights on strategic air taxi network infrastructure locations using an iterative constrained clustering approach," Transportation Research Part E: Logistics and Transportation Review, Vol. 128, 2019, pp. 470–505.

[20] Sinha, A. A. and Rajendran, S., "A novel two-phase location analytics model for determining operating station locations of emerging air taxi services," Decision Analytics Journal, Vol. 2, 2022.

[21] Arellano, S. I., Moeckel, R., and Rothfeld, R., A Data- and Demand-Based Approach at Identifying Accessible Locations for Urban Air Mobility Stations, Master's thesis, Technical University of Munich, 2020.

[22] Daskilewicz, M. J., German, B., Warren, M., Garrow, L. A., Boddupalli, S., and Douthat, T., "Progress in vertiport placement and estimating aircraft range requirements for evtol daily commuting," 2018 Aviation Technology, Integration, and Operations Conference, 2018.

[23] Chen, L., Wandelt, S., Dai, W., and Sun, X., "Scalable Vertiport Hub Location Selection for Air Taxi Operations in a Metropolitan Region," INFORMS Journal on Computing, Vol. 34, 11 2021.

[24] Rath, S. and Chow, J. Y., "Air taxi skyport location problem with single-allocation choice-constrained elastic demand for airport access," Journal of Air Transport Management, Vol. 105, 2022.

[25] Zhang, J., Liu, Y., and Zheng, Y., "Overall eVTOL aircraft design for urban air mobility," Green Energy and Intelligent Transportation, Vol. 3, No. 2, 2024.

[26] Ratei, P., Naeem, N., and Prakasha, P. S., "Development of an urban air mobility vehicle family concept by system of systems aircraft design and assessment," Journal of Physics: Conference Series, Vol. 2526, No. 1, jun 2023.

[27] Manning, C. D., Raghavan, P., and Schütze, H., Introduction to Information Retrieval, Cambridge University Press, Cambridge, UK, 2008.

[28] NYSDOT, Office of Policy, Planning Performance, "A Journey to Work (JTW) flow comparison report," Census Bureau for the Transportation Community, 10 2010, Accessed on 23 September 2024.

[29] U. S. Census Bureau, "Ttime Leaving Home to Go to Work," U.S. Census Bureau, Accessed on 18 October 2024.

[30] Bureau], U. C., "US County Boundaries," U.S. Census Bureau, 04 2017, Accessed on 05 October 2024.

[31] Boscoe, F. P., Henry, K. A., and Zdeb, M. S., "A nationwide comparison of driving distance versus straight-line distance to hospitals," The Professional Geographer, Vol. 64, No. 2, 2012, pp. 188–196.

[32] Bacchini, A. and Cestino, E., "Electric VTOL Configurations Comparison," Aerospace, Vol. 6, 02 2019.

[33] Wang, S., Lima Pereira, L. T., and Ragni, D., "A preliminary design exploration of UAM vehicles," 03 2024.

[34] Arora, J. S., Introduction to Optimum Design, chap. Chapter 17 - Multi-objective Optimum Design Concepts and Methods, Academic Press: Boston, 2012.

[35] Ahmed, S. S., Fountas, G., Eker, U., Still, S. E., and Anastasopoulos, P. C., "An exploratory empirical analysis of willingness to hire and pay for flying taxis and shared flying car services," Journal of Air Transport Management, Vol. 90, 2021.

[36] Ilahi, A., Belgiawan, P. F., Balac, M., and Axhausen, K. W., "Understanding travel and mode choice with emerging modes; a pooled SP and RP model in Greater Jakarta, Indonesia," Transportation Research Part A: Policy and Practice, Vol. 150, 2021.

Appendix A - Vertiport locations

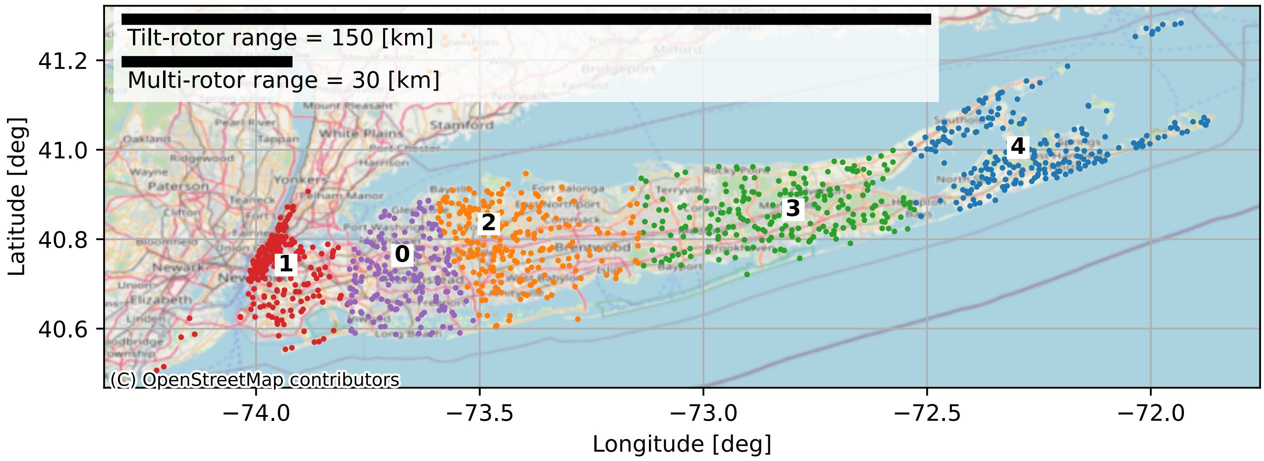

(a) 5 Vertiport network

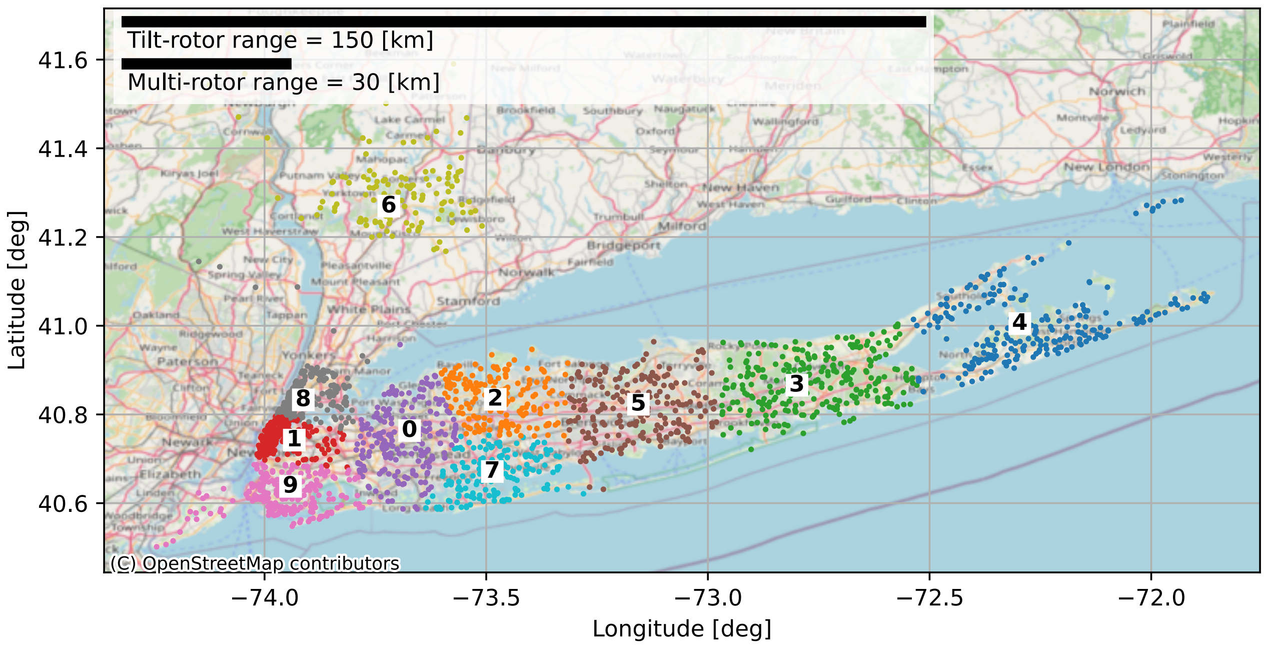

(b) 10 Vertiport network

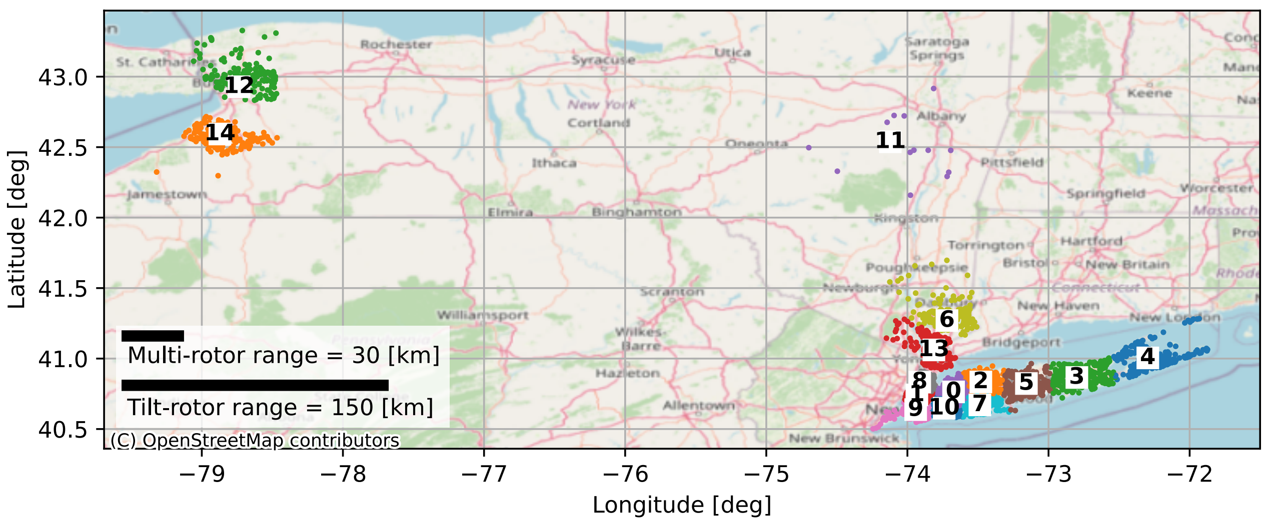

(c) 15 Vertiport network

Figure 1.19: Vertiport locations and filtered demand as a result of varying number of vertiports.

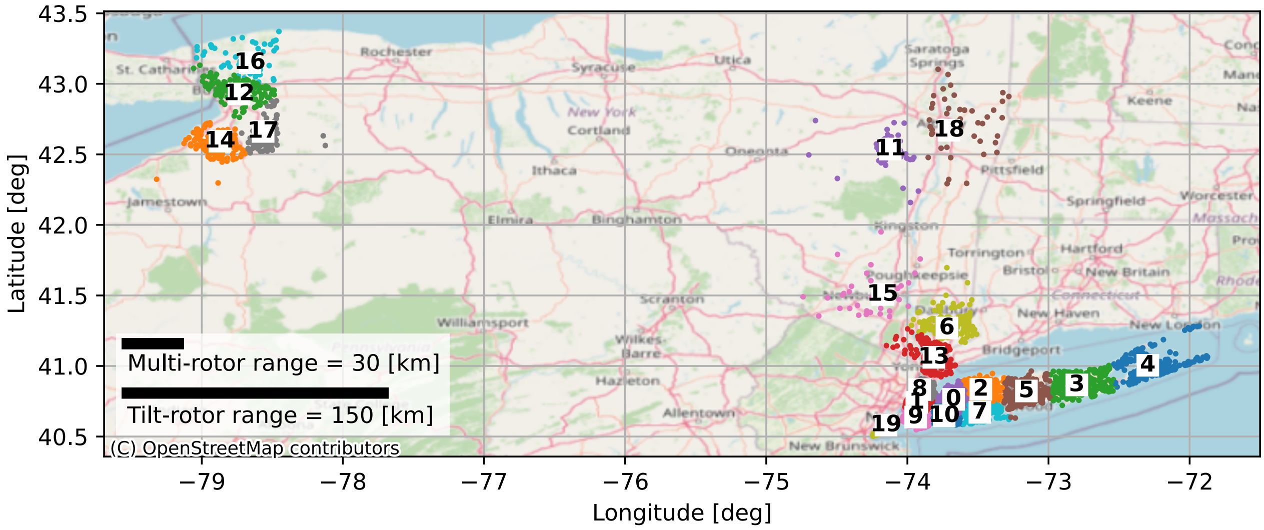

(d) 20 Vertiport network

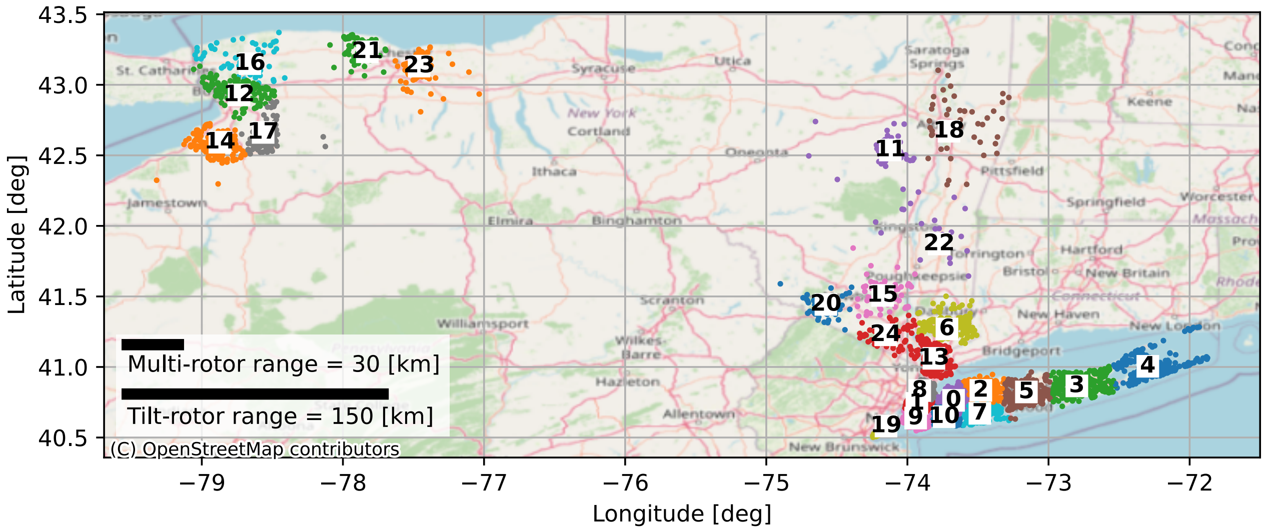

(e) 25 Vertiport network

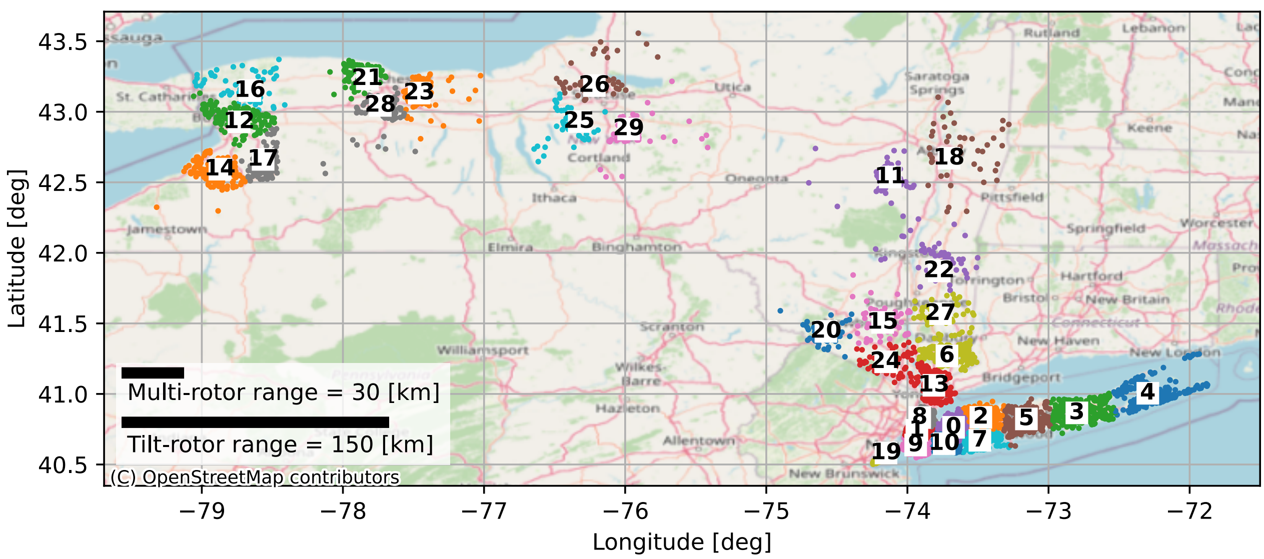

(f) 30 Vertiport network

Figure 1.19: Vertiport locations and filtered demand as a result of varying number of vertiports.

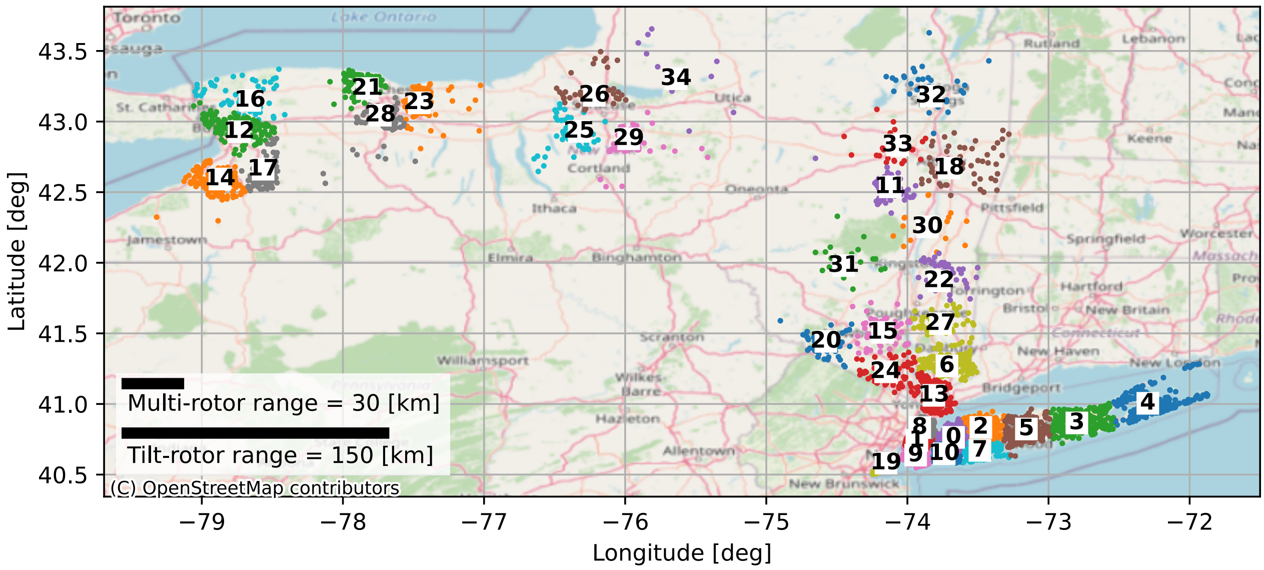

(g) 35 Vertiport network

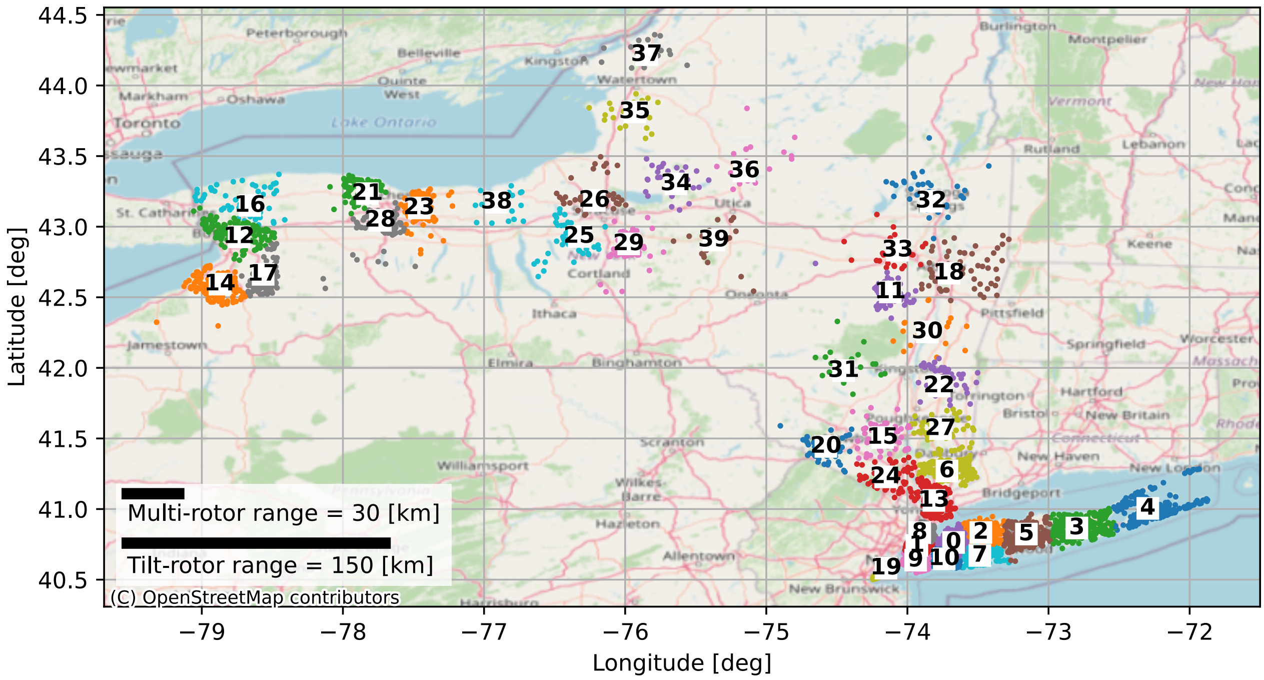

(h) 40 Vertiport network

Figure 1.19: Vertiport locations and filtered demand as a result of the number of vertiports in the AAM network.

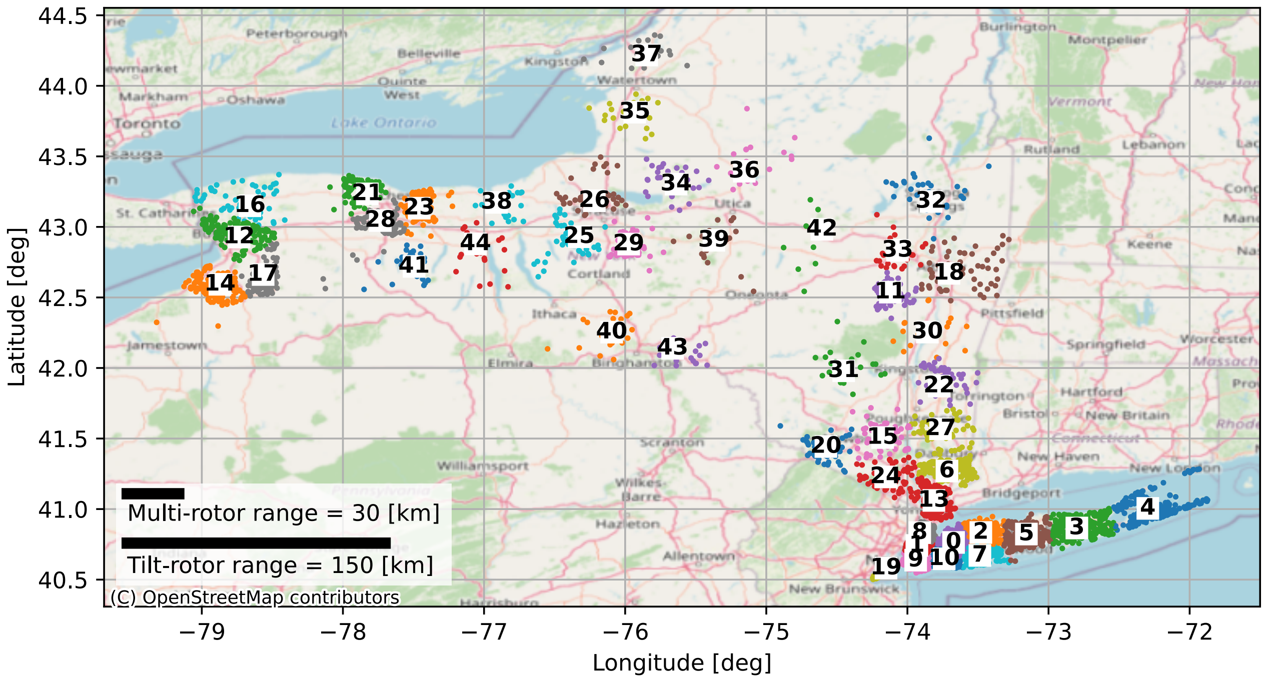

(i) 45 Vertiport network

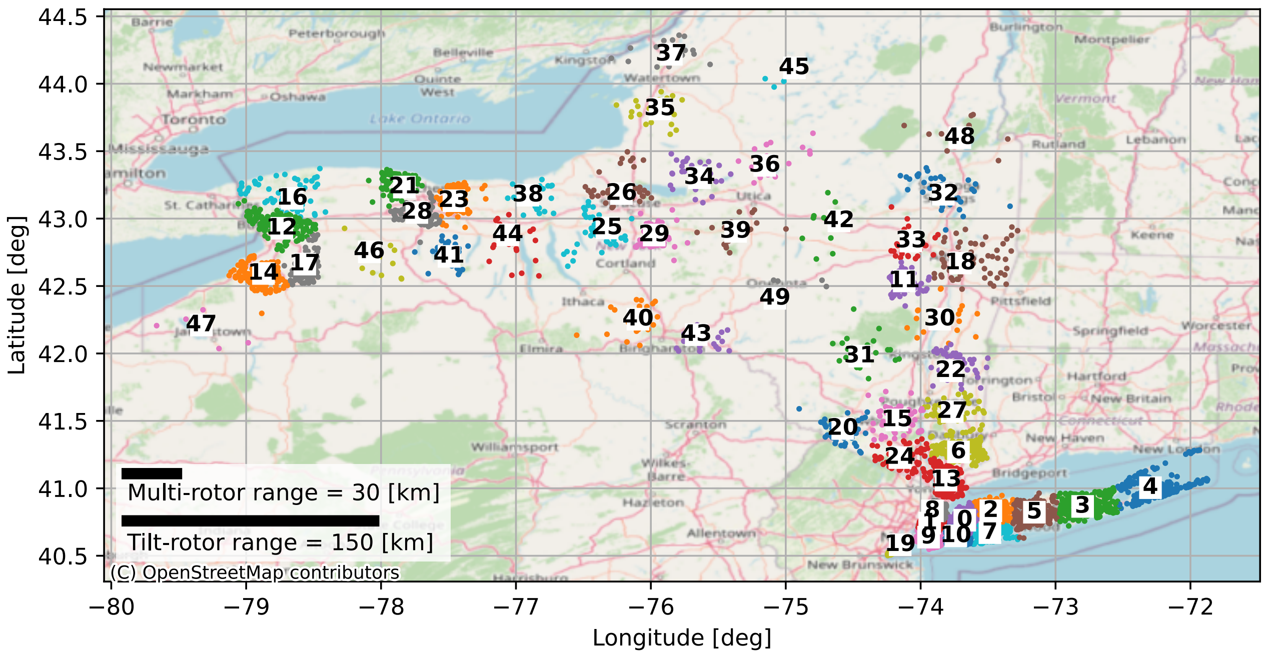

(j) 50 Vertiport network

Figure 1.19: Vertiport locations and filtered demand as a result of the number of vertiports in the AAM network.

Table 1.6: Longitude (Lon.) and Latitude (Lat.) of the largest vertiport network assessed in this study.

Vertiport label	**Lon.** [°]	**Lat.** [°]	**Vertiport label**	**Lon.** [°]	**Lat.** [°]	**Vertiport label**	**Lon.** [°]	**Lat.** [°]
0	-73.6729	40.7635	17	-78.5654	42.6626	34	-75.6389	43.3033
1	-73.9329	40.7421	18	-73.7055	42.6707	35	-75.9321	43.8132
2	-73.4796	40.8341	19	-74.1515	40.5817	36	-75.1556	43.3945
3	-72.7992	40.8658	20	-74.5776	41.4435	37	-75.8479	44.2183
4	-72.2964	41.0048	21	-77.8272	43.2340	38	-76.9113	43.1737
5	-73.1568	40.8230	22	-73.7752	41.8718	39	-75.3716	42.9050
6	-73.7198	41.2695	23	-77.4599	43.1326	40	-76.0956	42.2540
7	-73.4863	40.6713	24	-74.1540	41.2280	41	-77.4960	42.7198
8	-73.9126	40.8329	25	-76.3259	42.9305	42	-74.6057	42.9830
9	-73.9414	40.6379	26	-76.2183	43.1856	43	-75.6636	42.1397
10	-73.7393	40.6477	27	-73.7655	41.5687	44	-77.0606	42.8796
11	-74.1213	42.5378	28	-77.7349	43.0451	45	-74.9363	44.1173
12	-78.7357	42.9284	29	-75.9752	42.8783	46	-78.0873	42.7534
13	-73.8124	41.0613	30	-73.8588	42.2546	47	-79.3323	42.2107
14	-78.8717	42.5932	31	-74.4515	41.9802	48	-73.7093	43.6003
15	-74.1755	41.5071	32	-73.8318	43.1805	49	-75.0802	42.4087
16	-78.6589	43.1499	33	-74.0701	42.8336			

Appendix B - Value Functions

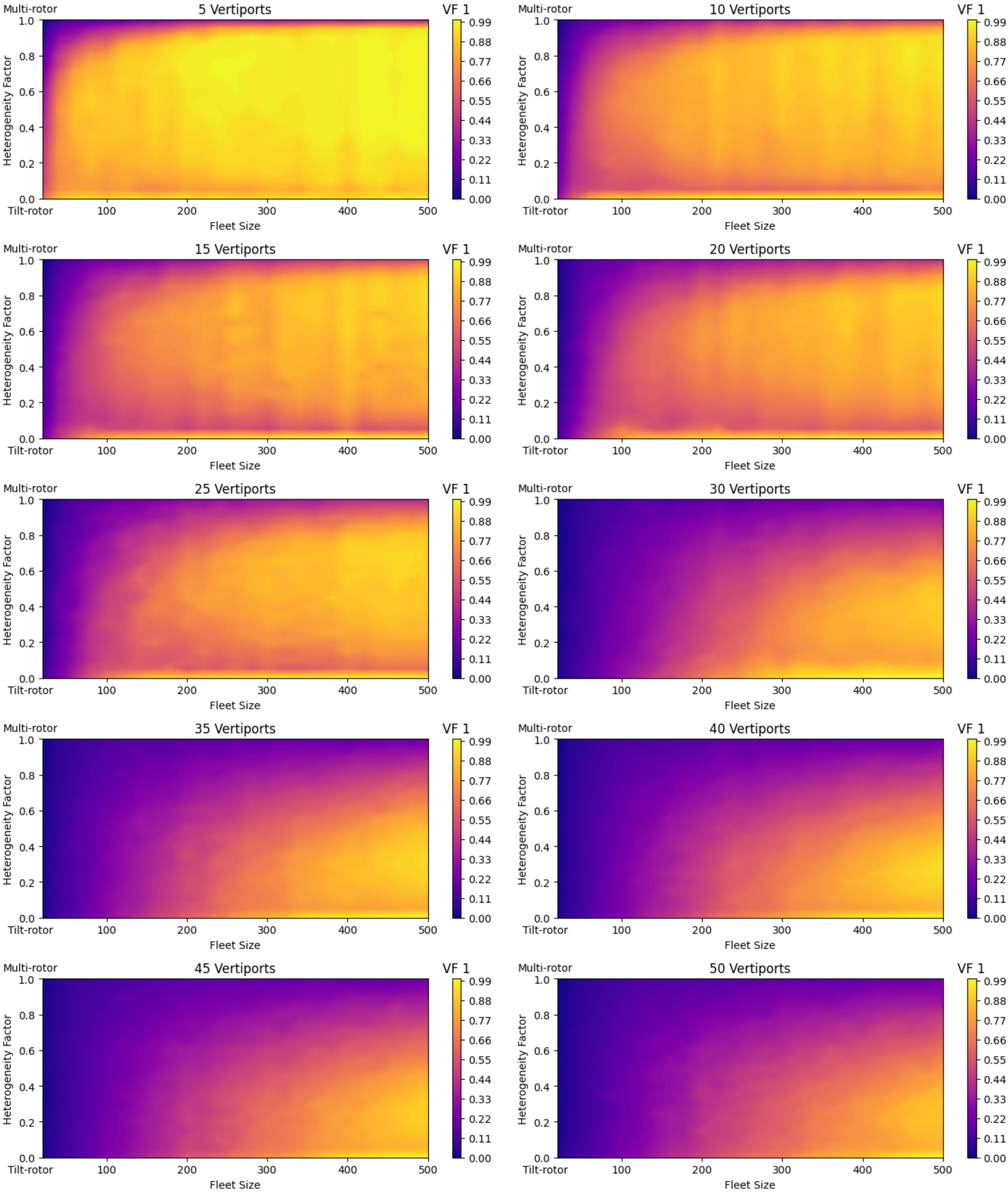

Figure 1.20: VF$_I$ - Served demand/Filtered demand as a result of number of vertiports and fleet

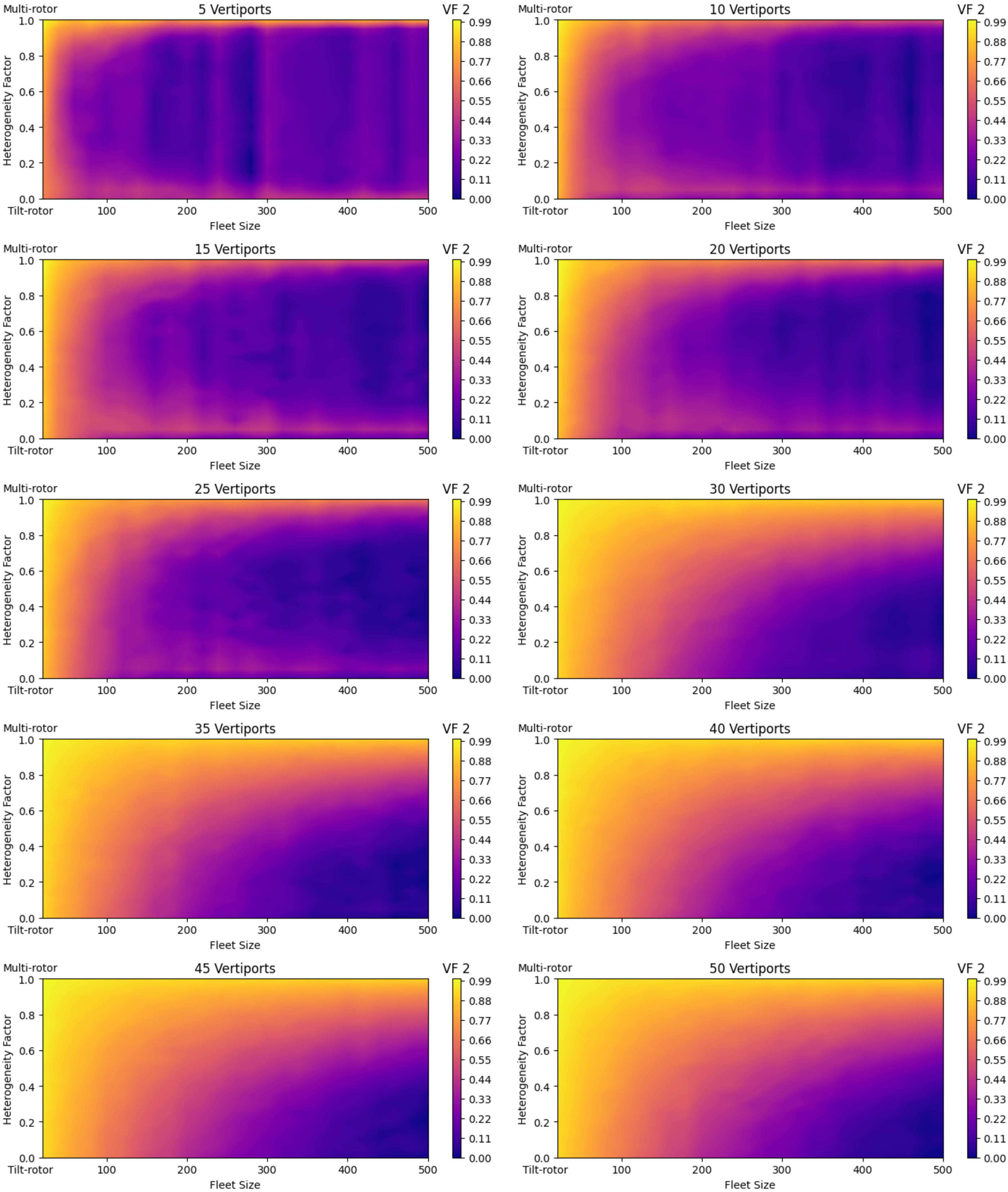

Figure 1.21: VF_{II} - Inverse fleet energy as a result of number of vertiports and fleet

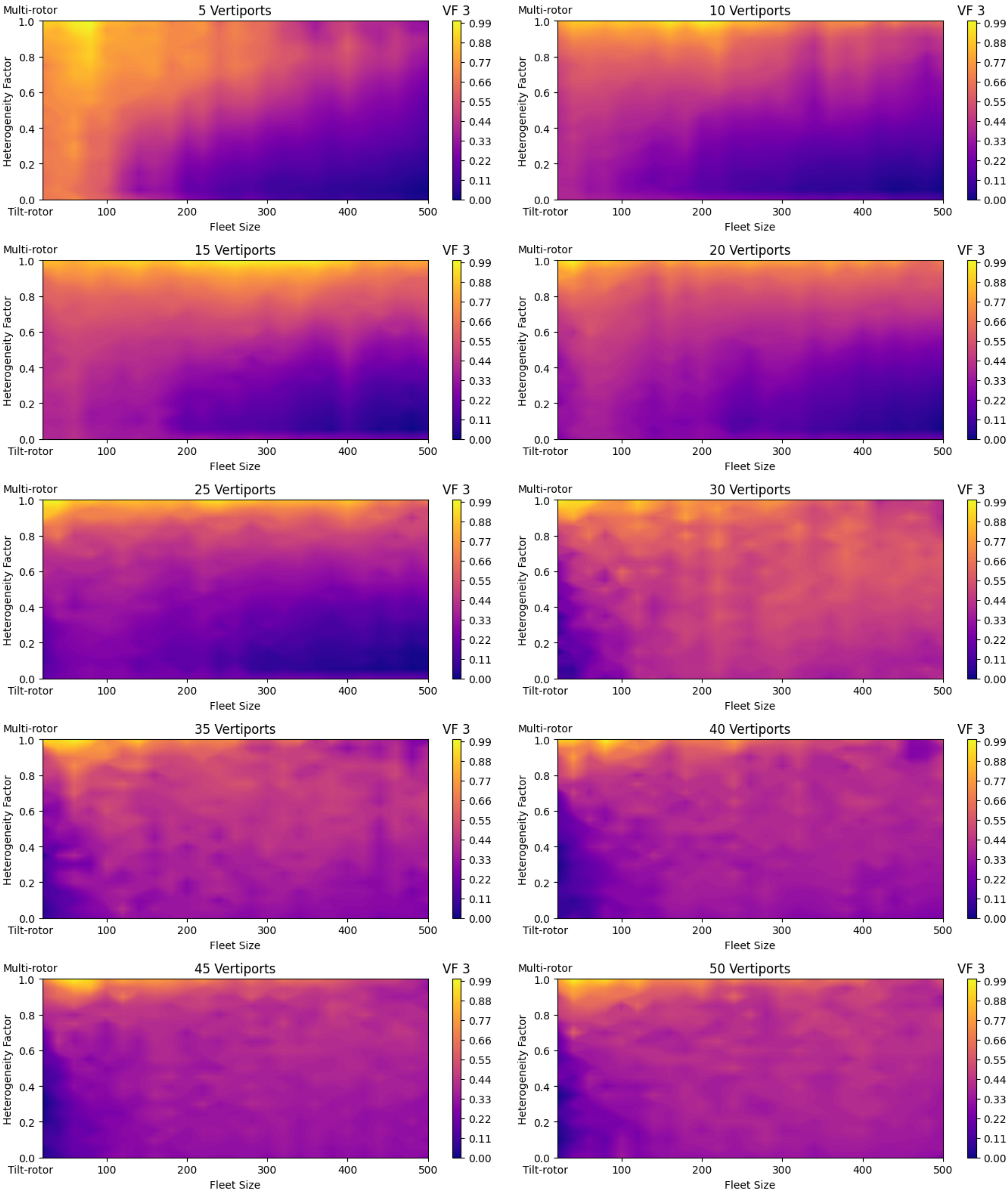

Figure 1.22: VF_{III} - Average load factor as a result of number of vertiports and fleet

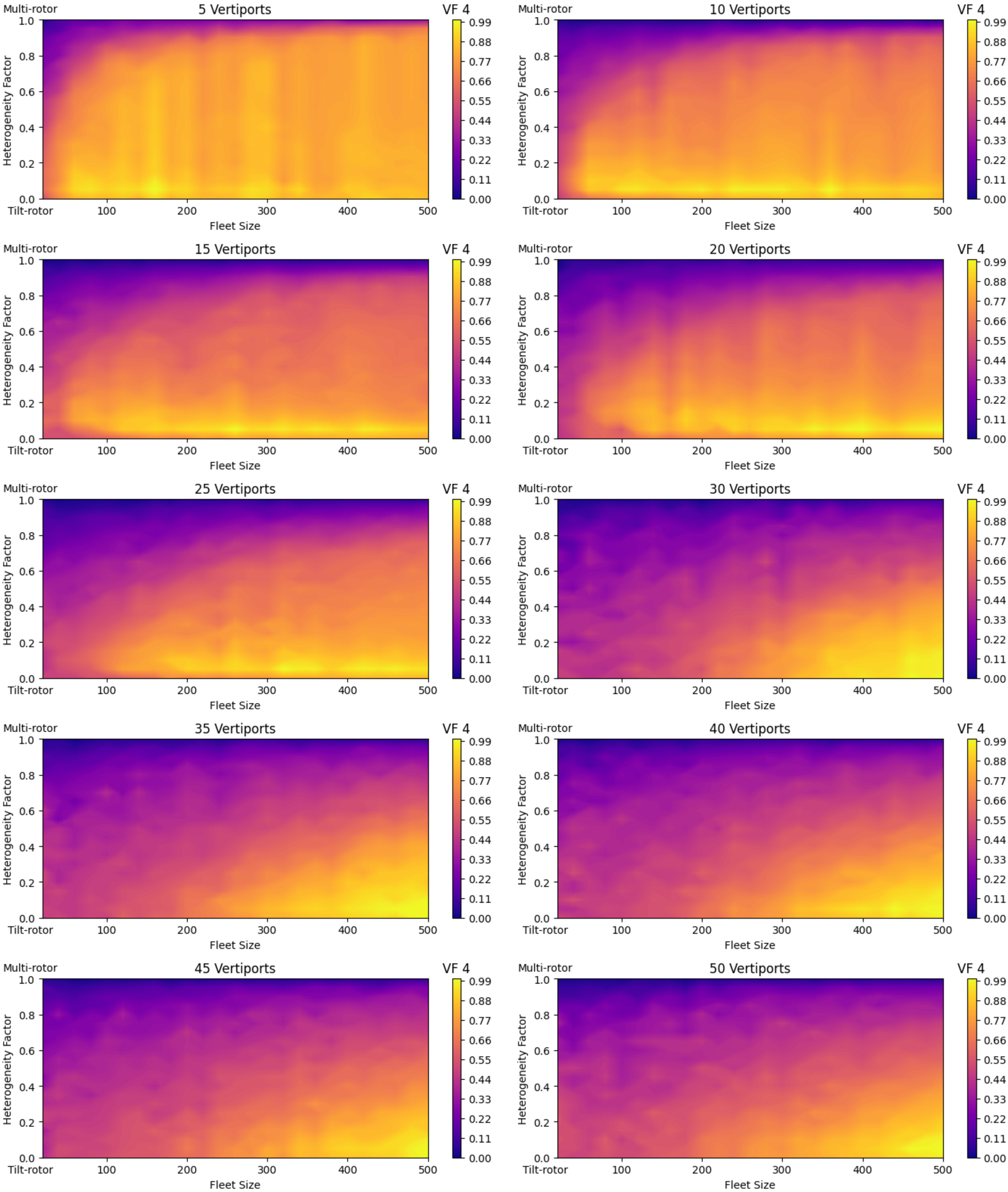

Figure 1.23: VF_{IV} - Average time saved as a result of number of vertiports and fleet

Appendix C - Measure of Effectiveness

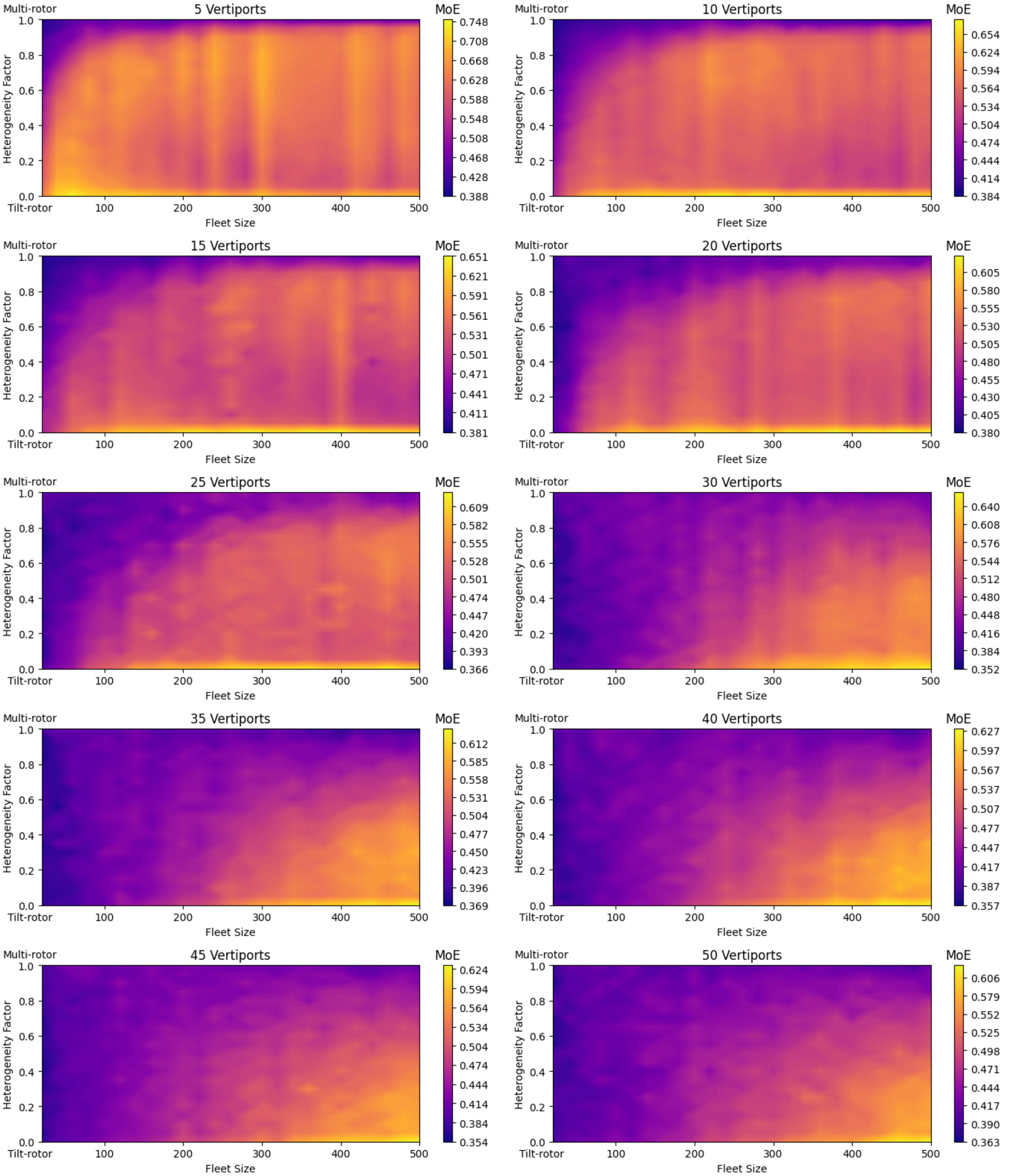

Figure 1.24: MoE - AAM transportation system measure of effectiveness as a result of number of vertiports and fleet

2

Literature review

1. Introduction and Relevance

Advanced Air Mobility (AAM), also known as Innovative Air Mobility (IAM) is a new transportation market which has not yet entered into service, but is gaining increasing amounts of attention from the various stakeholders involved [1, 2]. The motivation behind this increase in attention comes from multiple directions, namely, the need to improve door-to-door mobility travel times [3], increasingly constricting regulations on carbon emissions, and the alleviation of traffic congestion. The birth of this market has been enabled through major advancements in technology in various fields e.g. distributed propulsion, electric powertrains, battery technology, traffic management, artificial intelligence.

As opposed to conventional aviation, in which the airspace density is comparatively low, the AAM market introduces a new operational scenario in which small aircraft will be operating on a large scale within a relatively confined airspace. Apart from aggravating the load on traffic management, this increases the complexity of the system substantially and emphasises the interdependencies between the various components of the system (e.g. aircraft performance and sizing, traffic management, vertiport operations and allocation). Furthermore, due to the electric nature of the aircraft, the importance of efficiently designing and sizing it, and developing the network it is to serve, are accentuated. Apart from the complexity, this provides an indication of the vastness of the research field, which can be segmented into the vehicle side and the operations side.

Even though the distinction between studies focusing on the vehicle or operations side can be made, the operations side is highly dependent on the performance and sizing of the aircraft, and vice versa. For example, aircraft sizing is based on the top level aircraft requirements (TLARs). The TLARs are generally a result of a market analysis, more specifically, customer demand and details on the trips to be served. On the other hand, operational aspects are in part determined, or rather, constrained by the aircraft size and performance capabilities. As a result, one is unable to derive detrimental conclusions about sizing of the aircraft and operations within the emerging AAM market without the use of an integrated framework.

Accordingly, this review starts by introducing studies in which AAM frameworks have been developed in section 2 for a number of objectives. The frameworks encompass the operations side as well as the vehicle side to draw relevant conclusions. In order to make a top-level system assessment, generally multiple aspects on the operations side are linked to one another within these frameworks. As such, to gain an understanding of the complexity and interdependencies, an overview of the most relevant operational components is provided in section 3. Furthermore, in order to get awareness of aircraft sizing and performance, and the connection to the operations side, an overview of the most important aspects pertaining the aircraft are covered in section 4. Finally, the research gap and consequently, the research objective are provided in section 5 and 6, respectively.

2. Assessment frameworks

The operations and vehicle side of AAM truly come together in studies regarding assessment frameworks, which focus on various overall system level aspects [4, 5]. On the operations side, the frameworks commonly encompass an analysis of the demand to be served (subsection 3.1), the allocation of vertiports (subsection 3.2) and aspects related to traffic management (subsection 3.3). Furthermore, the frameworks generally include a vehicle sizing module to determine the vehicle performance characteristics and operational constraints. The two sides are then coupled in an agent-based or scheduled simulation, over an extended period of time. Consequently, performance of the system based on the framework inputs (specific operational scenario and initial vehicle size) are established. Evidently, these frameworks follow a feed-forward process. Thus, in order to observe the effect of various operational and vehicle parameters on the performance of the transportation system, a sensitivity analysis in which relevant parameters are varied, is usually conducted.

Fu et al. [4] established five operational scenarios in which the fleet size, available technologies, infrastructure placement and pricing strategies were varied. They fed these into an agent-based simulation implemented in MATSim [1] with the goal to analyse the potential demand of UAM. Their results show that the system configuration greatly impacts the UAM demand; infrastructure capacity and fleet size were identified to be the main bottlenecks. Furthermore, even though peak hours and trips up to 20km created high levels of demand, the modal share of UAM in none of the operational scenarios caused an alleviation of ground-based congestion.

Shiva Prakasha et al. [5] developed a framework (see Figure 1) to assess the aircraft architecture and the fleet size. Even though Figure 1 shows a feedback step from the System of Systems (SoS) agent-based simulation back to the aircraft design optimization module is not included in the framework ultimately used. Consequently, they varied an array of operational and vehicle parameters (provided in Table 1) and ultimately analysed approximately 5,000 design points in the design exploration. Overall, their results show 'the complex interaction between UAM aircraft architectures, technology assumptions, fleet operations, agent dispatching logic, and UAM throughput' [5].

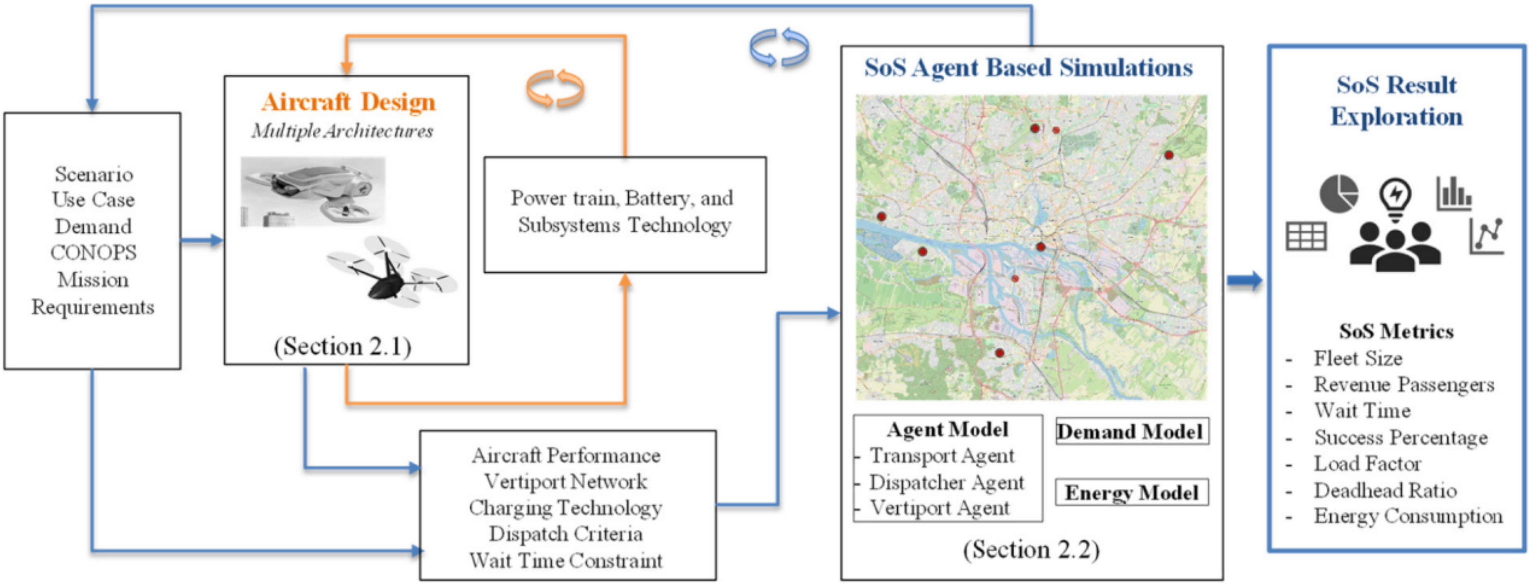

Figure 1: System of systems (SoS) framework developed by Shiva Prakasha et al. [5].

Table 1: Inputs for the design of experiments by Shiva Prakasha et al.[5]

Parameter	**Count**	**Specific design point(s)**
Scenario	2	Near-term, Far-term
Sizing mission	2	Single-flight, multi-flight
Aircraft architecture	4	Multirotor, compound helicopter, lift+cruise, tilt-rotor
Cruise speed, m/s	3	20, 40, 55
Passenger capacity	2	2, 4
Charging power	3	250, 500, 1000
Passenger demand	2	Low (max. 24/h), high (max. 48/h)
Fleet size	9	12, 18, 24, 30, 36, 42, 48, 54, 60
Vertiport capacity	1	100 (unlimited)

Escribano Macias et al. [6] developed a framework which contains a feedback loop between a vertiport placement model, an aircraft sizing model, and a vertiport infrastructure model. This was done with the

[1] Agent-based simulation software MATSim: `https://matsim.org/install/` [accessed on 08/08/2024]

purpose of solving the vertiport allocation problem, and the objective to minimise the total cost of the system and maximise the total travel time savings. The vehicle sizing model assumed an aircraft structural mass of 50%, and a combined payload and battery mass of 50% of the maximum take-off mass [7]. By doing so, only the battery size and passenger capacity were affected throughout the simulation. Furthermore, the study maintained the number of vertiports at a fixed value, and varied the number of take-off and landing pads, and charging pads to determine the optimal operational configuration.

To summarise, the frameworks provide valuable insights into the complexity of the AAM transportation system and prove the importance of a holistic approach when conducting research in the field of AAM. They generally account for a wide range of operational aspects, but do so for a specific operational scenario and based on a defined number of vertiports. On one hand, the frameworks fail to incorporate the sequential allocation of vertiports as to mimic the growth of the AAM network over time. Furthermore, apart from the framework developed by Escribano Macias et al. [6], which contains a feedback loop between the operations side and vehicle side, the frameworks are based on a feed-forward process. Thus, on the other hand, the vehicle sizing model by Escribano Macias et al. [6] can be expanded, or the intended feedback step (from the SoS agent-based simulation to the vehicle sizing module) as seen in Figure 1 can be established. To better understand the importance and effects of the relevant components on the operations side, an overview thereof is provided in section 3.

3. Operations

The AAM market can be segmented into Urban Air Mobility (UAM) and Regional Air Mobility (RAM), where the difference lies in the ranges of the trips to be served. Furthermore, multiple fields of use cases have been identified within the AAM market. The most prominent fields include passenger transport, package delivery and emergency response [8, 9]. This entails a vast research field and consequently, the review conducted here confines itself to the passenger transport segment of the AAM market.

Seeing as the AAM market has not yet entered service, the operations side could potentially be developed as a hub-to-hub (e.g. airport to airport as seen in conventional aviation), point-to-hub (emergency response site to a hospital), point-to-point (origin to destination address as is done using a taxi) system or a combination thereof. Due to the complexity and the relatively high costs associated with the AAM transportation system, the passenger transport segment will most likely initially develop as a hub-to-hub system [10]. Based on that, the implementation of the AAM transportation system for passenger transport purposes introduces a set of use cases. To this extent, Asmer et al. [11] identified five distinct use cases as can be seen in Figure 2. According to these definitions, they analysed TLARs along with the optimal aircraft type per use case, of which the results are provided in Table 2. Observing the range and the vehicle type, one can conclude that the multi-rotor type performs best for short to medium range use cases, whereas the fixed-wing types are more suitable for the longer range use cases.

Table 2: AAM use cases as identified by Asmer et al. [11]

	Sub-Urban	**Intra-city**	**Inter-city**	**Airport shuttle**	**Mega-city**
Capacity	4 pax+hand luggage (4x90 [kg])	2-4 pax, possibly 1 pilot (90 [kg] p/person)	6-10 pax (90 [kg] p/person)	4 pax+luggage (4x110 [kg])	4-6 pax, possibly 1 pilot (90 [kg] p/person)
Range	≤ 70 [km]	≤ 50 [km]	>100 [km]	≤ 30 [km]	≤ 100 [km]
Speed	100-150 [km/h]	80-100 [km/h]	>100 [km/h]	100-150 [km/h]	100-150 [km/h]
Vehicle type	Multi-rotor	Multi-rotor	VTOL fixed-wing	Multi-rotor	Conventional helicopter/ VTOL rotary-wing/ VTOL fixed-wing
Mission steps	Vertiport → Vertiport	Vertiport→Vertistop→ Vertistop→Vertiport	Vertiport→Vertiport	Vertiport→Vertiport	Vertiport→Vertistop→ Vertiport

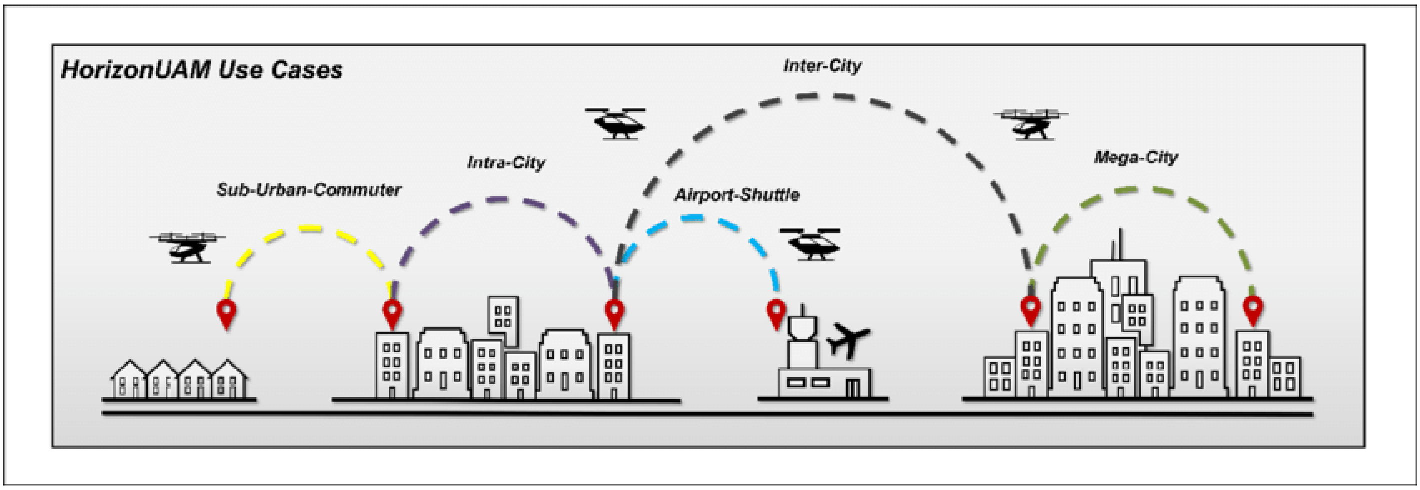

Figure 2: Potential use cases within the AAM transportation system [11]

The availability of the use cases as seen in Figure 2 depends on the area in which the AAM transportation system is to be introduced. Furthermore, the use cases also depend on the commuters to be served by the system. Thus, in order for the AAM system to become successful and widely adopted, a thorough understanding of the market it is to serve, is of utmost importance. As a result, this section starts with an overview of the studies focused on the potential demand to be served by the system in subsection 3.1. As will be evident in subsection 3.1, the potential demand is greatly affected by the allocation of vertiports. The design and operation of the vertiports may also have a significant impact on the success of the AAM system. For this reason, studies on the relevant aspects regarding the vertiport are introduced in subsection 3.2. Finally, apart from the vertiport throughput, the airborne vehicle density could potentially lead to conflicts and unsafe operations. Accordingly, the outlook and studies on traffic management within the AAM market is discussed in subsection 3.3.

3.1. Demand

Within any transportation system, having insights into the market to be served by the system is crucial. This allows for an estimation of the potential demand, and accordingly, the development of a balanced transportation system, which is able to efficiently and effectively serve its users. This holds even more so for the AAM market as a result of the complex coupling of various aspects, the level of technological innovation, the risks pertaining safety and security, and the potential annoyance factor of the system. Accordingly, numerous survey studies have been performed and have identified key influencing factors with regards to user-acceptance of the AAM transportation system as well as the users' willingness to pay. Apart from the survey studies, the potential demand within a number of cities has been analysed based on its' commuter data. Some studies have also included socio-demographic data. The survey studies have proven it to have a non-negligible impact on the potential demand. As a result, the survey studies along with their findings are elaborated upon in subsubsection 3.1.1, and the potential demand analyses are introduced in subsubsection 3.1.2.

3.1.1. Survey studies

EASA [12] performed a survey study focused on the societal acceptance of the UAM transportation system. The survey consisted of three parts, namely, a quantitative survey with the general public as respondents, a qualitative survey focused on the stakeholders of the UAM market and a noise perception survey to estimate an acceptable noise level. The results show an overall positive attitude towards and general acceptance of UAM by those who are open to innovation and improvement of the quality of life [12]. This acceptance is coupled to the requirement to uphold suitable levels of safety, security and environmental protection, and that no discomfort resulting from UAM operations is brought upon any citizen.

Focusing on the commuters which the AAM system is to potentially serve, Ahmed et al. [13] conducted an exploratory analysis on the users' willingness to pay for the UAM service. Their study consisted of a three-part survey of which the data was then analysed using a correlated grouped random parameters bivariate probit modeling framework. Their results showed that socio-demographic aspects (gender, age, ethnicity, education level, income level, household population), user-specific factors (driving experience, accident history, vehicle maintenance expenses) and the users' attitude towards the benefits and challenges of the UAM system impact the overall user acceptance thereof. Respondents' age and cost-related factors showed to have a negative effect, whereas the potential benefits had a positive impact on the users' willingness to pay [13]. They concluded that 'implementation of an attractive pricing and regulatory framework for flying taxis and shared flying car services has the potential to significantly alter the currently dominant conventional ground transportation system as well as the mobility and daily travel patterns' [13]. Ilahi et al. [14] also investigated the users' willingness to pay. By their definition, it encompasses the users' value of travel time savings and the elasticity for all mode choice alternatives. To this extent, they conducted a new travel diary and mode choice survey applied to the Greater Jakarta area to establish Revealed Preference (RP) and Stated Preference (SP) data sets. They were able to identify the highest market potential to originate from high-income and long-distance travellers within the Greater Jakarta area. Furthermore, they established safety and security to be a requirement when it comes to user acceptance of the transportation system. Finally, they recognised that for the UAM system to be able to provide adequate coverage and service, time is required to develop and build the required infrastructure [14].

Boddupalli et al. [15] specifically assessed commuters' mode choice with the introduction of UAM into the mix of existing transportation systems and found that it causes changes in the dynamic travel behaviours. Furthermore, travel time and cost were found to be detrimental decision drivers i.e. a combination of higher AAM ticket price and longer total travel time would cause commuters to choose another form of transportation. In contrast to previous authors, Boddupalli et al. [15] found users' income to have a negligible effect on the mode choice.

Al Haddad et al. [16] analysed the overall users' acceptance and adoption of UAM through an online global preference survey. Their results are in line with those found by Ahmed et al. [13] with regards to socio-demographic aspects and the respondents' attitude towards the benefits and challenges of the UAM system. Furthermore, they found trust and safety to be cumbersome aspects with regards to acceptance and adoption i.e. related to the presence of in-vehicle cameras and operators, and the performance of the system with regards to service reliability and potential travel delay. Secondary influencing factors were found to be data and ethical concerns, value of time and costs, and high affinity to social media. With the findings, the need for regulatory bodies to develop a unified framework on the safety standards and allowed noise levels becomes evident.

To summarise, studies have been performed on the societal acceptance, user acceptance, users' willingness to pay, etc. Primarily, the results align with one another in terms of showing an overall acceptance towards AAM as a transportation system. Furthermore, socio-demographic, users' attitude towards the benefits and challenges, and user-specific factors were found to have an impact on user acceptance of the AAM system. Finally, these results were found to be reliant on the need to uphold suitable levels of safety and security pertaining the users as well as bystanders, and uphold environmental protection regulations. Taking into account that these studies were performed globally, this validates the need for a unified framework on safety standards and allowable noise levels [16].

3.1.2. Potential demand analysis

Translating the qualitative findings outlined in subsubsection 3.1.1 into potential user data which can be used is crucial for top-level assessment of the transportation system. Using commuter and in some studies, socio-demographic data, the potential AAM demand in a number of cities/areas has been analysed. As such, Rajendran and Zack [17] used New York City taxi data to derive the potential UAM demand for the placement of vertiports. The demand is then filtered based on a number of trip-related factors e.g. maximum distance to be flown, minimum travel time saved, first and last leg trips should be less than one mile each, and takes ten minutes. Rajendran et al. [18] used the previously introduced data set and applied machine learning algorithms to better estimate the potential demand with the inclusion of temporal (month, day of week, time of day, weekday indicator and location id) and weather-related (temperature, weather condition, visibility, wind speed, humidity and fog) factors. Four machine learning algorithms were adopted, namely multinomial logistic regression, artificial neural network, random forests and gradient boosting to establish the link between the previously mentioned factors and the resulting demand level.

Haan et al. [19] used cell phone data to develop a regular commuter data set and used socio-demographic data to determine the potential demand in the United States. They then applied a mode choice model to better estimate the percentage of the potential demand willing to use the system. They performed a sensitivity analysis with variations in access and egress times, and different eVTOL designs. The results show that the overall demand is highly sensitive to the placement of vertiports and operating costs. They also found that aircraft with shorter ranges (airport shuttle or intra-city use case) and lower operating costs will generate more demand than a long range (mega-city or inter-city use case) and higher operating costs aircraft. Justin et al. [20] used a number of historical data sets (e.g. airfares, airports with commercial air services, air travel times, driving times and observed mode choice) to develop a utility model which is then used in a multinomial logit model to predict the potential demand.

Bulusu et al. [21] used commuter data of the San Francisco Bay area produced by the Mobiliti team at Berkeley Lab using the San Francisco County Transportation Authority (SFCTA) Champ 6 model. The travel time and road distances are then determined under congested conditions. This study aimed to determine the maximum potential demand. However, the study did not include the users' willingness to pay, which as elaborated upon in subsubsection 3.1.1 can have a significant effect on the demand. Nevertheless, the results show that under highly congested road conditions, around 45% of commuters benefit from UAM based on the travel time. In uncongested conditions, this percentage drops to around 3%.

3.2. Vertiport

As found by Haan et al.[19], the potential AAM demand is highly sensitive to the placement of vertiports. This shows the importance of the proper placement of the hubs, which has given rise to the vertiport placement problem. Consequently, numerous studies on the allocation of vertiports have been conducted, of which an overview is provided in subsubsection 3.2.1. Furthermore, when comparing the operational scenario of conventional aviation with that expected within to be the case in the AAM market, one can observe a higher vehicle throughput to be fulfilled by vertiports compared to conventional airports. The need to be able to meet such throughput requirements becomes even more important when accounting for the electric nature of the aircraft within the AAM market. As such, studies conducted on the design and operation of vertiports are outlined in subsubsection 3.2.2.

3.2.1. Vertiport allocation

The vertiport allocation problem has been tackled by numerous researchers whom have adopted a variety of methods. Brunelli et al. [2] identified four main groups into which the studies may be segregated, namely based on, location requirements and limitations, geographic data comparison methods, k-means approaches and objective-based approaches.

The **location requirements and limitations approach** is directly coupled to the specific location under investigation [22, 23]. It investigates whether a or which location is suitable for the placement of a vertiport based on 1. the physical space required for the vertiport, 2. obstacle clearance and 3. environmental constraints [2]. Antcliff et al. [24] identified highway cloverleaf areas as a good match for the placement of vertiports based on a number of operational, environmental and financial prerequisites. Furthermore, they addressed the privacy concerns by limiting the flights to a minimum flight altitude of 500 ft over private properties. With regards to the aircraft, the noise generation was found to be a detrimental factor when looking at the resulting user acceptance of and accordingly, demand within the AAM system. Due to the hub-to-hub nature of the system, the first- and last-mile problem is introduced. The first-mile problem refers to the passenger requiring another form of transportation to travel from the origin to the departure vertiport. Likewise, the last-mile problem concerns travel from the arrival vertiport to the users' destination.

For this reason, integration with existing modes of transportation is crucial for the large-scale acceptance and use of the AAM system. Otte et al. [25] addressed the importance of integration as a means to alleviate the current load on the public transportation system and on traffic congestion.

The **geographic data comparison approach** (GIS) utilises geographic, environmental and/or socio-economic data to determine optimal vertiport location(s) [26–28]. This method, in principle, allocates the vertiports based on the highest expected demand while accounting for the location requirements of a vertiport. Key factors here are socio-economic variables, points of interest (POIs), integration with ground transportation nodes, existing helipads and suitable infrastructure, and regulatory factors (e.g. low-noise, no low-altitude). Delgado Gonzalez [26] conducted a rooftop suitability analysis in Manhattan (New York, U.S.) by utilizing Lidar imagery in combination with rooftop footprints. By doing so, he was able to map the rooftop elevation and flatness of the rooftops within a designated area. Furthermore, Delgado Gonzalez conducted a parallel place suitability analysis based on POI, census blocks and socio-economic and environmental data and combined the results of the two analyses to develop a vertiport allocation suitability map.

The **k-means clustering approach** uses commuter data to group the population into k clusters of which the centres represent optimal vertiport locations in terms of serving demand [29, 30]. The centroid of the cluster is defined as seen in Equation 1 [31]. Once the centroid has been determined, the residual sum of squares (RSS) can be calculated through Equation 2. The algorithm then minimises the RSS by adapting the centroids.

$$\underline{\mu}(\omega) = \frac{1}{|\omega|} \sum_{\underline{\mathbf{x}} \epsilon \omega} \underline{\mathbf{x}} \tag{1}$$

$$RSS = \sum_{k=1}^{K} \sum_{\underline{\mathbf{x}} \epsilon \omega} |\underline{\mathbf{x}} - \underline{\mu}(\omega_k)|^2 \tag{2}$$

Rajendran and Zack [17] adopted an iterative k-means algorithm with a multi criteria warm start technique based on multi-modal transportation. The authors found that the percentage of time savings and "willingness to fly" rate did not significantly impact location decisions and the number of sites' [17]. Furthermore, Sinha and Rajendran [32] adopted a similar iterative k-means clustering method with a multi criteria warm start technique to improve the resulting vertiport locations. Most prominently, this version of the k-means method allows for the incorporation of socio-economic attributes such as demand satisfaction and user acceptance amongst others.

The **objective-based approach** determines the optimal vertiport locations based on a specific (set of) objective function(s). Arellano et al. [33] utilized a GIS approach based on a number of criteria and allocating the vertiports according to the objective to maximize served demand. The framework produced a higher UAM demand and the travel time savings were comparatively lower than if the network was manually developed. Daskilewicz et al. [34] used commuter data and allocated the vertiports with the objective to maximize the combined travel time savings of the commuters compared to driving. They were able to show that irrespective of the network size, based on current data, 'short trips under 30 miles dominate the electric vertical take-off and landing (eVTOL) commuter market' in Los Angeles and San Francisco [34]. Furthermore, objective-based approaches have been applied which minimise the travel costs [35] or maximize the revenue of the AAM system [36].

3.2.2. Vertiport operations

Apart from the importance of proper allocation of vertiports, the design of the vertiports determines the maximum throughput of eVTOL aircraft and passengers, and could potentially pose constraints on the scale of the AAM system. Improper design and sizing of the vertiports introduces risks, especially when accounting for the limited electric energy supply of the eVTOL aircraft operating within the system, the scale of operations and environmental aspects [37–39]. The goal when designing a vertiport is to 'maximize the throughput of a vertiport, minimize its physical footprint, and increase its robustness to off-nominal operations' [40]. As a result, Ahn and Hwang [41] established 'design criteria for touchdown and liftoff (TLOF) pads, final approach and takeoff (FATO), safety areas, gates, and taxiways' based on the regulations as set by the Federal Aviation Administration (FAA) and the European Union Aviation Safety Agency (EASA) separately. They established various vertiport designs based on a variety of topologies. The satellite, linear and pier topologies according to the regulations on vertiport design and operations set by EASA [22] can be found in Figure 4-5 respectively [41]. They proceeded by analysing the performance of the respective designs by applying them to Gimpo International Airport (South Korea) and found varying results as to which layout performs best depending on which set of regulations was adopted. This shows the correlation between the optimal vertiport design and the available space.

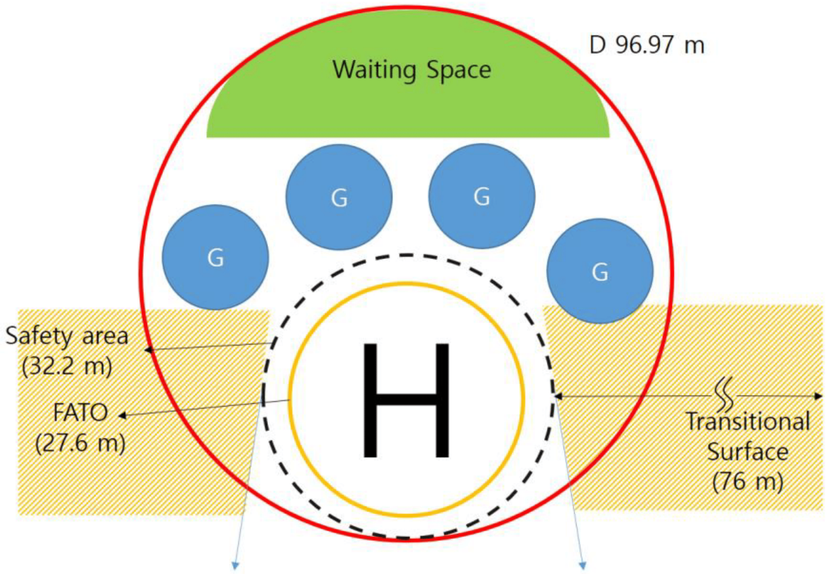

Figure 3: Vertiport satellite topology according to EASA's regulations [41] [22]

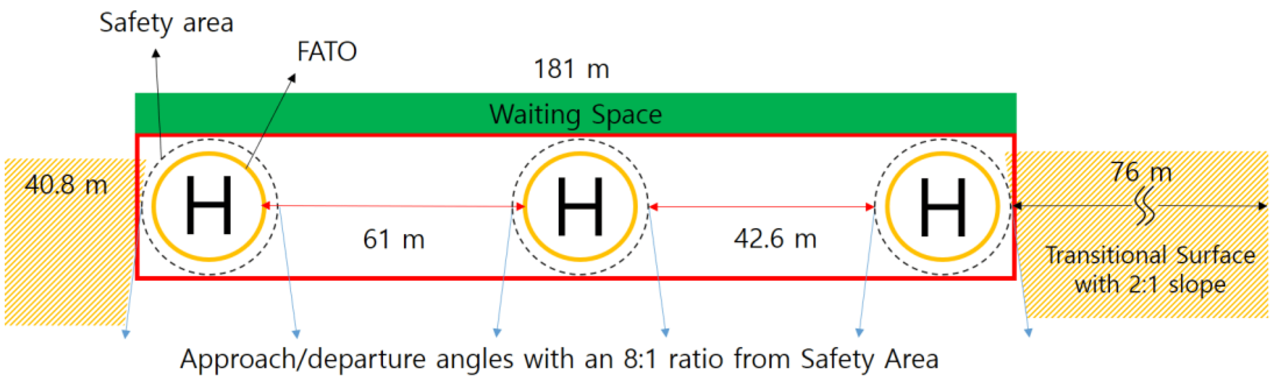

Figure 4: Vertiport linear topology according to EASA's regulations [41] [22]

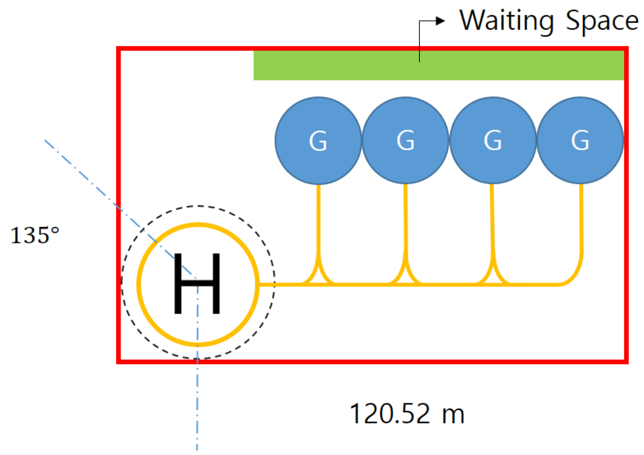

Figure 5: Vertiport pier topology according to EASA's regulations [41] [22]

Guerreiro et al. [42] adopted a first-come first-served scheduling approach to determine the capacity of a variety of vertiport designs. They were able to establish that the first-come first-served approach introduced inefficiencies in terms of the use of vertiport resources, which worsened with increasing number of resources [42]. Vascik and Hansman [40] developed an Integer Programming (IP) approach to determine the capacity envelop of a vertiport and applied it to 156 vertiport layouts. They utilised the previously introduced topologies (Figure 4-5) as well as a 'remote apron' topology to define the vertiport layouts. The results show the 'importance of balancing the number of touchdown and liftoff pads with the number of gates to achieve maximum vehicle throughput per vertiport footprint' [40]. Furthermore, they found that allowing simultaneous take-off and landing operations increases the vertiport throughput significantly [40]. Taylor et al. [39] developed a vertiport design tool for the analysis of operational trade-offs. They adopted a stochastic Monte Carlo simulation to determine the vertiport throughput and found that it increases with one vehicle per hour with every 420 m^2 of added vertiport surface area [39].

3.3. Traffic management

Besides proper vertiport allocation, and design and operation, the AAM market introduces a new operational scenario compared to conventional aviation. This operational scenario entails small aircraft which will be operating on a large scale within a constrained airspace. Consequently, the complexity of and load on air traffic control will be unlike what has been observed so far. In order to ensure continuous safe operation, major improvements in air traffic management are required. This has given rise to a number of studies targeting an array of aspects within the field of AAM air traffic management, namely focused on path planning, collision avoidance, airspace structure, etc. The fields come together in studies regarding autonomous traffic control and management.

The new operational scenario requires a level of automation within air traffic control and management in order to ensure safe and conflict free operations [43, 44]. Deniz et al. [45] developed a multi-agent reinforcement learning (MARL) model for the purpose of autonomous traffic control and management at merging points and intersections within a corridor based airspace. Training and evaluation of their model is realised using a neural network architecture within the BlueSky environment. Tang et al. [44] developed an Automated Flight Planning System (AFPS) to provide AAM operators with airspace and traffic management services. The system comprises of a Low-Altitude Airspace Management System (LAMS), to establish an airspace structure, and a Low-Altitude Traffic Management System (LTMS) for conflict-free operation. They incorporated the multiplication model for the preservation of fairness within a competitive market. A computational guidance algorithm was developed by Yang and Wei in order to permit autonomous on-demand operations within a free-flight airspace [43]. It serves to guide eVTOL aircraft, collision free, to its destination through adjustments in its bank angle and acceleration. The algorithm is based on a Markov Decision Process (MDP), which is solved by a Monte Carlo Tree Search (MCTS) algorithm.

Cummings and Mahmassani [46] developed macroscopic air traffic flow models based on a free-flight airspace for the purpose of relating key traffic variables to one another. The models serve to generate insights for the prediction of air traffic flow, and accordingly, potential conflicts. They did so by individually varying the traffic density, spacing requirements or the maximum vehicle speed, and observed the effects on the system performance. Their results show that with increasing traffic density, 'the conflict rate increases much more quickly' [46]. Furthermore, with increase in traffic density, decrease in vehicle speed and throughput was observed. The results also show that larger spacing requirements lead to deterioration with regards to conflicts, vehicle speed and critical density. This effect also holds for increase in maximum vehicle speed. Wang et al. [47] also addressed the air traffic assignment problem through the development of two-phase algorithm which optimises UAM traffic flow. Their model is based on a fixed-route structure airspace, known as volume segments. Their algorithm was able to efficiently allocate the traffic flow. Song et al. [48] focused on the optimal design of the airspace surrounding vertiports. To do so, they proposed a scheduling technique and a balanced branch queuing approach (BBQA) as an approach model.

4. AAM vehicle design and sizing

With regards to the vehicle, the market comprises of aircraft using powertrains based on a variety of energy sources (e.g. electric, fuel cell, hybrid), and requiring various take-off and landing distances (short and vertical take-off and landing). Seeing the need for clean transportation methods and the electric trend which the market is primarily following, this study solely permits aircraft based on an electric powertrain within its design space. Furthermore, although short take-off and landing (STOL) require a short runway, the available space within major cities is already very limited. For this reason, the research to be conducted confines itself to electric vertical take-off and landing (eVTOL) aircraft. Based on that, an overview of the eVTOL aircraft types is provided in subsection 4.1. subsection 4.2

4.1. Vehicle types

Due to the emergence of distributed electric propulsion, the design space of eVTOL aircraft is vast. As such, numerous eVTOL designs have been developed [1]. The various vehicles can be classified as has been done within the aircraft directory as done by eVTOL news [1], or as is presented in Figure 6 [49].

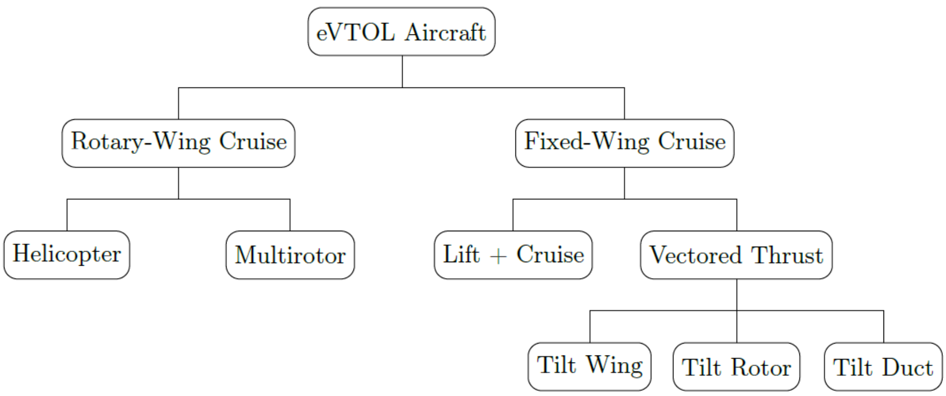

Figure 6: eVTOL aircraft classifications according to their cruise segment [49].

The rotary-wing cruise classification contains the e-helicopter and the multirotor designs. Example e-helicopter and multirotor designs are the FlyNow Aviation eCopter [2] and the eHang EH216-S [3], and can be seen in Figure 7 and Figure 8 respectively.

[1] eVTOL News aircraft directory: `https://evtol.news/aircraft` [accessed 25.06.24]
[2] FlyNow Aviation eCopter: `https://www.flynow-aviation.com/` [accessed 25.06.24]
[3] eHang EH216-S aircraft: `https://www.ehang.com/ehangaav/` [accessed 25.06.24]

Figure 7: Example of the electric helicopter type: FlyNow Aviation eCopter

Figure 8: Example of the multirotor type: eHang EH216-S

On the other hand, the fixed-wing cruise types have a very efficient cruise segment compared to the rotary-wing cruise types, but contain take-off and landing segments which require a high power output. This is a result of the relatively high disk loading associated with the hover phase. An example of the lift+cruise type is the aircraft by Ascendance Flight Technologies as seen in Figure 9 [4]. The lift+cruise type contains a set of rotors for the take-off and landing segments, and separate rotor(s) for the cruise segment. This allows for the optimisation of both sets of rotors for their respective operating conditions. The drawback of this type is the increase in weight as a result of the addition of rotors.

Figure 9: Example of the lift+cruise type: Beta Alia

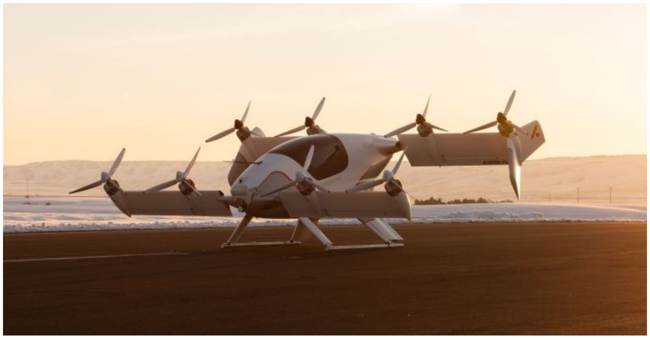

Figure 10: Example of the tilt-wing type: Airbus Vahana

As seen in Figure 6, the vectored thrust category consists of the tilt-wing, tilt-rotor and tilt-duct eVTOL aircraft types. Airbus designed the Vahana (Figure 10 [1]), a tilt-wing aircraft which was used for research purposes. During hover, the wings are in vertical position. The transition phase then entails tilting of the wing into horizontal position such that the cruise configuration is attained. Furthermore, two designs which are currently undergoing certification are the tilt-rotor Joby S4 aircraft (Figure 11 [2]) and the tilt-duct Lilium jet (Figure 12 [3]). Tilting of the rotors and ducts are the same as for the tilt-wing type, but as the name already states, the rotors and ducts are tilted for these types instead of the wing(s).

[4] Beta Alia: `https://www.beta.team/` [accessed 09.07.24]
[1] Airbus Vahana: `https://acubed.airbus.com/projects/vahana/` [accessed 25.06.24]
[2] Joby S4: `https://www.jobyaviation.com/` [accessed 25.06.24]
[3] Lilium jet: `https://jet.lilium.com/` [accessed 25.06.24]

Figure 11: Example of the tilt-rotor type: Joby S4

Figure 12: Example of the tilt-duct type: Lilium jet

Unlike the lift+cruise type, the rotors of these types need to be optimised for the hover and forward flight configurations. As a result, both flight segments contain less than optimal propeller designs since the flight conditions widely vary. Apart from that, tilting of the wing/rotor/duct requires a tilting mechanism able to bear the loads created in the hover, cruise and transition from hover to cruise configurations. The tilting mechanisms add weight as well as complexity to the aircraft. However, these types allow for an efficient cruise segment compared to the rotary-wing types. Furthermore, the addition of weight as a result of the cruise propeller, and drag as a result of the hover rotors as found in the lift+cruise type is not present in the vectored thrust types.

To get an indication of the performance of an eVTOL aircraft during hover and cruise, one could observe its disk loading and lift-to-drag ratio. With increasing disk loading, the aircraft becomes less efficient during hover. On the other hand, with increasing lift-to-drag ratio, the aircraft becomes more efficient during cruise. An overview of the disk loading and lift-to-drag ratio of the various types can be seen in Figure 13 [11]. One can observe a very low (in comparison to the other types) disk loading for rotary wing types, which indicates their efficiency during their hover flight segments. This efficiency comes at the detriment of the cruise segment, which can be observed by the relatively low lift-to-drag ratios compared to the fixed wing types. Consequently, these types are most suitable for short range, multi-leg trips [11, 50]. When looking at the fixed-wing types, one can observe a high lift-to-drag ratio as well as a high disk loading. This translates into inefficient hover segments, but very efficient forward flight segments.

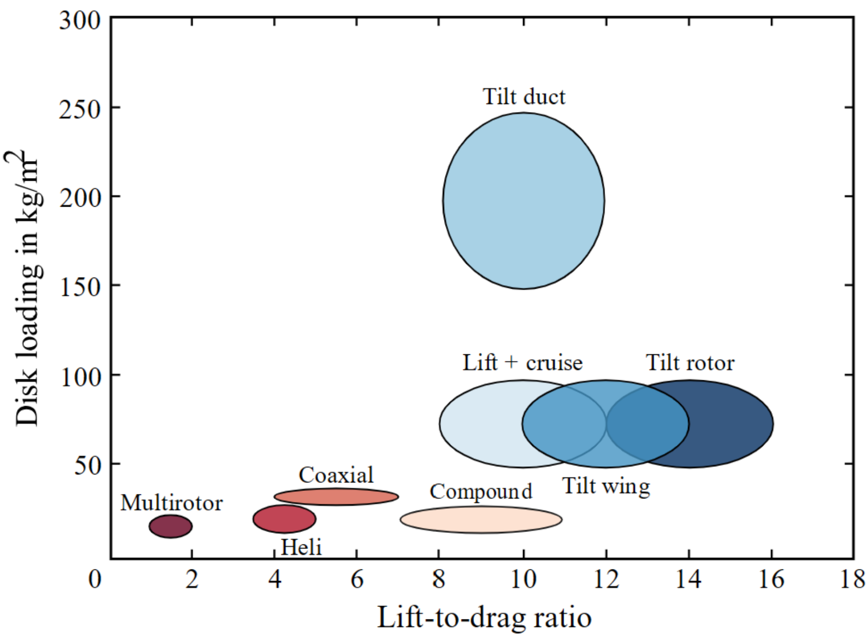

Figure 13: Disk loading vs lift-to-frag ratio for the eVTOL aircraft types [11].

4.2. Vehicle sizing

A number of methodologies have been established for the conceptual and preliminary sizing of eVTOL aircraft [51–55]. The majority of the methodologies rely on analytical methods used for the sizing procedure of conventional aircraft. These are altered as to be applicable to eVTOL aircraft. Furthermore, semi-empirical methods are adopted for the weight estimation of the aircraft components as is done for conventional aircraft. The methodologies start with an initial estimate of the aircraft design parameters. These parameters are then altered by the developed software until mass convergence is achieved. A number of methodologies include a sensitivity analysis on certain TLARs and aircraft design parameters. Nathen et al. [56], and Bacchini and Cestino [50] established a method for the performance assessment of existent eVTOL aircraft.

Akash et al. [51] developed a tilt-rotor eVTOL aircraft for intercity travel. They thereby also developed an extensive sizing methodology, which includes an assessment of the aircraft' stability and control, as well as a cost estimation and technological forecast. Ugwueze et al. [52] developed a concise sizing methodology for all types of eVTOL aircraft based on whether it is a rotary-wing or fixed wing concept. They applied a number of convergence methods (bisection, fixed-point iteration, Newton-Raphson and hybrids) in order to assess their respective performance in terms of convergence time and quality of the results. Zhang et al. [53] developed a tilt-duct concept with a range of 120 km and a cruise velocity of 241 km/h. Their sizing methodology includes a noise assessment. Shiva Prakasha et al. [54] provide their mass convergence algorithm with mission, rotor sizing and wing sizing inputs. The rotor and wing are sized and their performance characteristics are established. This is followed by an airframe weight estimation and sizing of the onboard systems. A convergence check is performed and the previously mentioned steps are performed until convergence is reached. An example sizing loop in provided in Figure 14 [54].

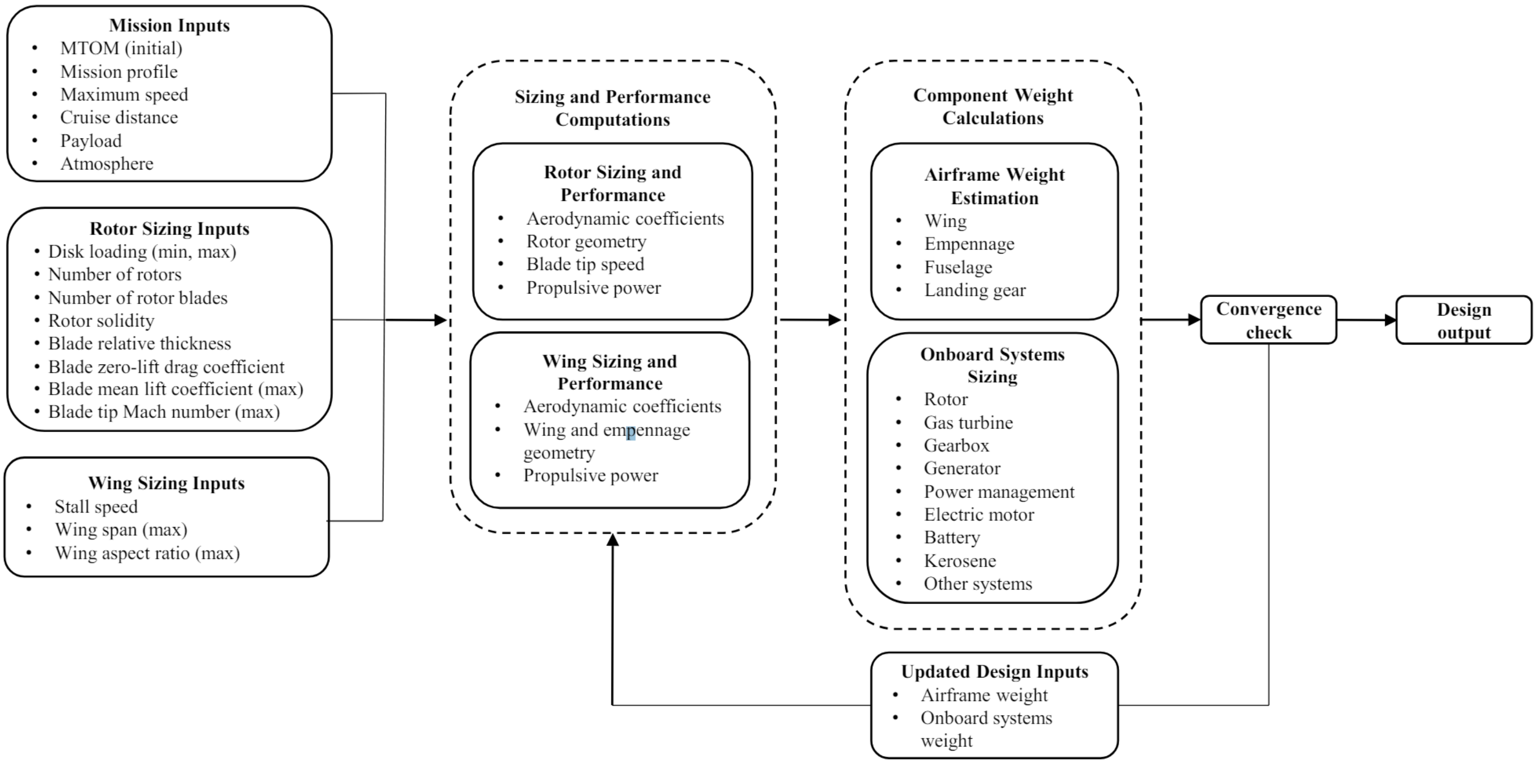

Figure 14: eVTOL aircraft sizing loop as developed by Shiva Prakasha et al. [54].

Apart from the previously introduced methodologies, a number of design software exist. One of these is the NASA Design and Analysis of Rotorcraft (NDARC) software, which is based on low-fidelity models [57] [1]. Furthermore, NASA also developed Open Vehicle Sketch Pad (OpenVSP), an open source parametric geometry software [2]. The software also has the capability to perform certain analysis methods to determine the performance of the design e.g. aerodynamics, structures.

One of the most important differences compared to conventional aircraft and the methods used to size them is the electric powertrain of the eVTOL aircraft. As per the definition by Ugwueze et al. [52], the aircraft mass comprises of the aircraft empty mass and the payload mass. The empty mass encompasses the battery mass, airframe mass and propulsion system mass. Generally, the airframe mass and the propulsion system mass are estimated using the methods established by Roskam [58]. The battery mass is determined based on either the energy required to complete the entire mission or the maximum power required throughout the mission segments. The total mission energy is a summation of the energy required in each of the flight segments, which are a direct result of the respective segment power requirement and the time required to complete the segment. An overview of the method established by Ugwueze et al. [52] to determine the power (P) requirements of the respective mission segments is provided in Table 3.

Table 3: Power required for the various flight segments based on the type of eVTOL vehicle [52].

Flight Segment	**Vehicle Configuration**	**Power Model**	
Take-off, hover	Both	$P_{hv} = \frac{T^{3/2}}{FM\sqrt{2\rho A}}$	
Climb	Both	$\frac{P_{cb}}{P_{hv}} = \frac{V_v}{2v_{hv}} + \sqrt{\left(\frac{V_v}{2v_{hv}}\right)^2 + 1}$	
Cruise	Fixed-wing	$P_{cr} = \frac{1}{\eta_{prop}} D V_{cr}$	
Cruise	Rotary-wing	$P_{cr} = T(V_{cr} sin\alpha + v_i)$	
Descent	Both	$\frac{P_{ds}}{P_{hv}} = \frac{V_v}{2v_{hv}} + \sqrt{\left(\frac{V_v}{2v_{hv}}\right)^2 - 1}$	for $V_{ds}/v_{hv} \leq$ -2
		$P_{ds} \approx P_{hv}$	for -2 $\leq V_{ds}/v_{hv} \leq 0$
Landing, hover	Both	$P_{hv} = \frac{T^{3/2}}{FM\sqrt{2\rho A}}$	

The power required for the hover segments (Table 3) is a result of the thrust (T), which is generally determined using actuator disk theory [59]. Based on steady hover flight, the thrust is assumed to be equal to the weight (W) of the aircraft. In order to account for aerodynamic losses, the figure of merit (FM) is introduced. Furthermore, ρ and A represent the air density and rotor area, respectively. For the climb segment, a power ratio is determined, which is a result of the relative vertical velocity (V_v/v_{hv}). In the climb segment, the relative vertical velocity is positive, whereas in the descent segment, it is negative. In the descent segment, a distinction in calculation method is made based on the magnitude of the relative velocity. With regards to the cruise segment for the fixed-wing types, the aerodynamic losses are accounted for through the propeller efficiency (η_{prop}). Furthermore, the power required is also dependent on the drag (D) produced by the aircraft as seen in Equation 3.

$$D = \frac{1}{2}\rho V_{cr} S \left(c_{D_0} + \frac{c_L^2}{\pi ARe}\right) \tag{3}$$

The drag consists of the parasitic drag and the lift induced drag. The lift induced drag is a direct result of the lift produced by and the efficiency of the wings. On the other hand, the parasitic drag is a result of the shape, size and surface roughness of the aircraft. Finally, pertaining the rotary-wing types, the power required is dependent on the cruise velocity (V_{cr}), the induced velocity (v_i), the thrust and the angle of attack. The angle of attack is determined using Equation 4 [52].

[1] NASA Design and Analysis of Rotorcraft (NDARC) software: `https://software.nasa.gov/software/ARC-16265-1` [accessed 26.06.2024]

[1] Open Vehicle Sketch Pad (OpenVSP) software: `https://openvsp.org/` [accessed 26.06.2024]

$$\alpha = tan^{-1}\frac{D}{T} \tag{4}$$

This is followed by the calculation of the energy requirement using the time required to complete the respective flight segments [52, 56]. Once the total energy required for the mission has been determined, the battery is then either sized based on the total energy required for or based on the maximum power required throughout the mission as can be seen in Equation 5 [54]. Here, SP_{bat} and SE_{bat} represent the battery specific power and specific energy, respectively. The current state of battery technology requires a trade-off between the battery specific power and the specific energy i.e. the battery either has a high specific energy at the detriment of the specific power, or vice versa. The battery and relevant aspects are further discussed in subsubsection 4.2.1.

$$m_b = max\left(\frac{P_{bat,max}}{SP_{bat}}, \frac{E_{bat}}{SE_{bat}}\right) \tag{5}$$

4.2.1. Electric powertrain - Batteries

The batteries pose the highest risk in the development and advancement of the AAM market. Batteries are widely known to drop in performance beyond a certain state of charge (SOC), as can be seen in Figure 15 [60]. One can also observe the effect of the operating temperature on the open circuit voltage (OCV), or in general, on the discharge performance of the battery. As introduced in subsection 4.1, especially the vectored thrust eVTOL types require a very high power output during its take-off and landing flight segments due to their relatively high disk loading. Thus, in order to ensure safe operation, a minimum SOC of about 10-20% is generally adopted when sizing the battery [52, 54, 56].

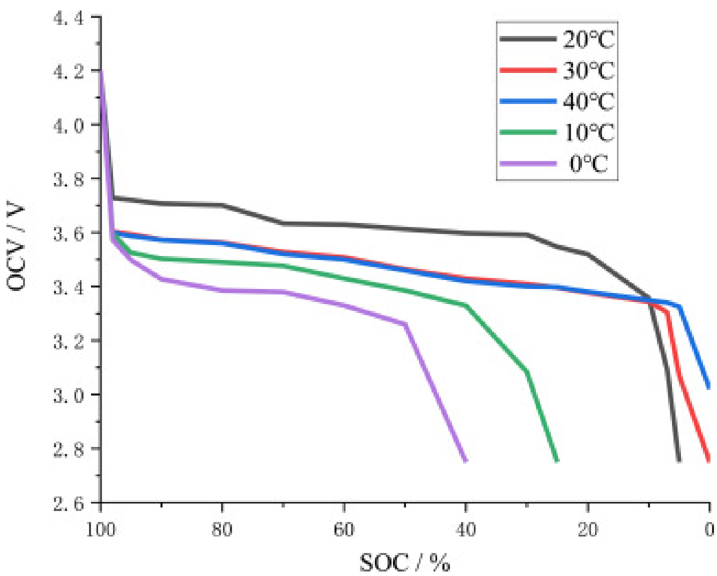

Figure 15: Discharge voltage as a result of the state of charge (SOC) [60].

Apart from the minimum SOC, a maximum SOC is adopted in some methodologies. This is done since the charging efficiency of a battery declines beyond a certain percentage, as seen in Figure 16 [61], causing the battery to charge at a much slower pace. Furthermore, by charging and discharging a battery completely, its state of health rapidly deteriorates. This can be observed in the number of life cycles associated with various depths of discharge (DOD) in Figure 17 [62].

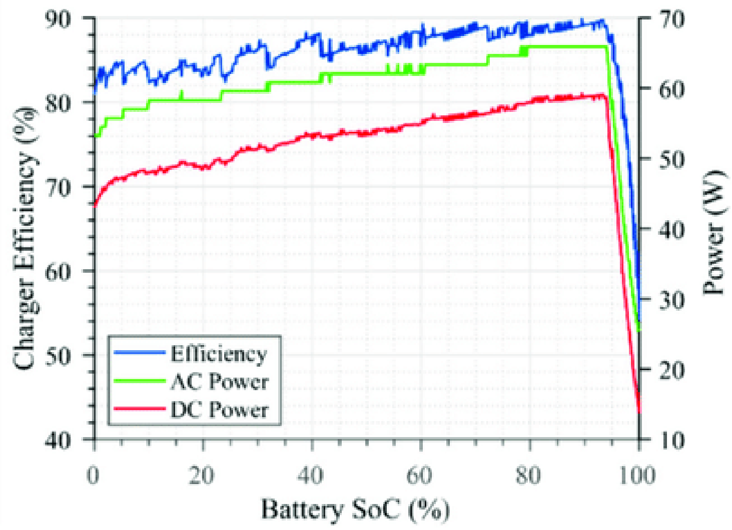

Figure 16: Charging efficiency as a result of the state of charge (SOC) [61].

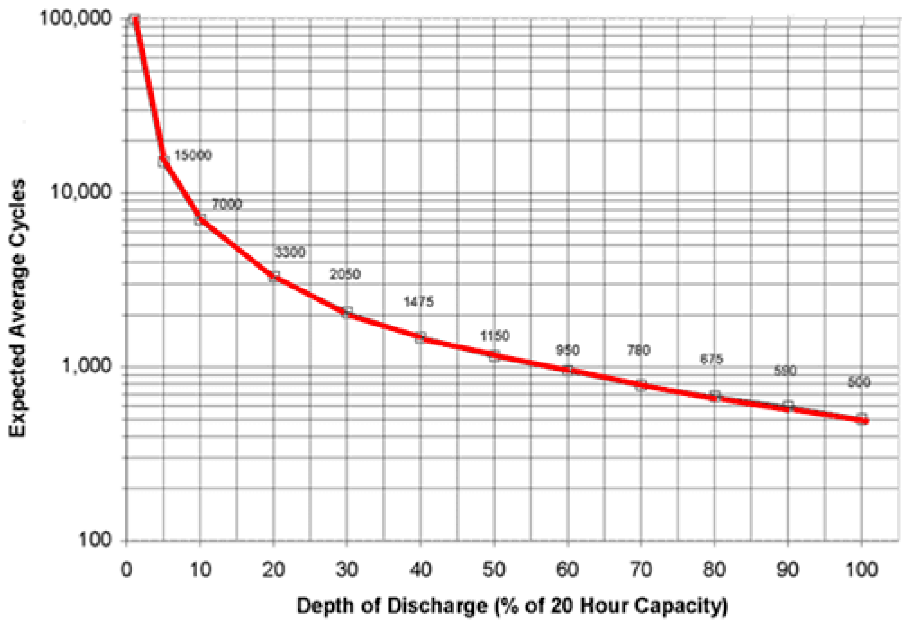

Figure 17: Number of life cycles as a result of depth of discharge (DOD) [62].

5. Research gap

To conclude, an overview of frameworks developed to determine various system-level performance metrics is provided in section 2. It has been shown how these frameworks encompass the operations and vehicle side, and couple them within an agent-based or scheduled simulation. In order to develop such a framework, an understanding of the most important aspects on the operations side is necessary. An overview thereof has been provided in section 3. The same holds for the vehicle design and sizing part, which has been provided in section 4.

Current studies filter the demand based on a variety of aspects, and consequently optimise for a single or multiple (unconnected) operational objectives. Generally, the growth of the market is accounted for by increasing the demand within a given operational scenario. Growth of the market is further simulated through sensitivity analyses by some. Furthermore, apart from the study by Escribano et al. [6] (who accounted for sizing of the aircraft based solely on the weight of its battery), present studies do not incorporate eVTOL aircraft sizing within their vertiport allocation optimisation or convergence loop.

Whereas these studies do provide crucial insights into how the system could be introduced into service and how it could respond to growth in the market, they exclude the impact on the formation of the network itself i.e. the sequential placement of vertiports within a city. Seeing the cost of developing a vertiport, the overall complexity of the system, the interdependencies between the components of the system and the electric nature of the aircraft, the need for efficient vertiport allocation becomes evident. Even more so, this shows the importance of a long term sequential allocation and overall, development plan which includes the (performance) limitations introduced by the aircraft.

6. Research objective

The master thesis proposed in this report aims to fulfil the following purpose statement: Formation of a unified framework for the development of a sequential vertiport allocation plan in conjugation with vehicle sizing and performance.

In order to aid in satisfying above-mentioned purpose statement, the following research questions along with sub-questions will be answered:

- How does the network evolve according to the number of vertiports?
  - What are the locations of the vertiports as a result of the number of vertiports?
  - How does the demand evolve according to the number of vertiports?
  - How can performance of the transportation system be measured and how does it evolve according to the number of vertiports?
  - How do the TLARs (i.e. range, capacity, cruise velocity) evolve according to the number of vertiports?
- How does the fleet evolve according to the scale of the network?
  - What is the optimal fleet size as a result of the number of vertiports?
  - What is the effect on the size of the vehicle as a result of the number of vertiports?
  - What is the effect on the vehicle performance as a result of the number of vertiports?
- What is the impact of the scale of the network on the vertiport capacity requirements?
  - What is the effect of the number of vertiports on the required inflow and outflow of vehicles per vertiport?
  - What is the effect of the number of vertiports on the required inflow and outflow of passengers per vertiport?
  - What is the effect of the number of vertiports on the energy requirement (for vehicle charging) per vertiport?
- What is the impact of the number of vertiports on the AAM traffic density?

7. Planning

The work to be done is split up into workpackages (WPs). The first consists of defining the exact methodology, including the variables and equations. In workpackage 2, the modules as established in workpackage 1 are to be coded into a coding software. Workpackage 3 consists of running the simulation (optimization) for five cases, in which the number of vertiports is increased from case I to V to mimic growth of the transportation system within a city i.e. stepwise increase in number of vertiports within the system. Next, the results are compiled and assessed in workpackage 4. This workpackage includes validation of the vehicle and the vertiport network separately. The validation steps are completed through comparison with existing literature. Finally, workpackage 5 consists of the overall reporting requirements of the study.

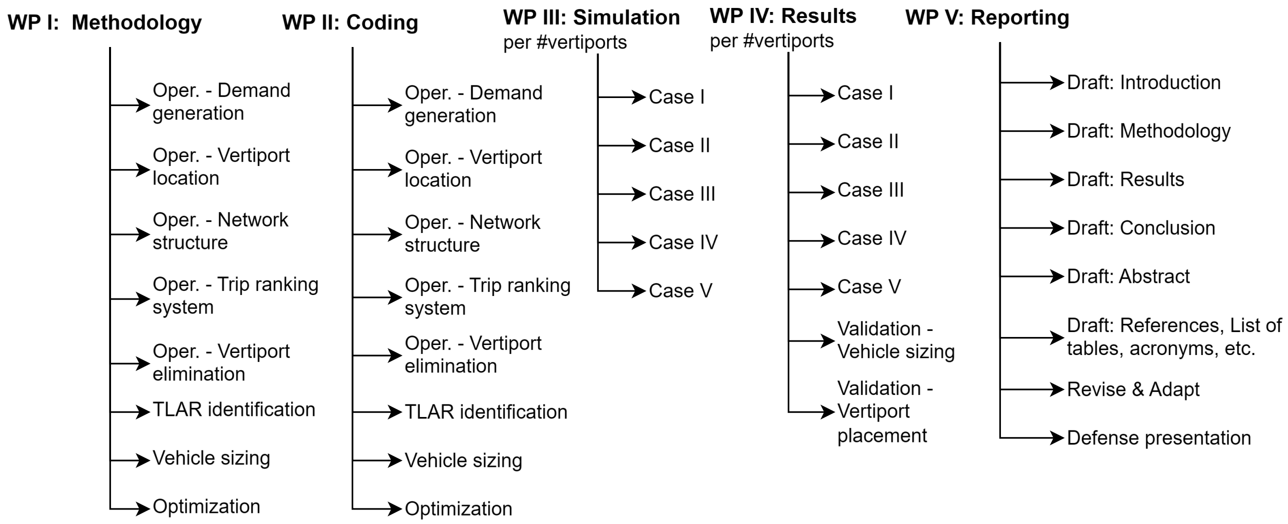

Figure 18: Work Breakdown Structure

Bibliography

[1] Long, Q., Ma, J., Jiang, F., and Webster, C. J., "Demand analysis in urban air mobility: A literature review," Journal of Air Transport Management, Vol. 112, 2023.

[2] Brunelli, M., Ditta, C. C., and Postorino, M. N., "New infrastructures for Urban Air Mobility systems: A systematic review on vertiport location and capacity," Journal of Air Transport Management, Vol. 112, 2023.

[3] Commission, E., for Mobility, D.-G., Transport, for Research, D.-G., and Innovation, Flightpath 2050 – Europe's vision for aviation – Maintaining global leadership and serving society's needs, Publications Office, 2011.

[4] Fu, M., Straubinger, A., and Schaumeier, J., "Scenario-Based Demand Assessment of Urban Air Mobility in the Greater Munich Area," Journal of Air Transportation, Vol. 30, No. 4, 2022, pp. 125 – 136.

[5] Shiva Prakasha, P., Naeem, N., Ratei, P., and Nagel, B., "Aircraft architecture and fleet assessment framework for urban air mobility using a system of systems approach," Aerospace Science and Technology, Vol. 125, 2022.

[6] Escribano Macias, J., Khalife, C., Slim, J., and Angeloudis, P., "An integrated vertiport placement model considering vehicle sizing and queuing: A case study in London," Journal of Air Transport Management, Vol. 113, 2023.

[7] Silva, C., Johnson, W., Antcliff, K. R., and Patterson, M. D., "VTOL urban air mobility concept vehicles for technology development," 2018.

[8] Gillis, D., Petri, M., Pratelli, A., Semanjski, I., and Semanjski, S., "Urban Air Mobility: A State of Art Analysis," Lecture Notes in Computer Science (including subseries Lecture Notes in Artificial Intelligence and Lecture Notes in Bioinformatics), Vol. 12950 LNCS, 2021, pp. 411 – 425.

[9] Goyal, R., Reiche, C., Fernando, C., and Cohen, A., "Advanced air mobility: Demand analysis and market potential of the airport shuttle and air taxi markets," Sustainability (Switzerland), Vol. 13, No. 13, 2021.

[10] Holden, J. and Goel, N., Fast-Forwarding to a Future of On-Demand Urban Air Transportation (white paper), UBER Elevate, 2016.

[11] Asmer, L., Pak, H., Shivaprakasha, P., Schuchardt, B., Weiand, P., Meller, F., Torens, C., Becker, D., Zhu, C., Schweiger, K., Volkert, A., and Jaksche, R., "Urban Air Mobility Use Cases, Missions and Technology Scenarios for the HorizonUAM Project," 08 2021.

[12] EASA, Study on the societal acceptance of Urban Air Mobility in Europe, 2021.

[13] Ahmed, S. S., Fountas, G., Eker, U., Still, S. E., and Anastasopoulos, P. C., "An exploratory empirical analysis of willingness to hire and pay for flying taxis and shared flying car services," Journal of Air Transport Management, Vol. 90, 2021.

[14] Ilahi, A., Belgiawan, P. F., Balac, M., and Axhausen, K. W., "Understanding travel and mode choice with emerging modes; a pooled SP and RP model in Greater Jakarta, Indonesia," Transportation Research Part A: Policy and Practice, Vol. 150, 2021.

[15] Boddupalli, S.-S., Garrow, L. A., and Welch, T. F., Estimating demand for an electric vertical landing and takeoff (eVTOL) air taxi service using discrete choice modeling, Master's thesis, Georgia Tech, 2019.

[16] Al Haddad, C., Chaniotakis, E., Straubinger, A., Plötner, K., and Antoniou, C., "Factors affecting the adoption and use of urban air mobility," Transportation Research Part A: Policy and Practice, Vol. 132, 2020.

[17] Rajendran, S. and Zack, J., "Insights on strategic air taxi network infrastructure locations using an iterative constrained clustering approach," Transportation Research Part E: Logistics and Transportation Review, Vol. 128, 2019, pp. 470–505.

[18] Rajendran, S., Srinivas, S., and Grimshaw, T., "Predicting demand for air taxi urban aviation services using machine learning algorithms," Journal of Air Transport Management, Vol. 92, 2021.

[19] Haan, J., Garrow, L. A., Marzuoli, A., Roy, S., and Bierlaire, M., "Are commuter air taxis coming to your city? A ranking of 40 cities in the United States," Transportation Research Part C: Emerging Technologies, Vol. 132, 2021.

[20] Justin, C., Payan, A., and Mavris, D., "Demand Modeling and Operations Optimization for Advanced Regional Air Mobility," 08 2021.

[21] Bulusu, V., Onat, E. B., Sengupta, R., Yedavalli, P., and Macfarlane, J., "A Traffic Demand Analysis Method for Urban Air Mobility," IEEE Transactions on Intelligent Transportation Systems, Vol. 22, No. 9, 2021.

[22] EASA, Prototype technical specifications for the dessign of VFR vertiports for operation with manned VTOL-capable aircraft certified in the enhanced category, 2022.

[23] Feldhoff, E. and Soares Roque, G., "Determining infrastructure requirements for an air taxi service at Cologne Bonn Airport," CEAS Aeronautical Journal, Vol. 12, No. 4, 2021, pp. 821 – 833.

[24] Antcliff, K. R., Moore, M. D., and Goodrich, K. H., "Silicon valley as an early adopter for on-demand civil VTOL operations," American Institute of Aeronautics and Astronautics Inc, AIAA, 2016.

[25] Otte, T., Metzner, N., Lipp, J., Schwienhorst, M. S., Solvay, A. F., and Meisen, T., "User-centered integration of automated air mobility into urban transportation networks," Vol. 2018-September, Institute of Electrical and Electronics Engineers Inc., 2018.

[26] Delgado González, C. J., Rooftop-place suitability analysis for urban air mobility Hubs: A GIS and neural network approach, Master's thesis, Universidade Nova de Lisboa, 2020.

[27] Fadhil, D. N., Rothfeld, R., and Moeckel, R., A GIS-based Analysis for Selecting Ground Infrastructure Locations for Urban Air Mobility, Master's thesis, Technical University of Munich, 2018.

[28] Kim, N. and Yoon, Y., "Regionalization for urban air mobility application with analyses of 3D urban space and geodemography in San Francisco and New York," Procedia Computer Science, Vol. 184, 2021, pp. 388–395.

[29] Lim, E. and Hwang, H., "The Selection of Vertiport Location for On-Demand Mobility and Its Application to Seoul Metro Area," International Journal of Aeronautical and Space Sciences, Vol. 20, No. 1, 2019, pp. 260 – 272.

[30] Jeong, J., So, M., and Hwang, H.-Y., "Selection of Vertiports Using K-Means Algorithm and Noise Analyses for Urban Air Mobility (UAM) in the Seoul Metropolitan Area," Applied Sciences, Vol. 11, No. 12, 2021.

[31] Manning, C. D., Raghavan, P., and Schütze, H., Introduction to Information Retrieval, Cambridge University Press, Cambridge, UK, 2008.

[32] Sinha, A. A. and Rajendran, S., "A novel two-phase location analytics model for determining operating station locations of emerging air taxi services," Decision Analytics Journal, Vol. 2, 2022.

[33] Arellano, S. I., Moeckel, R., and Rothfeld, R., A Data- and Demand-Based Approach at Identifying Accessible Locations for Urban Air Mobility Stations, Master's thesis, Technical University of Munich, 2020.

[34] Daskilewicz, M. J., German, B., Warren, M., Garrow, L. A., Boddupalli, S., and Douthat, T., "Progress in vertiport placement and estimating aircraft range requirements for evtol daily commuting," 2018 Aviation Technology, Integration, and Operations Conference, 2018.

[35] Chen, L., Wandelt, S., Dai, W., and Sun, X., "Scalable Vertiport Hub Location Selection for Air Taxi Operations in a Metropolitan Region," INFORMS Journal on Computing, Vol. 34, 11 2021.

[36] Rath, S. and Chow, J. Y., "Air taxi skyport location problem with single-allocation choice-constrained elastic demand for airport access," Journal of Air Transport Management, Vol. 105, 2022.

[37] Zelinski, S., "Operational Analysis of Vertiport Surface Topology," 10 2020, pp. 1–10.

[38] Goodrich, K. H. and Barmore, B. E., "Exploratory analysis of the airspace throughput and sensitivities of an urban air mobility system," American Institute of Aeronautics and Astronautics Inc, AIAA, 2018.

[39] Taylor, M., Saldanli, A., and Park, A., "Design of a Vertiport Design Tool," 2020 Integrated Communications Navigation and Surveillance Conference (ICNS), 2020.

[40] Vascik, P. and Hansman, R., "Development of Vertiport Capacity Envelopes and Analysis of Their Sensitivity to Topological and Operational Factors," 01 2019.

[41] Ahn, B. and Hwang, H.-Y., "Design Criteria and Accommodating Capacity Analysis of Vertiports for Urban Air Mobility and Its Application at Gimpo Airport in Korea," Applied Sciences, Vol. 12, No. 12, 2022.

[42] Guerreiro, N., Hagen, G., Maddalon, J., and Butler, R., "Capacity and Throughput of Urban Air Mobility Vertiports with a First-Come, First-Served Vertiport Scheduling Algorithm," 06 2020.

[43] Yang, X. and Wei, P., "Autonomous Free Flight Operations in Urban Air Mobility with Computational Guidance and Collision Avoidance," IEEE Transactions on Intelligent Transportation Systems, Vol. 22, No. 9, 2021.

[44] Tang, H., Zhang, Y., Mohmoodian, V., and Charkhgard, H., "Automated flight planning of high-density urban air mobility," Transportation Research Part C: Emerging Technologies, Vol. 131, 2021, pp. 103324.

[45] Deniz, S., Wu, Y., Shi, Y., and Wang, Z., "A reinforcement learning approach to vehicle coordination for structured advanced air mobility," Green Energy and Intelligent Transportation, Vol. 3, No. 2, 2024.

[46] Cummings, C. and Mahmassani, H., "Airspace Congestion, flow Relations, and 4-D fundamental Diagrams for advanced urban air mobility," Transportation Research Part C: Emerging Technologies, Vol. 159, 2024, pp. 104467.

[47] Wang, Z., Delahaye, D., Farges, J.-L., and Alam, S., "Complexity optimal air traffic assignment in multi-layer transport network for Urban Air Mobility operations," Transportation Research Part C: Emerging Technologies, Vol. 142, 2022.

[48] Song, K., "Optimal Vertiport Airspace and Approach Control Strategy for Urban Air Mobility (UAM)," Sustainability (Switzerland), Vol. 15, No. 1, 2023.

[49] Ratei, P., Wagner, M., and Shiva Prakasha, P., Conceptual Aircraft Design and Comparison of different eVTOL Aircraft for Urban Air Mobility, Master's thesis, HAW Hamburg, 2021.

[50] Bacchini, A. and Cestino, E., "Electric VTOL Configurations Comparison," Aerospace, Vol. 6, 02 2019.

[51] Akash, A., Raj, V. S. J., Sushmitha, R., Prateek, B., Aditya, S., and Sreehari, V. M., "Design and Analysis of VTOL Operated Intercity Electrical Vehicle for Urban Air Mobility," Electronics, Vol. 11, No. 1, 2022.

[52] Ugwueze, O., Statheros, T., Horri, N., Bromfield, M., and Simo, J., "An Efficient and Robust Sizing Method for eVTOL Aircraft Configurations in Conceptual Design," Aerospace, Vol. 10, 03 2023.

[53] Zhang, J., Liu, Y., and Zheng, Y., "Overall eVTOL aircraft design for urban air mobility," Green Energy and Intelligent Transportation, Vol. 3, No. 2, 2024.

[54] Shiva Prakasha, P., Ratei, P., Naeem, N., Nagel, B., and Bertram, O., "System of Systems Simulation driven Urban Air Mobility Vehicle Design and Fleet Assessment," 08 2021.

[55] Wang, S., Lima Pereira, L. T., and Ragni, D., "A preliminary design exploration of UAM vehicles," 03 2024.

[56] Nathen, P., Bardenhagen, A., Strohmayer, A., Miller, R., Grimshaw, S., and Taylor, J., "Architectural performance assessment of an electric vertical take-off and landing (e-VTOL) aircraft based on a ducted vectored thrust concept," 2021.

[57] Johnson, W., "NDARC-NASA Design and Analysis of Rotorcraft: Theory-Vol 1," 2022.

[58] Roskam, J., Airplane design. 5, component weight estimation, DAR corporation, 2003.

[59] Chattot, J., "Actuator Disk Theory—Steady and Unsteady Models," Journal of Solar Energy Engineering, Vol. 136, 08 2014.

[60] Ji, H., Pan, X., and Zhang, L., "Analysis of the performance decline discipline of lithium-ion power battery," Journal of Loss Prevention in the Process Industries, Vol. 74, 2022.

[61] Arango, I., Lopez, C., and Ceren, A., "Improving the Autonomy of a Mid-Drive Motor Electric Bicycle Based on System Efficiency Maps and Its Performance," World Electric Vehicle Journal, Vol. 12, 04 2021.

[62] Sepasi, S., Adaptive state of charge estimation for battery packs, Ph.D. thesis, 12 2014.